Chapter 6

Isochron Discordances and the Role of Inheritance and Mixing of Radioisotopes in the Mantle and Crust

Andrew A. Snelling, Ph.D.*

Abstract. New radioisotope data were obtained for ten rock units spanning the geologic record from the recent to the early Precambrian, five of these rock units being in the Grand Canyon area. All but one of these rock units were derived from basaltic magmas generated in the mantle. The objective was to test the reliability of the model and isochron "age" dating methods using the K-Ar, Rb-Sr, Sm-Nd, and Pb-Pb radioisotope systems. The isochron "ages" for these rock units consistently indicated that the α-decaying radioisotopes (^{238}U, ^{235}U, and ^{147}Sm) yield older "ages" than the β-decaying radioisotopes (^{40}K, ^{87}Rb). Marked discordances were found among the isochron "ages" yielded by these radioisotope systems, particularly for the seven Precambrian rock units studied. Also, the longer the half-life of the α- or β-decaying radioisotope, and/or the heavier the atomic weight of the parent radioisotope, the greater was the isochron "age" it yielded relative to the other α- or β-decaying radioisotopes respectively. It was concluded that because each of these radioisotope systems was dating the same geologic event for each rock unit, the only way this systematic isochron discordance could be reconciled would be if the decay of the parent radioisotopes had been accelerated at different rates at some time or times in the past, the α-decayers having been accelerated more than the β-decayers. However, a further complication to this pattern is that the radioisotope endowments of the mantle sources of basaltic magmas can sometimes be inherited by the magmas without resetting of the radioisotope

* *Geology Department, Institute for Creation Research, Santee, California*

"clocks" during ascent, intrusion, and extrusion in the earth's crust. This is particularly evident in recent or young rocks. Some evidence of open-system behavior was also found, and crustal contamination of some of the rock units was evident from their isotope geochemistry. Nevertheless, the overall systematic trend of radioisotope "ages" in the rock units according to their relative positions in the geologic record confirms that accelerated radioisotope decay was the dominant factor operating through earth history, with inheritance and mixing of radioisotopes from the mantle and crust as contributing factors in producing anomalous "ages." Within the Biblical framework of earth history, it is thus postulated that accelerated radioisotope decay accompanied the catastrophic geologic processes operating early in the Creation week and during the subsequent global Flood. Furthermore, because each of the three assumptions of conventional radioisotope dating—known initial conditions, closed-system behavior, and constancy of decay rates—have been clearly shown to be subject to failure, the radioisotope methods cannot, and should not, be relied upon to produce absolute "ages" for the earth's rock strata.

1. Introduction

It was in large part the discovery that modern lavas, particularly oceanic basalts, yielded old radioisotope "ages" which led to the recognition and definition of geochemical reservoirs in the earth's mantle where these lavas had been sourced. Thus *Zindler and Hart* [1986] delineated five end-member compositions in the mantle by which a variety of mixing processes were regarded as capable of explaining all the Sr-Nd-Pb isotope geochemical data on mid-ocean ridge and ocean-island basalts (MORBs and OIBs). Similarly, *Taylor et al*. [1984] had recognized three isotopic reservoirs in the continental crust, also characterized with respect to Sr, Nd, and Pb isotopes. What these mantle and crustal isotopic/geochemical reservoirs actually represent is still somewhat uncertain and very much a subject of current debate in the relevant literature as these reservoirs and their compositions have been linked in mantle-crust geodynamics models to the processes of

plate tectonics [*Doe and Zartman*, 1979; *Allègre et al*., 1983a,b*; Galer and O'Nions*, 1985; *Zindler and Hart*, 1986; *Allègre*, 1987; *Allègre et al*., 1988; *Zartman and Haines*, 1988; *Kramers and Tolstikhin*, 1997; *Albarède*, 1998; *Nägler and Kramers*, 1998; *Phipps Morgan and Morgan*, 1999; *van Keken et al*., 2002].

Snelling [2000a] concluded that the common thread among all the radioisotope systems is the role of these geochemical reservoirs in the mantle as the source of isotopic inheritance and mixing to give crustal rocks their isotopic signatures. This is now a well established explanation in the conventional literature, where mantle-crust geodynamics models have been used to link the characterized reservoir compositions to the different elements in the processes of plate tectonics. Thus it is envisaged that complex mixing has occurred through time as the upper and lower mantles have been stirred by subduction of plates, convection, and the ascent of plumes. Crustal growth has resulted. Defining what these mantle reservoirs represent is the subject of ongoing interpretation and debate. Even the so-called "Pb isotope paradox" seems to have been solved [*Murphy et al*., 2003], with the proposal that subducted oceanic crust and associated continental sediment stored as slabs in the mantle Transition Zone or mid-lower mantle are the terrestrial reservoir that plots to the left of the meteorite isochron (or geochron).

However, vast time spans of slow-and-gradual uniformitarian plate tectonics are unnecessary to produce, and are indeed incapable of producing, the required mixing, crustal growth, and mantle stirring, whereas catastrophic plate tectonics has the potential to explain, and be consistent with, even more of the real-world data within a young-earth time frame [*Austin et al*., 1994]. Indeed, state-of-the-art computer modeling of plate tectonics has demonstrated that the processes of subduction, plate movements, and mantle convection, and therefore crustal growth, occur catastrophically over a drastically shortened timescale [*Baumgardner*, 1994a, b, 2003].

Accelerated geological processes during Creation and the Flood, including catastrophic plate tectonics at least during the latter event, would have guaranteed that the present condition of the mantle and the crustal geologic record, which uniformitarians claim to have developed

over 4.57 Ga, would have instead developed within a young-earth time frame of 6000–10,000 years.

Snelling [2000a] reviewed each of the major long-age radioisotope dating methods and showed that two of the three basic assumptions upon which these methods are based face easily demonstrated difficulties. First, open-system behavior is rife, being readily recognized in weathered and hydrothermally altered samples. However, it is also subtly present even in otherwise fresh rocks, often enough to suggest that all samples could be affected to varying degrees. All parent-daughter pairs suffer at least some fractionation and/or disturbance as a result of the mobility of these isotopes in crustal fluids (ground and hydrothermal waters) and during metamorphism, including even the Sm-Nd system which is usually claimed to be immobile even under metamorphic conditions. Furthermore, isotopic differences, migration, and gains or losses are found at all observational scales down to zones within mineral crystals and different crystal faces. Resetting of the radioisotope systems is therefore common.

Snelling [2000a] also found that the initial conditions can either be uncertain or variable for cogenetic suites of rock samples. In the K-Ar system, excess $^{40}Ar^*$ (radiogenic ^{40}Ar) occurs in modern lavas which thus yield anomalously old "ages," but this same problem now has been documented in volcanic and crustal rocks of all "ages." Because $^{40}Ar^*$ is indistinguishable from non-radiogenic ^{40}Ar, there is no way of knowing whether the $^{40}Ar^*$ measured in all samples has been produced by *in situ* radioactive decay of ^{40}K, whether it is primordial ^{40}Ar inherited from the mantle, or whether it is mobile $^{40}Ar^*$ acquired from other crustal rocks via fluid transport. Whereas the isochron technique is supposed to provide by extrapolation the initial ratios (and therefore initial conditions) for the Rb-Sr and Sm-Nd systems in cogenetic rock suites, significant problems do arise. The ranges of the $^{143}Nd/^{144}Nd$ ratios are usually so small compared to the analytical uncertainties of the samples that the necessary long extrapolations cause appreciable error margins for the determined initial ratios, and introduce substantial uncertainties. In any case, variations in initial $^{87}Sr/^{86}Sr$ or $^{143}Nd/^{144}Nd$ ratios for cogenetic suites of young lavas from single volcanoes have

been found, meaning that the assumption of well-defined initial ratios for many suites of rocks is difficult to defend.

As a consequence of this inheritance and mixing of excess $^{40}Ar^*$ there have been numerous attempted explanations of the interaction of the geochemical reservoirs in the crust and mantle during plate tectonics processes throughout the earth's history [*Allègre et al*., 1996; *O'Nions and Tolstikhin*, 1996; *Albarède*, 1998; *Phipps Morgan*, 1998; *Davies*, 1999]. However, of particular interest are the observations made by *Damon and Kulp* [1958], who found excess $^{40}Ar^*$ in beryl crystals recovered from pegmatites and other magmatic rocks of various uniformitarian "ages" and geological locations. Beryl is a mineral that usually contains no ^{40}K whatsoever, so all the $^{40}Ar^*$ measured (significant quantities in fact) had to have been inherited as excess $^{40}Ar^*$ from the magmas and magmatic/hydrothermal fluids present when the beryl crystallized. It would seem to be highly significant that they reported a 100-fold difference in excess $^{40}Ar^*$ content between beryl crystals formed in the early Precambrian (with an "age" of about 3 Ga) and those from the Paleozoic (with "ages" of 280–320 Ma). Furthermore, they found no significant variation in the total volume of the volatile constituents in the beryl crystals and thus eliminated formation pressure as a direct cause of this "age" correlation. In fact, there is a systematic trend in the data, between the absolute amounts of excess $^{40}Ar^*$ in the beryl crystals and the uniformitarian/radioisotope "ages" of the beryl crystals. *Damon and Kulp* [1958] therefore interpreted this correlation as due to a more extensive mobilization of the lower crust and mantle in the past (in the earlier phases of earth history), with a consequent greater rate of degassing of inert gases than at present.

Snelling [2000a] has discussed the Biblical framework of earth history, and the possibility of two clearly-stated periods of non-uniformitarian, accelerated geological processes—Creation and the Flood (2 Peter 3:3–7). It is conceivable that the apparent overall systematic trend of K-Ar and Ar-Ar radioisotope "ages" through the geologic record might be explained by systematic inheritance of excess $^{40}Ar^*$ during these periods of accelerated geological processes at Creation and the Flood when the vast majority of the geologic record was formed. A lot of

outgassing would have occurred during Creation week, especially with crustal formation and associated catastrophic tectonics on Day 3 to produce the dry land, so rocks inheriting a lot of excess $^{40}Ar^*$ at that time would now appear to be vastly older than rocks formed subsequently during the Flood when less outgassing was occurring. Similarly, there would have been more outgassing of excess $^{40}Ar^*$ and inheritance at the beginning of the Flood, with the breaking up of the "fountains of the great deep" (Genesis 7:11), than during later phases of the Flood, so that early Flood rocks would now appear to be much older than late Flood rocks higher up the geologic record. The excess $^{40}Ar^*$ in beryl data are consistent with this model.

Similarly, with the use of Sr, Nd, and Pb isotopes in modern lavas to define the mantle geochemical reservoirs from which the magmas were sourced, the source and history of other lavas and ancient magmatic rocks can also be described on the basis of their Sr-Nd-Pb isotope geochemistry (for example, *Snelling* [2003a, 2003b]). Indeed, mantle-crust geodynamics models have demonstrated that the radioisotope ratios in lavas and magmatic rocks interpreted as "ages" could conceivably have been derived from progressively tapping magmas from an increasingly stirred mantle with geochemical reservoirs consisting of compositional "plums" and melt residues [*Phipps Morgan and Morgan*, 1999], which included different U-Th-Pb, Rb-Sr, and Sm-Nd isotopic signatures, and excess $^{40}Ar^*$ contents.

However, perhaps the most crucial observation made by *Snelling* [2000a] is that not all linear arrays on Rb-Sr, Sm-Nd, and Pb-Pb diagrams are true isochrons. Linear correlations are known to arise from mixing of the isotopic signatures of mantle and crustal sources, contamination, fractionation, and/or sampling bias. As already noted, recent lavas on ocean islands plot along Rb-Sr and Pb-Pb isochrons which correspond to exceedingly old "ages," so it is recognized that these inconsistent isotopic signatures represent characteristics of heterogeneous mantle sources rather than true "ages" of the lavas. The Pb-Pb system in these lavas is also totally at variance with all current models of Pb isotopic evolution built on the assumed primordial Pb isotopic composition of a mineral in one small meteoritic fragment which yields the earth's 4.57 Ga

"age." Similarly, Sm-Nd "model ages" are based on the assumption that Nd isotopic evolution commenced with a bulk earth composition at its 4.6 Ga origin of the average chrondritic meteorite. Thus the edifice of radioisotope "dating" is ultimately built on the foundation of assumed earth accretion from the solar nebula at 4.57 Ga. Furthermore, what constitutes accepted "ages" within the uniformitarian time framework is determined by consistency with the stratigraphic and biostratigraphic settings and with other radioisotope "ages." Such concordances appear to occur systematically through the geologic record.

It logically follows that if modern lavas have radioisotope signatures which yield artificially old "ages" because the lavas have been sourced in heterogeneous mantle reservoirs, then it is possible, and entirely reasonable to suppose, that "ancient" lavas may likewise appear to be artificially old because of being similarly sourced from the mantle. Indeed, isotopic mixing from mantle and crustal reservoirs to produce crustal rocks has been demonstrated, for example, *Snelling* [2003a, b]. Thus, it is conceivable that the radioisotope "ages" in most crustal rocks are an artifact of systematic mixing of mantle and crustal sources which were supplied with fundamental radioisotope/geochemical signatures as a result of the accelerated crustal development processes operating during the fiat creation origin of the earth. Very different radioisotope signatures in successive flows from the same volcanoes would seem to be consistent with such mixing processes.

The quality and integrity of the radioisotope data may often be doubtful on the one hand, because of the demonstrated prevalent open-system behavior of the radioisotope systems in the surface samples from which the data are obtained. However, on the other hand, the concordances and a systematic consistency within the uniformitarian timescale edifice remain, so the solution to these may therefore involve the geochemical and catastrophic, tectonic (geodynamic) processes in the mantle and crust that have unmistakably produced their geochemical and radioisotope signatures in the earth's crustal rocks, signatures that have been wrongly interpreted as old "ages."

Nevertheless, some radioactive decay has occurred, sufficient to produce mature (fully-formed) ^{238}U radiohalos [*Snelling*, 2000b, 2005a;

S*nelling and Armitage*, 2003; *Snelling et al*., 2003b], as well as some nuclear decay that has produced fission tracks [*Snelling*, 2005b]. But just how much radioisotope decay has occurred can really only be calculated from the physical evidence. Thus, for example, the development of fully-formed ^{238}U radiohalos would seem to require at least 100 million years of radioactive decay assuming constant decay rates at today's values [*Humphreys*, 2000; *Snelling*, 2000b], so the presence of fully-formed and overexposed ^{238}U radiohalos in granitic rocks at many levels throughout the Paleozoic-Mesozoic geologic record [*Snelling and Armitage*, 2003; *Snelling et al*., 2003b; *Snelling*, 2005a] is consistent with hundreds of millions of years worth of radioisotope decay (at today's slow and constant rates) having occurred during accumulation of that portion of the Phanerozoic strata record. This conclusion is also confirmed by the quantities of fission tracks in selected Phanerozoic tuff beds corresponding to the accepted biostratigraphic and radioisotope "ages" of those strata [*Snelling*, 2005b].

The assumption of the uniformitarian timescale undergirds the interpretation of all radioisotope data, because consistency with that timescale distinguishes "dates" that are acceptable from "anomalies" that need to be explained by open-system behavior, inheritance, etc. Thus it is difficult to quantify just how significant are multiple radioisotope concordances and what appears to be a consistent overall trend of lower strata in the geologic record dating older than upper strata. However, the impression gained from the detailed examination by *Snelling* [2000a] of the primary radioisotope "dating" systems is that if the uniformitarian timescale assumption were removed, where more than one radioisotope system has been utilized to "date" specific rock strata, radioisotope discordances would be in the majority. That such discordances are often the case has already been discussed by *Austin* [2000], and has been thoroughly tested and documented on some specific strata by *Austin and Snelling* [1998], *Snelling et al*. [2003a], and *Austin* [2005]. Furthermore, it is highly significant that there are no practical geologic or geochemical explanations evident for these discordances, so if it weren't for the assumed appropriate uniformitarian "ages" used as a supposed objective "yardstick," all the discordant isochron

"ages" could actually be "anomalous." Using the same reasoning, there is therefore no guarantee that even when and where radioisotope concordances do occur the resultant "dates" are somehow objectively correct. In any case, the "ages" derived from the radioisotope systems can really only be regarded as maximum ages because of the evidence of open-system behavior, mixing, inheritance, etc., and thus the true ages of the strata may be considerably, or even drastically, younger. Of course, this puts intolerable strain on the evolutionary timescale for uniformitarians, because it not only argues that the conventional interpretation of radioisotope dating is not secure, but that the evidence actually points towards a much younger earth. A very relevant example is the stark contrast between the U-Pb radioisotope "age" of 1500 Ma for the zircon grains in the Jemez granodiorite of New Mexico and the He (derived from U decay) diffusion age of the same zircon grains of only about 6000 years [*Humphreys et al*., 2003a,b, 2004; *Humphreys*, 2005].

One definite possibility suggested by numerous lines of evidence is that there was a burst of accelerated nuclear decay during the Flood, and perhaps also a similar burst during the early part of the Creation week [*Humphreys*, 2000, 2005]. Thus, the radioisotope ratios produced, if interpreted in terms of today's slow radioisotope decay rates, would suggest that the rocks are very old, when in fact most of the radioisotope decay occurred extremely rapidly. If this occurred during the Flood, then the deepest strata would have more accelerated decay products accumulated in them than shallower strata deposited later in the Flood, and so would yield radioisotope "dates" that were much older. Furthermore, the physical evidence of radioisotope and nuclear decay provided by ^{238}U radiohalos and fission tracks respectively would thus be accounted for by the large amount of decay that actually occurred, albeit extremely rapidly. However, just how much decay occurred is constrained by the physical evidence of at least 500 million years worth (at today's decay rates) during the Flood [*Snelling*, 2005b]. Fission track ages of zircons in Precambrian granites of over 1000 million years are known [*Naeser et al*., 1989], but much of that nuclear decay could be related to the Flood event, and 1000 million years is drastically short

of the claimed 4.57 billion years of radioisotope decay from the origin of the earth interpreted from radioisotope ratios. Thus, there is ample scope for an alternative explanation for the radioisotope ratios measured in the earth's crustal rocks, but any alternative model must also still explain the apparent overall trend in radioisotope "dates" through the geologic record.

Uniformitarians assume the earth accreted from the solar nebula at 4.57 Ga, and that the earth's initial bulk geochemical composition was that of the average chondritic meteorite, which then becomes the starting condition for isotopic evolution through subsequent earth history. As argued by *Baumgardner* [2000], the plethora of geochemical data now available and the robustness of geochemical and geophysical modeling strongly suggest that at its creation the earth's bulk geochemical composition was probably that of the average chondritic meteorite. Of course, any associated inference about accretion from a solar nebula is totally rejected, given the unequivocal Biblical statements that the earth was in fact created before the Sun. Therefore, the quest to model the radioisotope data in the framework of catastrophic mantle-crust geodynamics is potentially greatly aided by starting with the same initial bulk geochemical composition and utilizing the same plate tectonics processes for stirring the mantle and extracting the crustal geologic record, but of course, in the context of catastrophic accelerated geological processes at Creation and during the Flood.

Therefore, in this concept of catastrophic mixing and inheritance to explain the radioisotope data, it is envisaged that the earth started after Creation with a radioisotope signature equivalent to an age approaching 4.57 Ga. Certainly, it is envisaged that some nuclear decay has occurred since Creation that has added to the initial radioisotope signature of the earth to now give it the uniformitarian "age" of 4.57 Ga, that nuclear decay having occurred at least during the Flood, as evidenced by mature ^{238}U radiohalos and fission tracks. This contribution may have been the equivalent of many millions, if not, hundreds of millions of years. Accelerated global tectonics processes during the Creation week to produce the dry land on Day 3 would then have extracted from the "primitive" mantle the necessary crustal material. Whether these

processes were accompanied by some accelerated nuclear decay or not is uncertain. However, because sequential extraction to build the crust was involved, and thus progressively more fractionation and mixing, the resulting radioisotope signatures in the sequences of crustal rocks so formed during the Creation week could have conceivably displayed a "younging" trend. Then with catastrophic plate tectonics, and renewed mantle stirring and crustal growth, triggered by the breaking up of "the fountains of the great deep" at the outset of the Flood, the sequence of "new" crustal rocks progressively formed during the accompanying accelerated nuclear decay could conceivably have been endowed with even younger "ages" as the Flood event continued. However, radioisotope "age" anomalies would also have increasingly developed as oceanic crust and some ocean floor sediments were recycled back into the mantle, mixing their radioisotope signatures with those in the mantle, especially where melting occurred to produce magmas that then added new magmatic rocks to the crust again. Quite clearly, the "picture" that emerges is one of increasing complexity as these accelerated geological and tectonic processes continued. Repeated stirring of the mantle, extraction of the magmas from it, and also recycling of crustal rocks back into it, would have progressively complicated the pattern of radioisotope signatures in an increasingly "plum-pudding" mantle mixture. Migration of radioisotopes in crustal fluids would also have produced "age" anomalies.

This then is a description of the inheritance and mixing model proposed by *Snelling* [2000a], but it is still rudimentary and requires "fleshing out" with a more detailed description of the development through the earth's history of the radioisotope ratios found in crustal rocks. In this model, rather than the radioisotope systems being perturbed, complex, multi-faceted open-system behavior is proposed to explain how the radiogenic daughter isotopes are found in association with their radioactive parent isotopes in the proportions necessary to yield the false interpretation of long ages. Clearly, much research needs to be done to substantiate and refine this model if ever it is to become a viable explanation for the long "age" pattern of the radioisotopes in the earth's crustal rocks.

2. Rationale of the Present Study

The present study represents the first attempt to use radioisotope data derived from specific crustal rock units to test the inheritance and mixing model proposed by *Snelling* [2000a]. Of course, there is a huge volume of radioisotope data in the conventional literature for rock strata throughout the geologic record from all parts of the globe, so one approach would be to reprocess this huge volume of data to identify radioisotope discordances and the apparent overall trend in radioisotope "dates" through the geologic record, as well as focusing on the Sr-Nd-Pb isotope geochemistry of these rock units to explore if the data fit those rock units having been sourced in one of the identified mantle or crustal geochemical reservoirs. However, most rock units have only been subjected to selected radioisotope analyses, so often only limited radioisotope data are available for them. Yet even then there can be uncertainty, because sometimes only selected radioisotope data are published. If reasons are not given for why data were rejected, then one can't be sure whether they were simply rejected because they didn't fit the investigators' preconceived outcome, when in fact the rejected data may still be valid.

Thus a different approach was deemed more appropriate. Specific, strategic rock units whose geologic and tectonic contexts are well characterized were selected for exhaustive radioisotope "dating" studies. Fieldwork was undertaken to become familiar with these rock units, so as to then obtain carefully selected samples for the radioisotope analyses. The benefit of these "hands on" case studies is that the radioisotope data can then be compared with, and understood in the context of, field knowledge of the rock units, their petrography, mineralogy, and general geochemistry, as well as the history of those rock units in their context since their formation. The main radioisotope systems that are routinely used were targeted, namely, the K-Ar, Rb-Sr, Sm-Nd, and U-Th-Pb radioisotope systems. Once these radioisotope data were generated for the rock units in these case studies, it was then possible to compare the different radioisotope systems, the isochron "ages" and model "ages" (both whole-rock and mineral where possible)

to test for radioisotope concordances and discordances, as well as to determine whether the overall trend in the radioisotope "dates" through the geologic record is only apparent or is real and can thus be fully accounted for by accelerated radioisotope decay, as argued by *Humphreys* [2000, 2005], or whether the radioisotope inheritance and mixing (catastrophic mantle-crust geodynamics) model can better explain the radioisotope data.

3. The Case Studies

The main criterion for the selection of the case studies for this present project was to target areas that are already well studied, both by the conventional community and by creationists, or the chosen areas are appropriate extensions to well-studied areas. This potentially maximizes the consequent benefits. Thus, the rock sequence in the Grand Canyon and the surrounding area is well studied by both the conventional scientific community and by creationists, and it offers a good cross-section through the geologic record of the Flood and into the pre-Flood rocks beneath. So it was logical to focus in this area as a "type section." Then an equally important criterion was to make sure the rock units studied spanned the geologic record and thus the conventional timescale. Furthermore, because there are a wide range of rock types on which radioisotope analyses can be made, it was important to hone the selection to a narrow band of rock types or compositions so that the same types of rocks could be compared at the different levels in the geologic record from the different episodes of earth history. This also had the additional advantage of removing the bulk chemistry of the rocks as a variable, potentially simplifying the interpretation of the resultant radioisotope data. The choice was thus made to primarily focus on mafic (basaltic) rock units, because the parent magmas were derived from the mantle, and thus the radioisotope and isotopic data obtained should coincide with one of the mantle geochemical reservoirs, or indicate mixing between them, or even crustal contamination during ascent of the magmas. When these additional criteria are applied to the Grand Canyon type section, it is evident that there are not mafic

rock units evenly spaced within either the rock record or its associated conventional timescale, so additional choices were made to augment the selected Grand Canyon mafic rock units with case studies from adjoining or other suitable areas.

Thus, in the Grand Canyon type section the mafic units chosen were the Uinkaret Plateau basalts (Quaternary), the Cardenas Basalt and the related diabase sills (Middle Proterozoic), and the amphibolites (metamorphosed basalts) of the Brahma Schist in the Granite Gorge Metamorphic Suite (Lower Proterozoic). Even though it isn't of mafic composition, the Elves Chasm Granodiorite (Lower Proterozoic) was added to this selection from the Grand Canyon because it appears to be the oldest rock unit in the Grand Canyon sequence. To fill in the gaps in the span of these Grand Canyon rock units of the geologic record and its associated conventional timescale, several additional rock units were targeted, namely, the Mt. Ngauruhoe andesite flows, New Zealand (historic), the Somerset Dam layered mafic intrusion, Queensland, Australia (Jurassic-Triassic), the Apache Group basalts and diabase sills in central Arizona (Middle Proterozoic), and the Beartooth andesitic amphibolite in Wyoming (Archean). Additional reasons for selection of the Apache Group basalts and diabase sills, and the Beartooth andesitic amphibolite were that the former appear to be closely related to the Cardenas Basalt and diabase sills in the Grand Canyon, while the latter is regarded as one of the oldest rocks in the U.S.A.

Detailed descriptions of each of the rock units chosen for these case studies are provided in an Appendix. These descriptions include the geographical occurrence, petrography, and mineralogical and geochemical variations within each rock unit, and where available, observations relevant to understanding how it formed. Suitable location and geological maps are also provided as well as appropriate strata sequence diagrams. The sampling of each of the rock units is described, and where possible sample locations are shown on the maps and strata sequence diagrams. A total of one hundred and thirty-six samples were collected:-

- Mt. Ngauruhoe, New Zealand (historic)—11
- Uinkaret Plateau basalts, western Grand Canyon (Quaternary)—10

- Somerset Dam layered mafic intrusion, Queensland, Australia (Jurassic-Triassic)—15
- Cardenas Basalt, eastern Grand Canyon (Middle Proterozoic)—15
- Diabase sills, central Grand Canyon, including the Bass Rapids sill (Middle Proterozoic)—16
- Apache Group basalts and diabase sills, central Arizona (Middle Proterozoic)—30
- Brahma Schist amphibolites, central Grand Canyon (Lower Proterozoic)—27
- Elves Chasm Granodiorite, Grand Canyon (Lower Proterozoic)—8
- Beartooth andesitic amphibolite, Wyoming (Archean)—1

4. Radioisotope Analytical Procedures

Two procedures were used for the handling and processing of the collected samples, depending on where the initial handling occurred. After the initial handling of the samples, they were sent to various laboratories for the different analytical work required.

Those samples that were taken to the petrographic laboratory at the Institute for Creation Research were sawed to remove exterior surfaces which could be contaminated. Thin-sawed slices of each rock sample were dispatched for preparation of thin sections for petrographic analysis. Interior blocks representative of each rock sample were then washed, dried, and crushed in an iron mortar to be prepared as whole-rock powders for chemical and isotopic analyses. After milling and grinding, the powders were sieved. All equipment used was thoroughly cleaned and washed after processing of each sample in order to eliminate contamination between samples. Approximately 20 g of particles finer than 200 mesh were submitted for bulk geochemical analyses (66 elements) to the XRAL Laboratories of Don Mills, Ontario, Canada, where XRF (x-ray fluorescence), ICP (inductively coupled plasma), and ICP-MS (inductively coupled plasma–mass spectrometry) methods were used to analyze the whole-rock powders. Other splits of the whole-rock powders containing 80–200 mesh (0.18–0.075 mm) particles were sent for K-Ar radioisotope analyses to the Geochron Laboratories

of Cambridge, Massachusetts, where they were analyzed under the direction of Dr. Richard Reesman, the K-Ar laboratory manager, who undertook standard K-Ar radioisotope analyses. The concentration of K_2O (weight %) was measured by the flame photometry method, and the ^{40}K concentration (ppm) was calculated from the terrestrial isotopic abundance using the measured concentration of K. The concentration in ppm of $^{40}Ar^*$, the supposed "radiogenic argon," was derived by the conventional formula from isotope-dilution measurements on a mass spectrometer by correcting for the presence of atmospheric Ar whose isotopic composition is known [*Dalrymple and Lanphere*, 1969]. Other splits of the powdered samples with particles <200 mesh (0.075 mm) were sent to the isotope laboratory at the University of Colorado at Boulder, where Professor G. Lang Farmer analyzed the samples by mass spectrometry for Rb-Sr, Sm-Nd, and Pb-Pb isotopes. These University of Colorado measurements of the Sr, Nd, and Pb isotopes were carefully calibrated by internationally recognized standards, and all the resultant isotopic data were then analyzed and isochrons plotted using the computer program called *Isoplot* [*Ludwig*, 2001]. For some of the rock units sampled, one or two of the samples were processed to split them into their mineral constituents. To do this, the –140 to +270 mesh grains were progressively concentrated into their various mineral constituents by centrifugation in different heavy liquids, followed by further cleaning using a strong magnet. X-ray diffraction (XRD) analysis and optical microscopy were used to confirm the identity and purity of the minerals concentrated. These mineral concentrates were then sent to the isotope laboratory at the University of Colorado at Boulder where Professor G. Lang Farmer undertook mass spectrometry measurements of the Sr, Nd, and Pb isotopes in the minerals. The resultant isotopic data were plotted as mineral isochrons for each radioisotope system, again using the *Isoplot* computer program.

Those samples whose processing was based in Brisbane, Australia, followed a slightly modified procedure. Split by hammering, a portion of each sample was sent for thin sectioning for subsequent petrographic analysis. Approximately 100 g splits of each of the samples were then dispatched to the Amdel laboratory in Adelaide, South Australia, where

each sample was crushed and pulverized. Whole-rock analyses were then undertaken by total fusion of each powdered sample followed by digesting them before ICP-OES (inductively coupled plasma-optical emission spectrometry) for major and minor elements, and ICP-MS (inductively coupled plasma-mass spectrometry) for trace and rare earth elements. Separate analyses for Fe as FeO were also undertaken by wet chemistry methods that were also able to record the loss on ignition, primarily representing H_2O or any carbonate (given off as CO_2) in the samples. A second representative set of 100 g pieces of each of the samples was sent to the K-Ar dating laboratory at Activation Laboratories in Ancaster, Ontario, Canada, for whole-rock K-Ar dating under the direction of the laboratory manager, Dr. Yakov Kapusta. After crushing of the whole-rock samples and pulverizing them, the concentrations of K (weight %) were measured by the ICP technique. The ^{40}K concentrations (ppm) were then calculated from the terrestrial isotopic abundance using these measured concentrations of K. The concentrations in ppm of $^{40}Ar^*$, the supposed radiogenic ^{40}Ar, were derived using the conventional formula from isotope dilution measurements on a noble gas mass spectrometer by correcting for the presence of atmospheric Ar whose isotopic composition is known [*Dalrymple and Lanphere*, 1969]. Finally, a third representative set of 100 g pieces of each of these samples was sent to the PRISE laboratory in the Research School of Earth Sciences at the Australian National University in Canberra, Australia, where under the direction of Dr. Richard Armstrong whole-rock Rb-Sr, Sm-Nd, and Pb-Pb isotopic analyses were undertaken. After the sample pieces were crushed and pulverized, the powders were dissolved in concentrated hydrofluoric acid, followed by standard chemical separation procedures for each of these radioisotope systems. Once separated, the elements in each radioisotope system were loaded by standard procedures onto metal filaments to be used in the solid source thermal ionization mass spectrometer (TIMS), the state-of-the-art technology in use in this laboratory. Strontium isotopes were measured using the mass fractionation correction $^{86}Sr/^{88}Sr = 0.1194$, and the $^{87}Sr/^{86}Sr$ ratios were reported normalized to the NBS standard SRM 987 value of 0.710207.

Neodymium isotopes were corrected for mass fractionation using $^{146}Nd/^{144}Nd = 0.7219$ and were normalized to the present-day $^{143}Nd/^{144}Nd$ value of 0.51268 for standard BCR-1 (a Columbia River basalt, Washington, sample). Lead isotope ratios were normalized to NBS standard SRM 981 for mass fractionation. Again, all the resultant isotope data were analyzed and isochrons plotted for each radioisotope system using the *Isoplot* computer program [*Ludwig*, 2001].

5. Results

5.1 K-Ar Model and Isochron Dating

The results of the K-Ar radioisotope analyses on the samples from all of these case studies are summarized in Table 1. The K-Ar model "ages" were calculated for each sample analyzed using the standard model-age equation, which assumes that 10.5% of the ^{40}K atoms in each sample decay to $^{40}Ar^*$ atoms. Furthermore, because ^{40}Ar is a common atmospheric gas which can leak into rocks and minerals making them appear older than their actual ages, in conventional K-Ar model age determinations it is assumed that a certain proportion of the ^{40}Ar in each rock sample is contamination, and therefore, a certain proportion of the total ^{40}Ar determined in the laboratory on each sample, in accordance with the ^{40}Ar to ^{36}Ar ratio of the present atmosphere, is subtracted so that only what is thus assumed to be the radiogenic ^{40}Ar in each sample is used in the model-age calculations [*Dalrymple and Lanphere*, 1969]. Furthermore, it is conventional to assume that no radiogenic ^{40}Ar (written as $^{40}Ar^*$) was present in the rock when it initially formed, so that all the $^{40}Ar^*$ now measured in the rock has been derived from *in situ* radioactive decay of ^{40}K. The reported error listed with each model "age" in Table 1 represents the estimated 1σ uncertainty due to the analytical equipment and procedure.

As already noted, the *Isoplot* computer program of *Ludwig* [2001], which is now commonly utilized by the geochronology community, was used to process the analytical data for each radioisotope system for each targeted rock unit. This program utilizes the least-squares linear

Table 1. K-Ar model and isochron "ages" obtained for the targeted rock units.

Rock Unit	Location	Conventional Age	Method	Number of Samples	Range of K-Ar Model Ages (Ma)		K-Ar Isochron Age (Ma)
					Minimum	Maximum	
Mt. Ngauruhoe andesites	Mt. Ngauruhoe, New Zealand	Historic flows (1949, 1954, 1975)	Direct observation	11 whole rocks (from 5 flows)	<0.27	3.5±0.2	Not applicable
Toroweap Dam	River Mile 179.4	1.16±0.18 Ma	K-Ar model	whole rock + 3 minerals	1.19±0.18 (whole rock)	20.7±1.3 (olivine)	Not applicable
Massive Diabase Dam	River Mile 202.5 Grand Canyon	0.443±0.041 Ma		whole rock + olivine	1.4±0.3 (whole rock)	46.5±4.3 (olivine)	
Somerset Dam layered mafic intrusion	Somerset Dam, southeast Queensland, Australia	216±4 Ma 225.3±2.3 Ma	K-Ar model composite Rb-Sr isochron	15 (whole rocks)	182.7±9	252.8±9	174±8
Cardenas Basalt	Eastern Grand Canyon, Arizona	1103±66 Ma	Rb-Sr isochron	15 (8 new, 7 existing)	577±12	1013±37	516±30
Bass Rapids diabase sill	Grand Canyon, Arizona	1070±30 Ma	Rb-Sr isochron	11 (whole rocks)	656±15	1053±24	841.5±164
Apache Group basalts	Central Arizona	1100 Ma	Assumed similar to diabase sills	9 (whole rocks)	513±13	968.9±25	Too much scatter
Apache Group diabase sills	Central Arizona	1120±10 Ma 1140±40 Ma	zircon U-Pb biotite K-Ar	21 (whole rocks)	267.5±14	855.8±17	Too much scatter
Brahma amphibolites	Grand Canyon, Arizona	1740–1750 Ma	zircon U-Pb concordia	27 (whole rocks)	405.1±10	2574.2±73	Too much scatter
Beartooth andesitic amphibolite	Northeast Wyoming	2790±35 Ma	Rb-Sr isochron	1 whole rock + 5 minerals	1520±31 (quartz-plag.)	2620±53 (hornblende)	Too much scatter

regression method of *York* [1969] to plot the isochron as the best-fit regression line through the data. The slope of the isochron is then used by the program to calculate the isochron "age" using the standard isochron-age equation. When plotted, each data point has assigned to it error bars that represent the estimated 2σ uncertainties due to the analytical equipment and procedure. The program also evaluates the uncertainties associated with the calculated isochron "age" using a statistic known as the "mean square of weighted deviates" (MSWD), which is roughly a measure of the ratio of the observed scatter of the data points from the best-fit line or isochron to the expected scatter from the assigned errors and error correlations (including, but not limited to, the analytical equipment). If the assigned errors are the only cause of scatter, so that the observed scatter approximates the expected scatter, then the value of the MSWD will tend to be near unity. MSWD values much greater than unity generally indicate either under-estimated analytical errors or the presence of non-analytical scatter [*Ludwig*, 2001], while MSWD values much less than unity generally indicate either over-estimated analytical errors or unrecognized error-correlations. Thus it is crucial to adequately estimate the analytical errors so that the observed scatter of the data points from the isochron line yields an MSWD near unity. This was the procedure adopted here, so that the isochron "ages" reported in Table 1 were calculated from isochrons with MSWDs near unity. The errors for each isochron age reported represent the estimated 2σ uncertainties. As *Ludwig* [2001] notes, this does not mean that the true age of the samples has a 95% probability of falling within the stated age interval, but rather only signifies that the mean of the infinitely-replicated regressions would yield an isochron age within this interval.

For recent and young rocks, such as the Mt. Ngauruhoe andesites and Toroweap Dam and Massive Diabase Dam basalts (Table 1), K-Ar isochrons simply could not be plotted to derive any meaningful K-Ar isochron "ages," so the K-Ar isochron method as expected is not applicable to these rocks. On the other hand, the oldest rock units in Table 1, their conventional ages being those reported in the geologic literature, yielded K-Ar isotope data that contained too much scatter

to yield statistically viable K-Ar isochrons and isochron ages. This would suggest that a significant component in the observed scatter of the data points from the best-fit regression lines is due to factors other than the scatter due to analytical errors. Such factors would likely include contamination of the K-Ar radioisotope system by open-system behavior such as additions from the host wall rocks, and/or perturbing of the radioisotope systems by subsequent hydrothermal alteration and/or during weathering.

The samples from most of the targeted rock units yielded large ranges of widely divergent or scattered K-Ar model "ages." The scatter of the model "ages" was often just as great in those rock units for which K-Ar isochron "ages" could be calculated as in those where there was too much scatter to yield statistically viable isochron "ages." Such scatter did not always prevent the fitting of isochrons to the data and calculation of isochron "ages." Nevertheless, it is highly likely that the same factors responsible for the excessive scatter of the data points from the best-fit regression lines, which prevented statistically viable isochron "ages" being calculated, were also responsible for the scatter in the model "ages," particularly as these factors would vary between the outcrops from which the samples were collected. Interestingly, in two of the three rock units for which K-Ar isochron "ages" could be determined, those isochron "ages" did not fall within the ranges of the K-Ar model "ages" for those rock units as might be expected, but were actually less than the lowest model "ages."

5.2 K-Ar, Rb-Sr, Sm-Nd, and Pb-Pb Isochron Dating

All the results of the K-Ar, Rb-Sr, Sm-Nd, and Pb-Pb isochron dating of the samples of the targeted rock units in this study are summarized in Table 2. As already indicated above, all the isotope data for each radioisotope system for each targeted rock unit was processed using *Isoplot* [*Ludwig*, 2001] to plot isochrons and calculate isochron "ages." Furthermore, all the comments above about the assessment of the 2σ uncertainties in both the isotope ratios obtained from each sample and in the calculated isochron "ages" are relevant to the data in Table 2.

Table 2. K-Ar, Rb-Sr, Sm-Nd, and Pb-Pb isochron "ages" obtained for the targeted rock units.

Rock Unit	Location	Conventional Age	Method	Number of Samples	Isochron Ages (Ma)			
					K-Ar	Rb-Sr	Sm-Nd	Pb-Pb
Mt. Ngauruhoe andesites	Mt. Ngauruhoe, New Zealand	Historic flows (1949, 1954, 1975)	Direct observation	11 whole rocks (from 5 flows)	Not applicable	133±87 (5 samples)	*197±160* (5 samples)	*3908±390* (7 samples)
Uinkaret Plateau basalts	Western Grand Canyon, Arizona	<1.16±0.18 Ma	K-Ar model	8 (whole rocks)	None	1143±220 (7 samples)	*916±570* (6 samples)	Not available
Somerset Dam layered mafic intrusion	Somerset Dam, southeast Queensland, Australia	216±4 Ma 225.3±2.3 Ma	K-Ar model composite Rb-Sr isochron	15 (whole rocks)	174±8 (15 samples)	393±170 (14 samples)	259±76 (13 samples)	*1425±1000* (13 samples)
Cardenas Basalt	Eastern Grand Canyon, Arizona	1103±66 Ma	Rb-Sr isochron	26 (whole rocks) (14 new, 12 existing)	516±30 (14 samples)	1111±81 (19) 892±82 (22)	1588±170 Ma (8 samples)	*1385±950 Ma* (4 samples)
Bass Rapids diabase sill	Grand Canyon, Arizona	1070±30 Ma	Rb-Sr isochron	11 whole rocks DI-13 + minerals (6) DI-15 + minerals (11) magnetites (7)	841.5±164 — — —	1055±46(11) 1060±24 (7) 1075±34 (12) 1007±79 (7)	Too much scatter 1379±140 (7) 1330±360 (9) 1336±380 (7)	1250±130 (11) Too much scatter *1584±420* (10) 1327±230 (6)
Apache Group basalts	Central Arizona	1100 Ma	Assumed similar to diabase sills	9 (whole rocks)	Too much scatter	*2295±300* (5)	Not enough spread	1304±69 (8)
Apache Group diabase sills	Central Arizona	1120±10 Ma 1140±40 Ma	zircon U-Pb biotite K-Ar	21 (whole rocks)	Too much scatter	*2067±380*(16)	Too much scatter	1142±98 (19) 1146±59 (18)
Brahma amphibolites	Grand Canyon, Arizona	1740-1750 Ma	zircon U-Pb concordia	27 (whole rocks)	Too much scatter	840±86 (25) 1240±84 (19)	1678±60 (24) 1655±40 (21)	1864±78 (27) 1883±53 (20)
Elves Chasm Granodiorite	Grand Canyon, Arizona	1840±1 Ma	zircon U-Pb	8 (whole rocks)	Not available	1512±140 (7 samples)	1664±200 (7 samples)	1933±220 (7 samples)
Beartooth andesitic amphibolite	Northeast Wyoming	2790±35 Ma	Rb-Sr isochron	1 whole rock + minerals (5)	Too much scatter	2515±110	2886±190	2689.4±8.6

Where possible, isochrons were fitted to the data so that the MSWD was close or equal to unity, so that the observed scatter from the best-fit regression lines or isochrons was equal to the assigned analytical errors. The 2σ uncertainties in the listed isochron "ages" in Table 2 were thus calculated on that basis. Where the 2σ uncertainties were so large as to render the calculated isochron "ages" statistically questionable, those isochron "ages" have been listed in italics. In one instance, the Cardenas Basalt, the large uncertainty in the Pb-Pb isochron "age" is probably due to the small sample set for which Pb-Pb isotope data is available. Otherwise, for several of the targeted rock units there was either not enough spread in the Sm-Nd isotope data to produce a valid isochron and isochron "age," or there was simply too much scatter in the data. This has already been noted above to also be the case with the K-Ar isotope data for some of the targeted Precambrian rock units.

Some of the data have already been published with full details, including isochron diagrams. The Mt. Ngauruhoe andesites have been discussed in detail by *Snelling* [1998, 2003a], the Somerset Dam layered mafic intrusion by *Snelling* [2003b], the Cardenas Basalt by *Austin and Snelling* [1998], the Bass Rapids diabase sill by *Snelling et al*. [2003] and *Austin* [2005], and the Beartooth andesitic amphibolite in *Austin* [2005]. The relevant isochron diagrams for the Brahma amphibolites are presented here in Figures 1, 2, and 3, while the isochron diagrams for the Elves Chasm Granodiorite are in Figures 4, 5, and 6. Many of the isochron "ages" listed in Table 2 are tightly constrained with large numbers of data points (samples) and excellent statistics. The isochrons for the Brahma amphibolites shown in Figures 1, 2, and 3 are excellent examples of this, with the Rb-Sr isochron defined by nineteen samples, the Sm-Nd isochron constrained by twenty-one samples, and the Pb-Pb isochron constrained by twenty samples (out of the twenty-seven analyzed). In each case the assigned analytical errors are low and yet the statistics are excellent because the observed scatter matches these low assigned analytical errors when the MSWD equals unity. The excellent statistics for these isochrons, coupled with the wide spread of the data points, yield isochron "ages" with low 2σ uncertainties. Table 2 also shows that for the Brahma amphibolites, if more samples

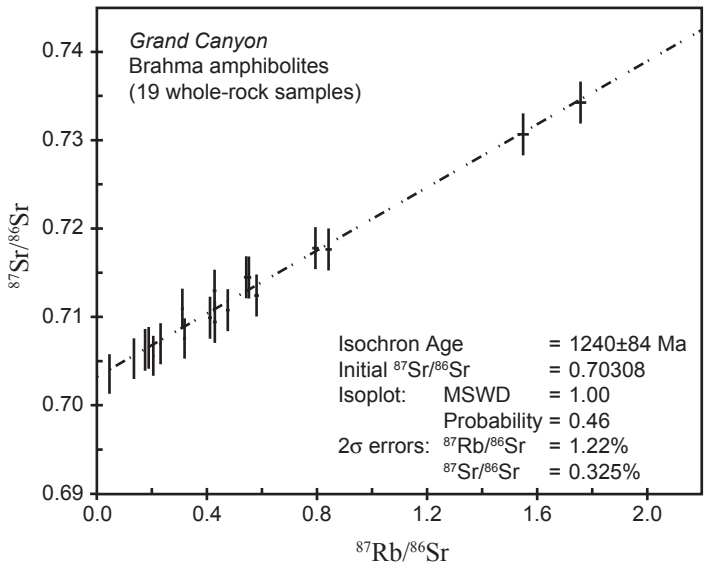

Figure 1. $^{87}Rb/^{86}Sr$ versus $^{87}Sr/^{86}Sr$ isochron diagram for the Brahma amphibolites in Grand Canyon. Nineteen of the twenty-seven whole-rock samples were used in the isochron and "age" calculations. The bars represent the 2σ uncertainties.

were included in the *Isoplot* analyses of the data, both the Sm-Nd and Pb-Pb isochron "ages" would essentially be the same apart from higher 2σ uncertainties, whereas the Rb-Sr isochron "age" would be significantly lower. Nevertheless, these three isochron "ages" for the Brahma amphibolites are very discordant. Indeed, most of the isochron "ages" listed in Table 2, when they are statistically valid, are discordant with one another for those rock units.

5.3 Sr-Nd-Pb Isotope Geochemistry

The Sr-Nd-Pb isotope geochemistry data obtained for the targeted rock units in this study are summarized in Table 3 and plotted on the respective isotope correlation diagrams in Figures 7–10. In these isotope correlation diagrams, where the isotope ratios of some of these samples plot beyond the margins of the diagrams, arrows point from the margins of the diagrams with the relevant sample symbols to indicate in which

direction those data points plot. The mantle isotopic reservoirs plotted in Figures 7–10 have been defined primarily by the isotope ratios in countless thousands of samples of modern and recent oceanic basalts, while the regions of lower and upper continental crust Pb-Pb isotope values plotted on Figure 10 are well established from isotope analyses of many crustal rocks.

Only two of the rock units in this study plotted in or near these mantle isotopic reservoirs. The gabbros of the Somerset Dam layered mafic intrusion plotted in the HIMU field in Figure 7, in the MORB field in Figure 8, almost in the PREMA field in Figure 9, and on the edge of the MORB field in Figure 10, thus indicating that the magma for this intrusion was derived from the upper mantle without crustal contamination during its passage and intrusion into the upper crust. As a group the Mt. Ngauruhoe andesite samples plot together but outside the fields of these mantle isotopic reservoirs, which suggests that if

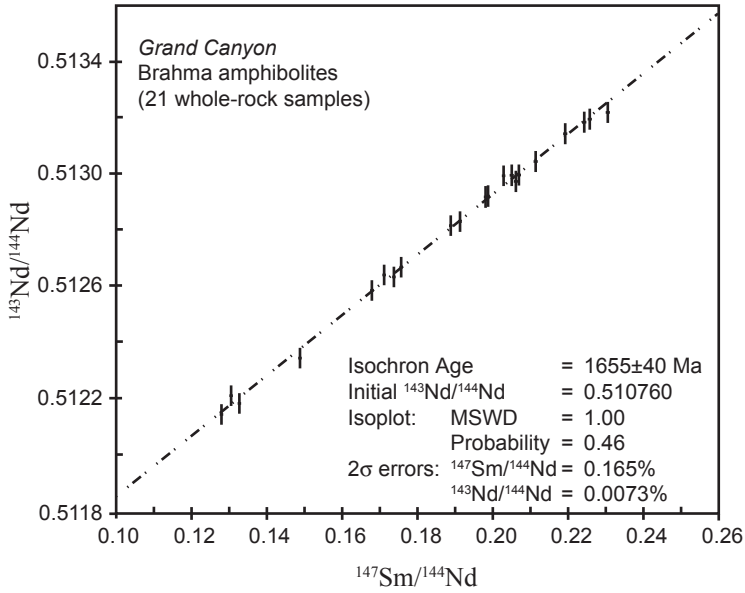

Figure 2. $^{147}Sm/^{144}Nd$ versus $^{143}Nd/^{144}Nd$ isochron diagram for the Brahma amphibolites in Grand Canyon. Twenty-one of the twenty-seven whole-rock samples were used in the isochron and "age" calculations. The bars represent the 2σ uncertainties.

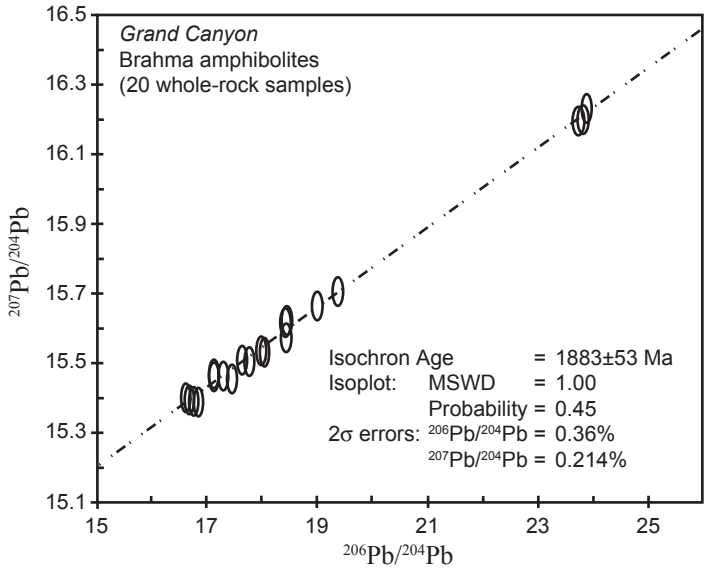

Figure 3. $^{206}Pb/^{204}Pb$ versus $^{207}Pb/^{204}Pb$ isochron diagram for the Brahma amphibolites in Grand Canyon. Twenty of the twenty-seven whole-rock samples were used in the isochron and "age" calculations. The ellipses represent the 2σ uncertainties.

this magma was sourced in the mantle, from where it would have been basaltic in composition, it was subsequently contaminated to produce its final andesitic composition. Otherwise, the samples from all of the other targeted rock units are scattered across these diagrams, though for some of the rock units some of these samples plot in and near the mantle array, suggesting a mantle component in their original magmas. This is even the case with the Elves Chasm Granodiorite, which would usually be regarded as being derived totally from magma sourced only in the lower crust. Furthermore, there appears to be a pattern to this scatter of the sample points plotted on these isotope correlation diagrams towards higher Sr isotope ratios in Figures 7–9, and towards higher Pb-Pb isotope ratios in Figure 10. The trend towards higher Sr isotope ratios, away from the mantle isotopic reservoirs, would appear to indicate significant crustal contamination in many of the rock units analyzed, while the strongly linear trend in the Pb-Pb isotope ratios in Figure 10 would appear to correlate with the respective Pb-Pb

isochrons for some of these rock units. Thus it is abundantly clear from the data plotted in these isotope correlation diagrams that for those rock units whose magmas were sourced in the mantle they have inherited at least some of their isotope compositions from those mantle sources, while there has been some crustal contamination of these radioisotope systems, particularly the Rb-Sr radioisotope system, during the passage and intrusion of these magmas into the upper crust or onto the earth's surface.

6. Discussion

6.1 K-Ar Dating, Model Ages, and Excess $^{40}Ar^*$

The K-Ar model "ages" of up to 3.5 Ma obtained for the recent andesite lava flows at Mt. Ngauruhoe in New Zealand (Table 1) clearly indicate that excess $^{40}Ar^*$ was present in those lavas when they erupted because

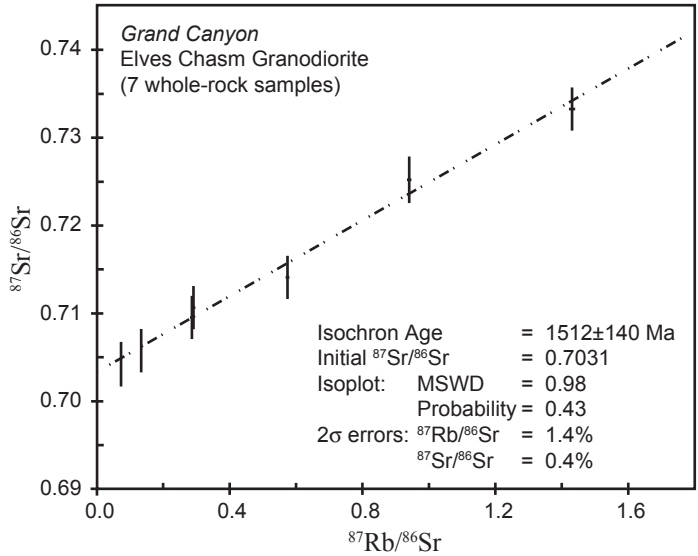

Figure 4. $^{87}Rb/^{86}Sr$ versus $^{87}Sr/^{86}Sr$ isochron diagram for the Elves Chasm Granodiorite in Grand Canyon. Seven of the eight whole-rock samples were used in the isochron and "age" calculations. The bars represent the 2σ uncertainties.

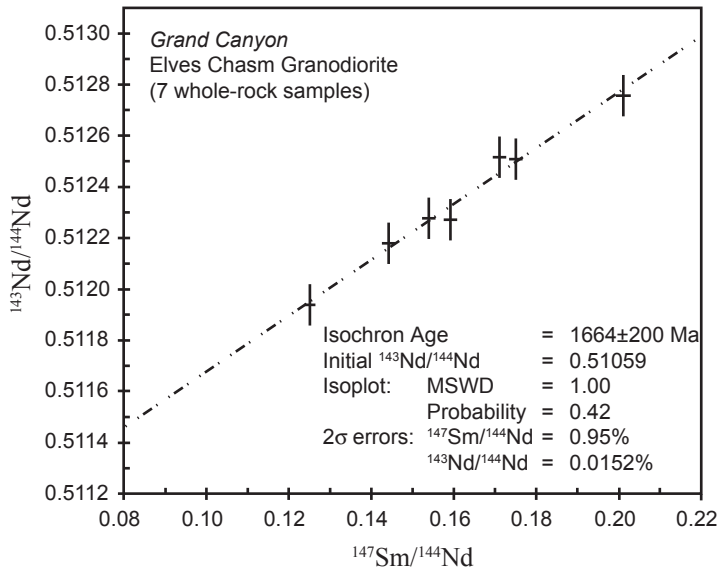

Figure 5. $^{147}Sm/^{144}Nd$ versus $^{143}Nd/^{144}Nd$ isochron diagram for the Elves Chasm Granodiorite in Grand Canyon. Seven of the eight whole-rock samples were used in the isochron and "age" calculations. The bars represent the 2σ uncertainties.

of being inherited from the mantle source of the magma [*Snelling*, 1998], and possibly also from the small component of crustal contamination [*Snelling*, 2003a]. Similarly, *Austin* [1996] found excess $^{40}Ar^*$ in dacite lava less than 10 years old at Mount St. Helens in Washington state, U.S.A. Furthermore, *Austin* [1996] found that the ferromagnesium mineral phases (amphibole and pyroxene) within that Mount St. Helens dacite yielded even larger anomalous K-Ar model "ages" than the whole rock, because the excess $^{40}Ar^*$ contained in them was supported by lower concentrations of parent ^{40}K. Similarly, when the minerals in the basalt of the Toroweap Dam in the western Grand Canyon were separated and analyzed, they yielded excessively older K-Ar model ages than the whole rock, especially the olivine with its low ^{40}K content ([*Rugg and Austin*, 1998] and Table 1). This is confirmed by the sample of the Massive Diabase Dam basalt, in which the excess $^{40}Ar^*$ in the

olivine yielded an extraordinarily old K-Ar model "age" (Table 1). This problem of excess $^{40}Ar^*$ being recognized and thus yielding anomalous old K-Ar model "ages" for historic, recent, and young volcanic rocks has now been widely documented, and has been extensively discussed by *Snelling* [1998, 2000a].

However, this begs the question: if excess $^{40}Ar^*$ is so well recognized and documented in historic, recent, and young volcanic rocks due to mantle inheritance and crustal contamination, then could excess $^{40}Ar^*$ likewise be present in ancient volcanic rocks, thus also producing anomalously old K-Ar model "ages" for them? This possibility, though, is easily dealt with by investigating the ancient rock units' K-Ar isochron diagrams, because if there is excess $^{40}Ar^*$ in them the isochrons will intercept the $^{40}Ar^*$ axes at positive $^{40}Ar^*$ values where the ^{40}K is zero. In this study only three of the ancient rock units studied yielded statistically

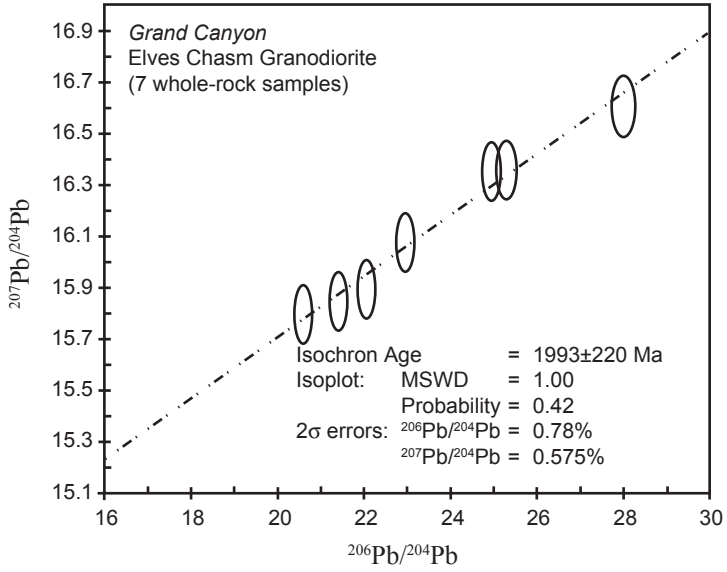

Figure 6. $^{206}Pb/^{204}Pb$ versus $^{207}Pb/^{204}Pb$ isochron diagram for the Elves Chasm Granodiorite in Grand Canyon. Seven of the eight whole-rock samples were used in the isochron and "age" calculations. The ellipses represent the 2σ uncertainties.

Table 3. Sr-Nd-Pb isotope geochemistry data obtained for the targeted rock units.

Rock Unit	Location	Conventional Age	Method	Number of Samples	Range of Isotope Ratios			
					$^{87}Sr/^{86}Sr$	$^{143}Nd^{144}Nd$	$^{206}Pb/^{204}Pb$	$^{207}Pb/^{204}Pb$
Mt. Ngauruhoe andesites	Mt. Ngauruhoe, New Zealand	Historic flows (1949, 1954, 1975)	Direct observation	11 whole rocks (from 5 flows)	0.705153 (min) 0.705660 (max)	0.512704 (min) 0.512778 (max)	18.797 (min) 18.842 (max)	15.620 (min) 15.637 (max)
Uinkaret Plateau basalts	Western Grand Canyon, Arizona	<1.16±0.18 Ma	K-Ar model	8 (whole rocks)	0.703749 (min) 0.707222 (max)	0.512494 (min) 0.512751 (max)	Not available	Not available
Somerset Dam layered mafic intrusion	Somerset Dam, southeast Queensland, Australia	216±4 Ma 225.3±2.3 Ma	K-Ar model composite Rb-Sr isochron	15 (whole rocks)	0.702740 (min) 0.703138 (max)	0.512902 (min) 0.512990 (max)	18.393 (min) 18.861 (max)	15.562 (min) 15.702 (max)
Cardenas Basalt	Eastern Grand Canyon, Arizona	1103±66 Ma	Rb-Sr isochron	15 (whole rocks)	0.71270 (min) 1.72104 (max)	0.512187 (min) 0.512611 (max)	19.017 (min) 20.110 (max)	15.613 (min) 15.712 (max)
Cardenas related diabase sills	Grand Canyon, Arizona	1070±30 Ma	Rb-Sr isochron	18 (whole rocks)	0.704502 (min) 0.83703 (max)	0.511992 (min) 0.512700 (max)	17.255 (min) 25.432 (max)	15.452 (min) 16.135 (max)
Apache Group basalts	Central Arizona	1100 Ma	Assumed similar to diabase sills	9 (whole rocks)	0.709802 (min) 0.835571 (max)	0.512363 (min) 0.512707 (max)	17.634 (min) 23.071 (max)	15.455 (min) 15.971 (max)
Apache Group diabase sills	Central Arizona	1120±10 Ma 1140±40 Ma	zircon U-Pb biotite K-Ar	21 (whole rocks)	0.704807 (min) 0.75208 (max)	0.512155 (min) 0.512565 (max)	16.290 (min) 35.764 (max)	14.439 (min) 16.927 (max)
Brahma amphibolites	Grand Canyon, Arizona	1740-1750 Ma	zircon U-Pb concordia	27 (whole rocks)	0.703565 (min) 0.757016 (max)	0.512118 (min) 0.513242 (max)	16.696 (min) 25.473 (max)	15.384 (min) 16.318 (max)
Elves Chasm Granodiorite	Grand Canyon, Arizona	1840±1 Ma	zircon U-Pb	8 (whole rocks)	0.704174 (min) 0.73335 (max)	0.511938 (min) 0.512758 (max)	20.583 (min) 33.178 (max)	15.800 (min) 16.607 (max)
Beartooth andesitic amphibolite	Northeast Wyoming	2790±35 Ma	Rb-Sr isochron	1 whole rock+ 5 minerals	0.70525 (titanite) 0.70988 (whole rock) 0.81352 (biotite)	0.509852 (biotite) 0.510492 (whole rock) 0.511381 (titanite)	14.455 (quartz-plag.) 16.306 (whole rock) 165.587 (titanite)	15.007 (quartz-plag.) 15.333 (whole rock) 42.666 (titanite)

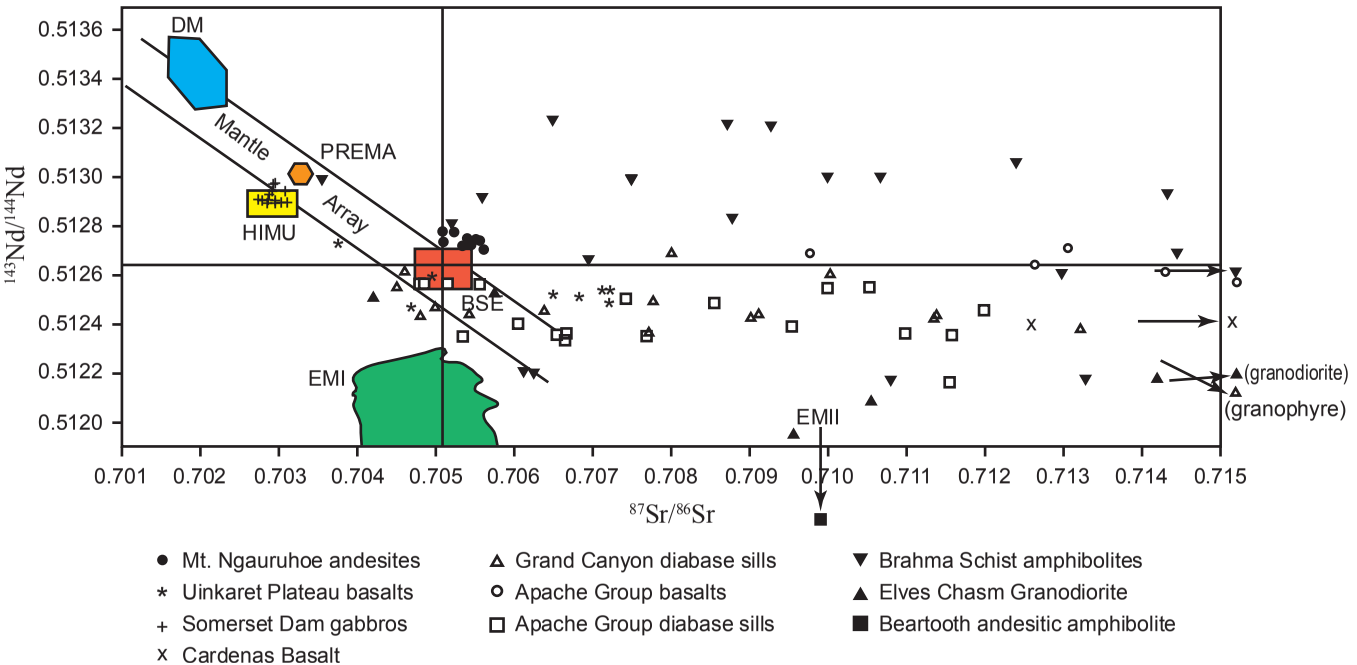

Figure 7. The $^{87}Sr/^{86}Sr$ versus $^{143}Nd/^{144}Nd$ isotope correlation diagram showing the main oceanic mantle reservoirs of *Zindler and Hart* [1986]: DM = depleted mantle; BSE = bulk silicate earth; EMI and EMII = enriched mantle; HIMU = mantle with high U/Pb ratio; PREMA = frequently observed PREvalent MAntle composition. The mantle array is defined by many oceanic basalts, and a bulk silicate earth value for $^{87}Sr/^{86}Sr$ can be obtained from this trend. The whole-rock isotope data for the samples from the rock units in this study are variously plotted and labeled on the diagram.

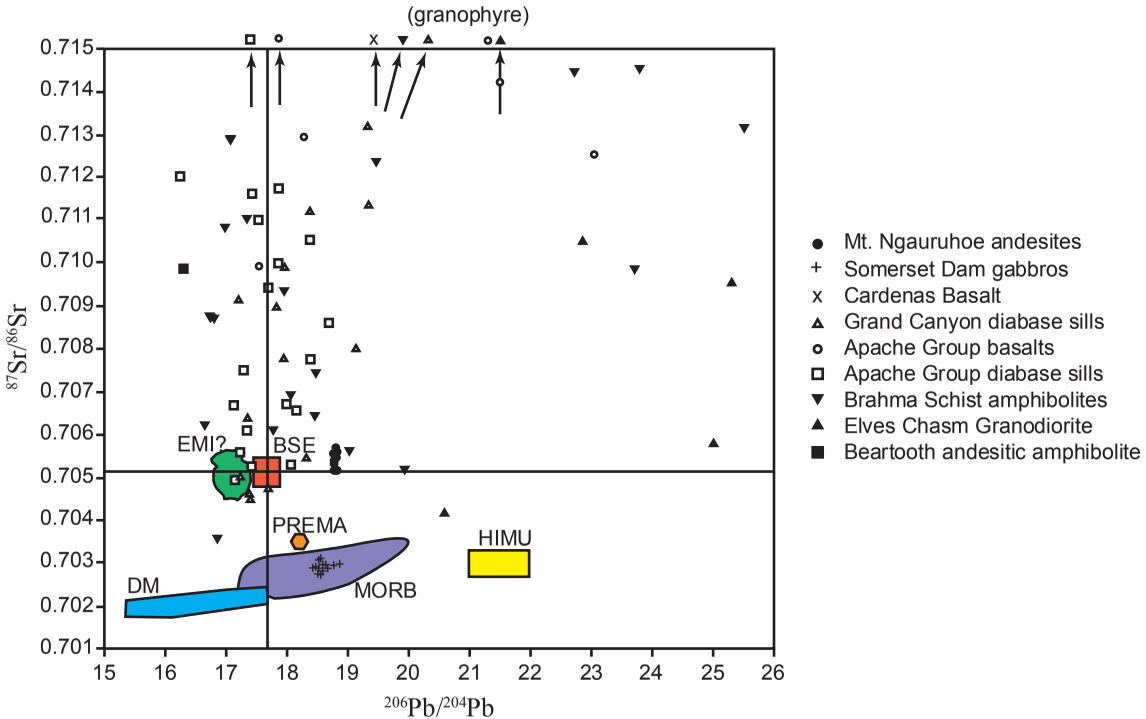

Figure 8. The $^{206}Pb/^{204}Pb$ versus $^{87}Sr/^{86}Sr$ isotope correlation diagram showing the positions of the mantle reservoirs identified by *Zindler and Hart* [1986]: DM = depleted mantle; BSE = bulk silicate earth; EMI and EMII = enriched mantle; HIMU = mantle with high U/Pb ratio; PREMA = frequently observed PREvalent MAntle composition. The $^{206}Pb/^{204}Pb$ value of the bulk silicate earth is taken from *Allègre et al.* [1988]. The whole-rock isotope data for the samples from the rock units in this study are variously plotted and labeled on the diagram.

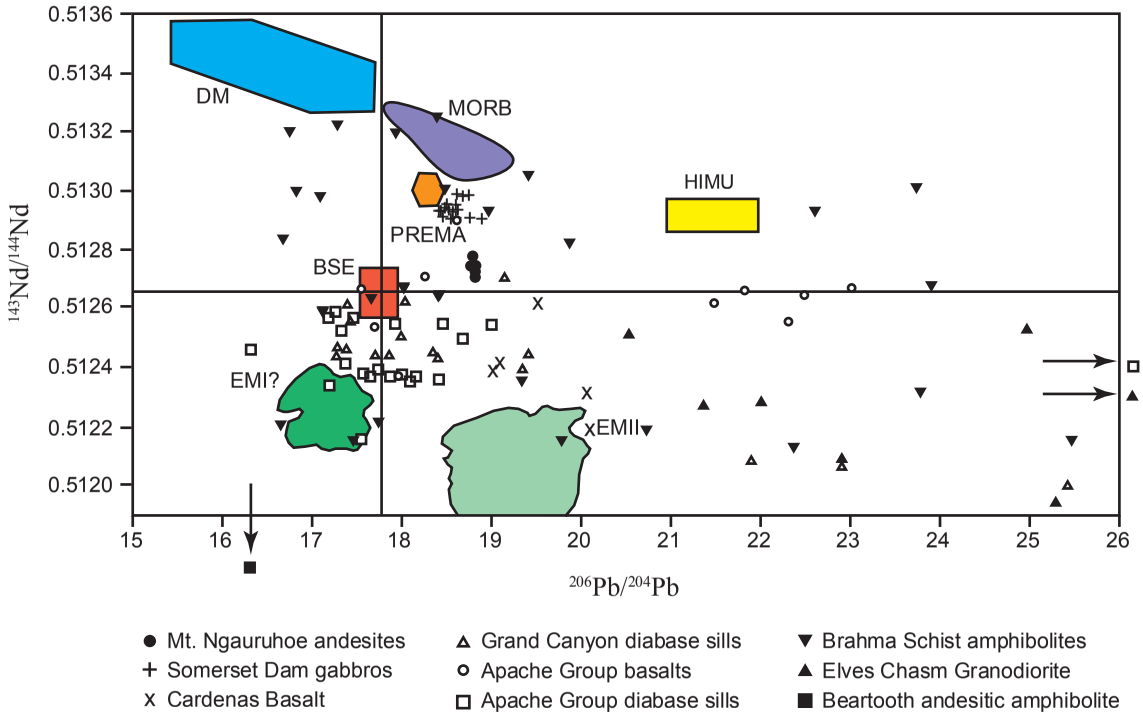

Figure 9. The $^{206}Pb/^{204}Pb$ versus $^{143}Nd/^{144}Nd$ isotope correlation diagram showing the positions of the mantle reservoirs identified by *Zindler and Hart* (1986): DM = depleted mantle; BSE = bulk silicate earth; EMI and EMII = enriched mantle; HIMU = mantle with high U/Pb ratio; PREMA = frequently observed PREvalent MAntle composition. The $^{206}Pb/^{204}Pb$ value of the bulk silicate earth is taken from *Allègre et al.* [1988]. The whole-rock isotope data for the samples from the rock units in this study are variously plotted and labeled on the diagram.

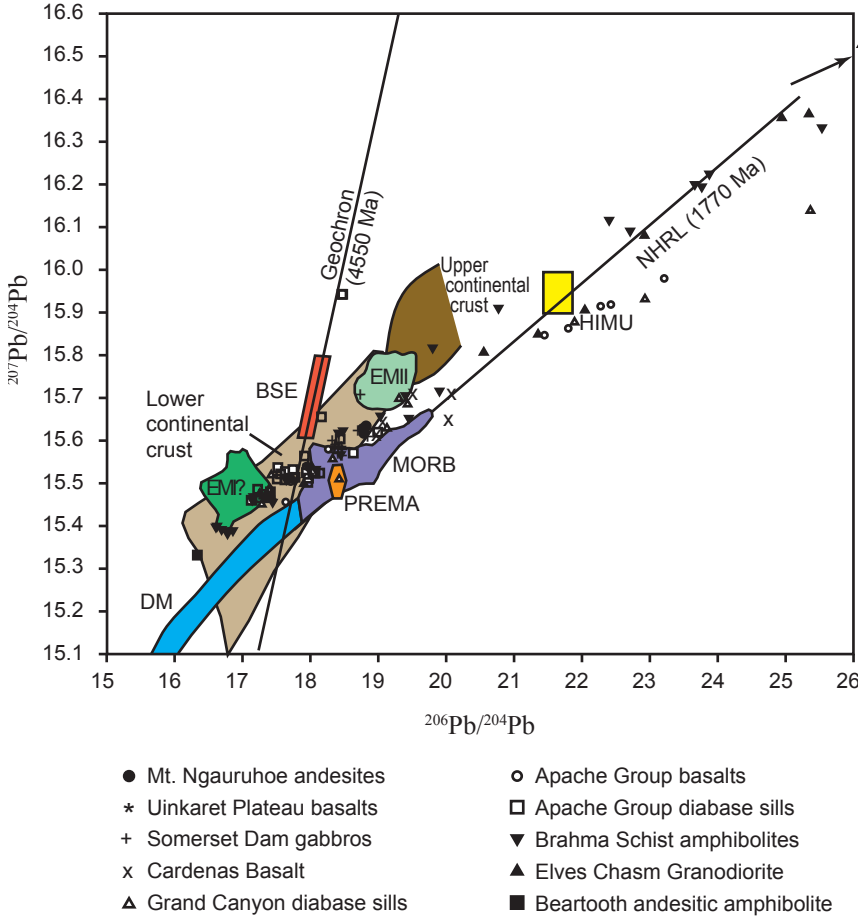

Figure 10. The $^{206}Pb/^{204}Pb$ versus $^{207}Pb/^{204}Pb$ isotope correlation diagram showing the position of the northern hemisphere reference line (NHRL), the slope of which has an age significance of 1770 Ma, and the geochron (4550 Ma). The mantle reservoirs of *Zindler and Hart* [1986] are: DM = depleted mantle; BSE = bulk silicate earth; EMI and EMII = enriched mantle; HIMU = mantle with high U/Pb ratio; PREMA = frequently observed PREvalent MAntle composition. The fields of the upper and lower continental crust, and of MORB (mid-ocean ridge basalts), are shown. The bulk silicate earth value is from *Allègre et al.* [1988]. The whole-rock isotope data for the samples from the rock units in this study are variously plotted and labeled on the diagram.

valid K-Ar isochrons (Table 1). In the K-Ar isochron diagrams for these three rock units, the isochron for the Bass Rapids diabase sill [*Snelling et al*., 2003; *Austin*, 2005] intersected at the origin of both the ^{40}K and ^{40}Ar* axes, indicating no excess ^{40}Ar*, whereas the isochrons for the Somerset Dam layered mafic intrusion [*Snelling*, 2003b] and for the Cardenas Basalt [*Austin and Snelling*, 1998] both intersected the ^{40}Ar* axis very close to the origin of the ^{40}K axis, consistent with negligible excess ^{40}Ar* being in these rock units, certainly not enough to account for the radioisotope "ages."

However, *Snelling* [2000a] reported much evidence of the mobility of ^{40}Ar* in crustal rocks, resulting in some instances of ^{40}Ar* loss from some rock units and some minerals within rock units, and excess ^{40}Ar* in other rock units and minerals. Thus, even if a magma inherited excess ^{40}Ar* from its mantle source, and from crustal contamination during its ascent and intrusion into the upper crust or extrusion onto the earth's surface, once intruded or extruded the fact that Ar is an inert gas which does not chemically bond within the crystal lattices of minerals means that it would be free to migrate through rock units. Thus ^{40}Ar* could be lost from some rock units to surrounding rock units or the atmosphere, while in other rock units excess ^{40}Ar* would accumulate. Indeed, because of the mobility of the Ar gas, even within single rock units there could be areas and minerals whose ^{40}Ar* content has been depleted and other nearby areas and minerals where excess ^{40}Ar* has accumulated. This explanation might well account for the wide variations in the individual sample K-Ar model "ages" for each of the ancient rock units reported in Table 1. Of course, the different samples in any one of these rock units contain different quantities of K and therefore ^{40}K (sometimes vastly different quantities). Nevertheless, all samples from the same rock unit are supposed to be the same "age," and no matter what their ^{40}K concentrations are, the constant rate of ^{40}K decay should have yielded the same proportional quantities of ^{40}Ar*, so that all samples would give the same model "ages." Thus the wide ranges of K-Ar model "ages" recorded for these rock units must be due to some other cause, so the mobility of ^{40}Ar* would seem a likely explanation.

For example, samples of the Brahma amphibolites in Grand Canyon yielded an enormously wide range of K-Ar model "ages," from 405.1±10 Ma to 2574.2±73 Ma, for a rock unit that is supposed to be 1740–1750 Ma. Even samples only 0.84 m apart in the same outcrop yielded K-Ar model "ages" of 1205.3±31 Ma and 2574.2±73 Ma. These differences could be explained easily by ^{40}Ar* loss from one part of the outcrop and accumulation of excess ^{40}Ar* in the other part of the same outcrop. This would also explain why there is too much scatter in the K-Ar isotope data for this rock unit to produce a viable isochron and a statistically valid isochron "age" for it. Interestingly, for the three rock units in this study where valid K-Ar isochron ages were obtained (Tables 1 and 2), the isochron for the Bass Rapids diabase sill intersected the origin of the isochron diagram thus indicating no excess ^{40}Ar*, and the resultant K-Ar isochron age is mid-way within the range of K-Ar model "ages" for the individual samples. In comparison, the isochrons for the Somerset Dam layered mafic intrusion and Cardenas Basalt intersected the ^{40}Ar* axes above the origin in their respective isochron diagrams indicating very small quantities of excess ^{40}Ar*, and in both instances the resulting isochron "ages" were less than the youngest K-Ar model "ages" in the ranges of model "ages" for the individual samples. In other words, the excess ^{40}Ar* made the individual sample K-Ar model "ages" appear older than they should be. Thus this disparity between excessively wide ranges of K-Ar model "ages" and the corresponding K-Ar isochron "ages" where they can be validly obtained, plus the uncertainty over ^{40}Ar* mobility and the role of excess ^{40}Ar*, casts some doubt over the reliability of K-Ar radioisotope dating.

6.2 Isochron Dating and the Discordance Pattern

Because of the much longer half-lives of the parent ^{238}U, ^{87}Rb, and ^{147}Sm isotopes, compared to that of the parent ^{40}K isotope, it is not usually expected that young intrusive and volcanic rocks will yield valid Rb-Sr, Pb-Pb, and Sm-Nd isochron "ages." The isochron "ages" obtained for the targeted rock units in this study (Table 2) confirm this. Only by the judicious selection of the most suitable data from

the recent Mt. Ngauruhoe andesite lava flows could a seemingly valid Rb-Sr isochron "age" of 133±87 Ma be obtained [*Snelling*, 2003a]. However, by comparison, the young Uinkaret Plateau basalts of the western Grand Canyon yielded a valid Rb-Sr isochron "age" of 1143±220 Ma. *Leeman* [1974] recognized that the $^{87}Sr/^{86}Sr$ ratios found in these basalts probably reflected their mantle origin. After *Sun and Hansen* [1975] found that the Rb-Sr data for fourteen different ocean island basalts when plotted on a isochron diagram yielded a positive correlation with a slope "age" of approximately 2000 Ma, *Brooks et al.* [1976a] called such "ages" "mantle isochrons." This mantle isochron concept was then extended to continental igneous rocks by *Brooks et al.* [1976b], who argued that these pseudo-isochrons were not mixing lines produced by crustal contamination of mantle-derived mafic magmas, but instead "dated" mantle differentiation events which had established domains of different Rb/Sr isotope ratios in the heterogeneous mantle sources of the magmas. Of course, a fundamental assumption of this mantle isochron model is that neither isotope nor elemental ratios are perturbed during magma ascent through the crust, an assumption that is now generally accepted as not being upheld with sufficient reliability to attribute age significance to such "erupted isochrons" [*Dickin*, 1995]. Nevertheless, *Leeman* [1982] and *Fitton et al.* [1988] have demonstrated conclusively that both the $^{87}Sr/^{86}Sr$ and $^{143}Nd/^{144}Nd$ isotope ratios in these western Grand Canyon basalts reflect the mantle source of their magma, compositional trends not being compatible with bulk crustal contamination but due to a heterogeneous mantle source. This is further confirmed by the Pb-Pb isotope data for these same basalts [*Alibert and Albarède*, 1986; *Austin*, 1994]. Thus the Rb-Sr isochron with its apparent 1143±220 Ma "age" obtained for these young basalts in the western Grand Canyon support the conclusion of *Zheng* [1989] that it is impossible to distinguish a valid isochron from an apparent isochron in the light of Rb-Sr isotope data alone, as an observed isochron does not necessarily define valid age information for a geological system, even if there is a good fit to the plotted data points.

However, it is certain that much radioactive decay has occurred throughout the earth's history, physical evidence for which is provided

by ^{238}U radiohalos [*Snelling*, 2000b, 2005a; *Snelling and Armitage*, 2003; *Snelling et al*., 2003b] and fission tracks [*Snelling*, 2005b]. This would thus imply that isochron "ages" yielded by ancient volcanic rocks should be due primarily to radioactive decay of parent radioisotopes. This is evident for the ancient intrusive and volcanic rock units targeted in this study whose isochron "ages" are listed in Table 2.

Austin [2005] has discussed the nature of the linear isotope plots for the Bass Rapids diabase sill and the Beartooth andesitic amphibolite. That discussion is equally relevant to the linear isotope plots obtained for the rock units listed in Table 2, and shown for the Somerset Dam layered mafic intrusion in *Snelling* [2003b], for the Cardenas Basalt in *Austin and Snelling* [1998], for the Brahma amphibolites in Figures 1–3, and for the Elves Chasm Granodiorite in Figures 4–6. All these isochron plots reveal an extraordinary linearity within the ^{40}K-^{40}Ar, ^{87}Rb-^{87}Sr, ^{147}Sm-^{143}Nd, and ^{207}Pb-^{206}Pb-^{204}Pb radioisotope systems. Of course, these are the successful isochron plots where the extraordinary linearity has produced statistically valid isochrons and isochron "ages," all the data points plotted following the linear trends within the error bars that represent the uncertainties assigned to each data point to account for analytical errors. As already indicated, the observed scatter in these plots has been fully accounted for by the assigned errors, as measured by the MSWD being at or near unity in each case. Not all attempted isochron plots using the *Isoplot* program [*Ludwig*, 2001] were successful, because as indicated in Table 2, either there was too much observed scatter to be accounted for by assigning reasonable analytical errors, or there was not enough spread in the data points to achieve statistically valid isochrons. This primarily occurred with respect to the ^{40}K-^{40}Ar radioisotope system for the reasons already discussed above. In several other instances the observed scatter was also too large in the Rb-Sr, Sm-Nd, and Pb-Pb radioisotope systems, which suggests that in those instances these radioisotope systems had been perturbed in those rock units by either contamination during their formation, or more likely, by post-formation alteration due to hydrothermal or metamorphic fluids, or groundwater and weathering.

For each of the ancient rock units listed in Table 2 it is clearly evident

that, where the radioisotope data have provided statistically valid and robust isochron "ages," there is disagreement between the different radioisotope systems as to the "ages" of these rock units. This is not so evident for the Somerset Dam layered mafic intrusion which occurs in the Phanerozoic part of the geologic record, but it is strikingly obvious for the other listed ancient rock units that are situated in the Precambrian part of the geologic record. Indeed, in many instances the isochron discordances are pronounced. *Snelling et al*. [2003a] and *Austin* [2005] have discussed explanations for these discordances and have concluded that the only explanation that can account for them is that the radioisotope decay constants have not always been constant. *Austin* [2005] also cited several examples from the geologic literature that similarly report discordant isochron ages for other rock units, most notably for the Great Dyke in Zimbabwe [*Mukasa et al*., 1998; *Oberthür et al*., 2002], for the Stuart dyke swarm of central Australia [*Zhao and McCulloch*, 1993], and the Uruguayan dike swarm in South America [*Teixeira et al*., 1999]. These examples in conjunction with the large number of rock units recorded in this study would strongly suggest that, where two or more of the commonly-used radioisotope pairs are applied to "date" rock units, discordances are the norm.

As already reported by *Austin* [2005], there is a pattern to the isochron discordances. The isochron "ages" listed in Table 2 consistently indicate that the α-emitters (^{238}U, ^{235}U, ^{147}Sm) yield older ages than the β-emitters (^{87}Rb and ^{40}K) when used to date the same geologic event, that is, the formation of each listed rock unit—for example, the extrusion of the Cardenas Basalt lavas, and the intrusion of the Bass Rapids diabase sill and Elves Chasm Granodiorite. In the case of the Brahma amphibolites, none of the listed isochron "ages" "date" the eruption of the original basalt lavas at 1740–1750 Ma. That "date" is based on U-Pb concordia dating of zircon grains in metamorphosed felsic volcanic lavas within the associated Brahma and Rama Schists that are believed to have survived the metamorphism without the U-Pb radioisotope system being reset [*Hawkins et al*., 1996; *Ilg et al*., 1996]. Nor do the isochron "ages" obtained "date" the metamorphism of the original basalt lavas to form the amphibolites, which has been determined as 1690–1710 Ma

based on U-Pb concordia dating of metamorphic monazite, xenotime, and titanite in the overlying Vishnu Schist and underlying Rama Schist [*Hawkins et al*., 1996; *Hawkins and Bowring*, 1999]. Nevertheless, assuming the isochron "ages" listed in Table 2 for each of the rock units are "dating" the same geologic event for each rock unit, then a logical explanation of these data is that the radioisotope decay of the various parent isotopes has not always proceeded at the rates described by the present-day decay "constants." Thus the discordances would instead be due to the different parent radioisotopes decaying at different rates over the same time periods since the geologic events represented by each rock unit. In other words, the decay of these parent radioisotopes was accelerated by different amounts. Thus the data in Table 2 are consistent with the possibility that α-decay was accelerated more than β-decay at some time or times in the past.

The correlation between the present radioactive decay "constants" for these α- and β-emitters and the isochron "ages" they have yielded for the geologic events associated with three of the targeted rock units is illustrated for the Cardenas Basalt in Figure 11, and for the Brahma amphibolites in Figure 12. *Austin* [2005] provides a similar isochron "age" versus mode of decay diagram for the radioisotope systems within the Bass Rapids diabase sill. In each of these examples the α-decaying isotopes (^{238}U and ^{147}Sm) yielded older isochron "ages" than the β-decaying isotopes (^{40}K and ^{87}Rb). Among the β-decaying isotopes, ^{87}Rb has the smaller decay constant and thus the longer half-life, yet it consistently yields the older "ages," double the K-Ar isochron "age" of the Cardenas Basalt in Figure 11. On the other hand, even though ^{147}Sm has the smaller decay constant (and thus the longer half-life) of the α-decaying isotopes, it does not always yield the older isochron "ages." It does for the Cardenas Basalt (Figure 11), for the Bass Rapids diabase sill, and for the Beartooth andesitic amphibolite [*Snelling et al*., 2003a; *Austin*, 2005], but not for the Brahma amphibolites (Figure 12) and the Elves Chasm Granodiorite (Table 2). Perhaps the metamorphism of the original basalt lavas may have reset the Sm-Nd radioisotope system in the resulting Brahma amphibolites but not perturbed the U-Pb radioisotope pairs. Similarly, the Elves Chasm Granodiorite may

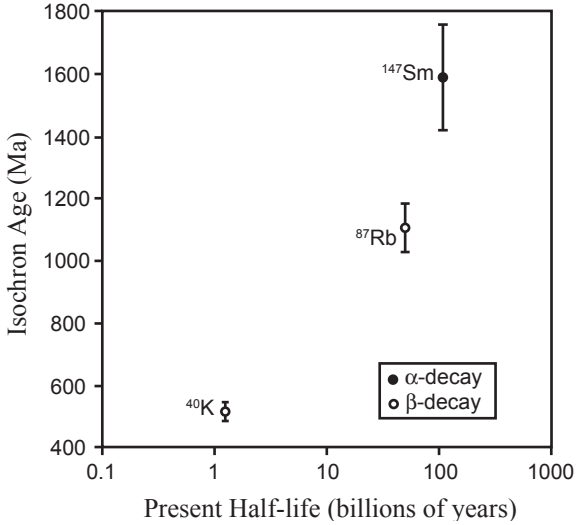

Figure 11. The isochron "ages" yielded by three radioisotope systems for the Cardenas Basalt, Grand Canyon, plotted against the present half-lives of the parent radioisotopes according to their mode of decay.

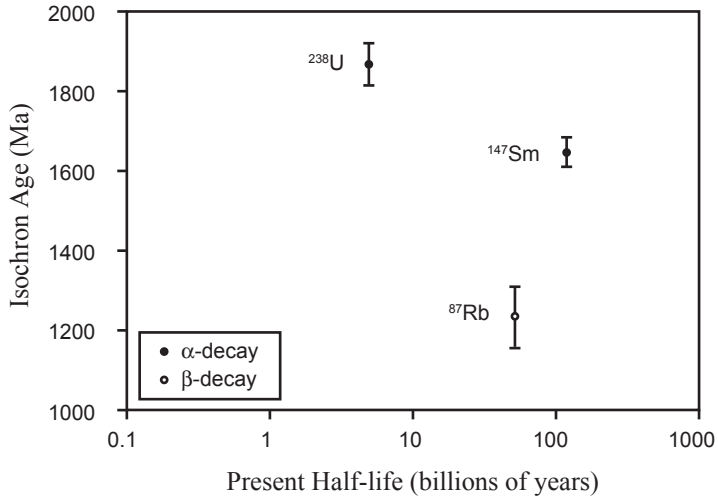

Figure 12. The isochron "ages" yielded by three radioisotope systems for the Brahma amphibolites, Grand Canyon, plotted against the present half-lives of the parent radioisotopes according to their mode of decay.

have suffered late-stage hydrothermal alteration and the subsequent effects of the same metamorphic event that produced the Brahma amphibolites, so again the Sm-Nd radioisotope system may have been perturbed relative to the U-Pb radioisotope pairs. On the other hand, if these isochron "ages" are plotted against the atomic weights of the respective parent isotopes (Figure 13), then there appears to be a trend of older isochron "ages" with increasing atomic weight that would seem to partly resolve this enigma over which α-decaying parent isotope might consistently give the older isochron "ages."

In any case, it is clear that the different radioisotope systems produced discordant isochron "ages" for the same geologic events, suggesting that their decay was accelerated at different rates over the same time periods since those geologic events, the α-decaying parent isotopes being accelerated more than the β-decaying parent isotopes. It is also possible that the longer the half-life of the α- or β-emitter, and/or the heavier its atomic weight, the more its decay has been accelerated relative to the other α- or β-emitters at some time or times in the past. Obviously, the isochron dating method cannot be relied upon to give true absolute "ages."

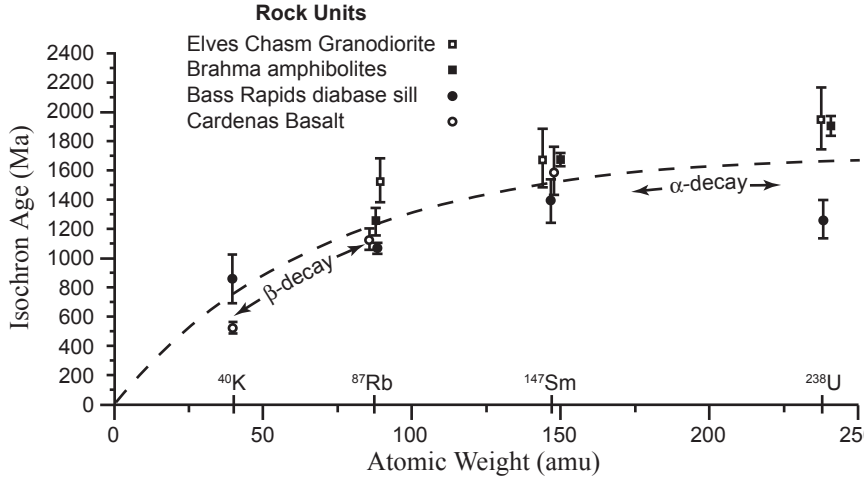

Figure 13. Composite plot of isochron age versus atomic weight for four radioisotope pairs and four Precambrian formations in Grand Canyon from *Austin* [2005] and this study.

6.3 Inheritance and Mixing of Sr, Nd, and Pb Isotopes

As already discussed, there is very clear evidence that modern, historic, and recent volcanic rocks have inherited radioisotope signatures of the mantle sources of the magmas that produced them, and this is now well documented in the geologic literature. For example, radioisotope analyses of the young Uinkaret Plateau basalts of the western Grand Canyon yield Rb-Sr, Sm-Nd, and Pb-Pb isochron "ages" that reflect isotopic heterogeneities inherited by their magma from its mantle source (Table 2) [*Leeman*, 1974, 1982; *Alibert et al*., 1986; *Fitton et al*., 1988; *Austin*, 1994]. This is also true of the historic andesite flows at Mt. Ngauruhoe, New Zealand, although the isochron "ages" in Table 2 were derived by selective manipulation of the data and have large errors due to the statistics of the observed scatter in the data [*Snelling*, 2003a]. Furthermore, these andesite flows yield depleted mantle Nd model "ages" ranging from 724.5 Ma to 1453.3 Ma, and even though their isotope data plot as tight clusters in Figures 7–10, they plot outside the fields of the mantle isotopic reservoirs. This indicates that even though the isotopic signature of these andesite lavas was inherited from the mantle source of what would have been originally a basaltic magma, when crustal contamination modified the mantle composition to produce these andesite lavas their isotopic signature was also modified by the crustal contamination [*Snelling*, 2003a].

Graham et al. [1992] demonstrated on an Sr-Nd isotope correlation diagram how the Ngauruhoe andesites would have been derived from a parent basalt magma sourced in the mantle below, but then contaminated with a small quantity (up to 10%) of the Torlesse metasedimentary strata that underlie the volcano. However, whereas *Graham and Hackett* [1987] and *Graham et al.* [1992] regarded this crustal contamination as thus being a secondary process in which the basalt magma composition was modified by assimilation of crustal rocks *en route* through the crust to the surface, *Gamble et al.* [1996] proposed that the crustal contamination was primary due to a source-modifying process of sediment subduction into the mantle under the volcano. Using combinations of the MORB (mid-ocean ridge basalt)-

source typical for the basalt magmas of the Taupo-Kermadec Volcanic Arc system to which the Ngauruhoe volcano belongs, with sediments typical of the adjacent offshore Kermadec Trench-Hikurangi Trough and with the Torlesse metasediments, *Gamble et al.* [1996] calculated bulk mixing curves based on the isotope pairs $^{206}Pb/^{204}Pb$ versus $^{143}Nd/^{144}Nd$ and $^{87}Sr/^{86}Sr$ (Figure 14). Thus they found that the incorporation of a relatively small amount (around 5%) of New Zealand continental sediment (equivalent to the average Torlesse metasediment [*Graham et al*., 1992]) to basalt magma from a MORB-source could have brought about massive shifts in the isotopic composition of the magma, the sediment-hosted Pb having a "swamping" affect on the "mantle Pb." Therefore, it could be reasonably concluded that the Ngauruhoe andesite lavas have resulted from the contamination of a basalt magma from a MORB-source with around 5% trench sediment consisting of eroded Torlesse basement metasediments subducted into the mantle under the Ngauruhoe volcano. This petrogenetic model favored by *Gamble et al.* [1996] envisages a zone of melt formation approximately below the volcanic front (which includes Mt. Ngauruhoe) in a region delimited by the interface of the subducting slab (of the Pacific Plate) with the mantle wedge under the arc lithosphere of continental New Zealand (Figure 15). Subducted trench sediment scraped from the upper surface of the slab is incorporated into the mantle wedge along the slab-mantle interface. Fluids liberated from the descending slab as it progressively dehydrates ascend into the mantle wedge, causing partial melting of both the mantle peridotite and the subducted sediment being mixed with it. The resulting lower density melt, now andesitic in composition, then rises and pools in an upwelling melt column, to eventually penetrate upwards into the overlying crust to fill magma chambers that then erupt when full.

If isotopic signatures are inherited from mantle sources of magmas and subsequently suffer crustal contamination during ascent and extrusion of modern and recent volcanic rocks, are these effects also evident in the case of ancient volcanic and intrusive rocks and their associated isochron "ages"? As already noted, the Phanerozoic gabbros of the Somerset Dam layered mafic intrusion plot in the isotope correlation diagrams of

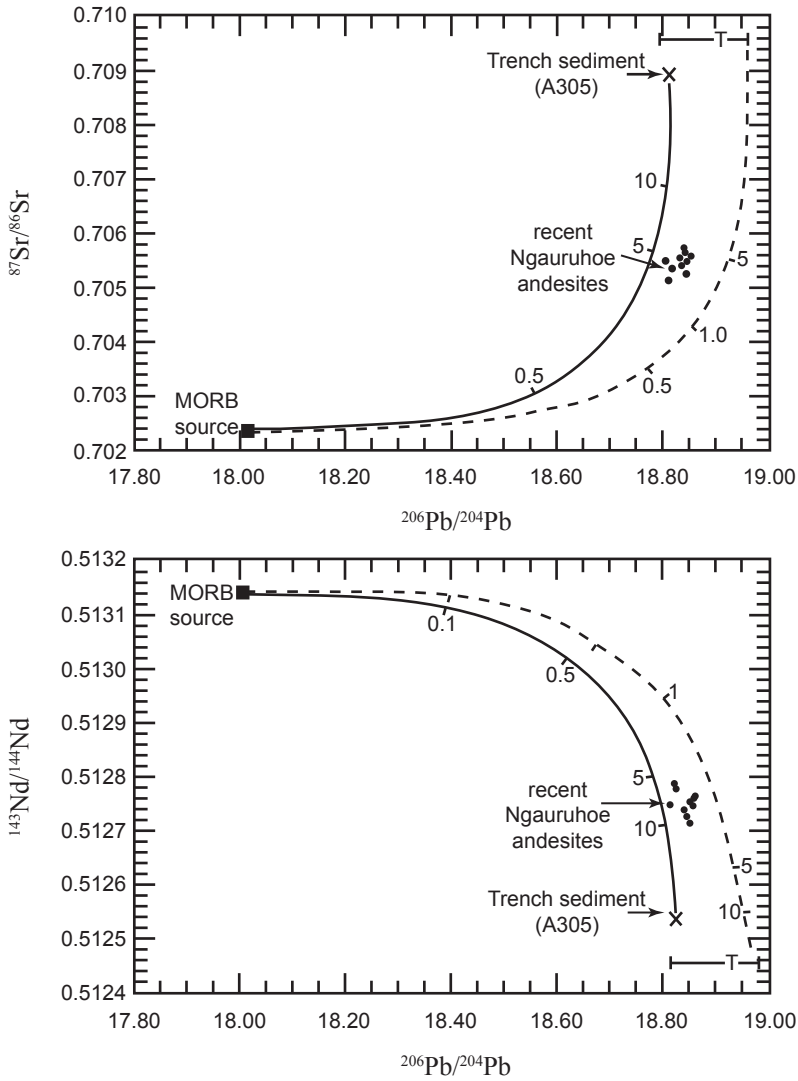

Figure 14. Plots of $^{87}Sr/^{86}Sr$ and $^{143}Nd/^{144}Nd$ versus $^{206}Pb/^{204}Pb$ for the recent Ngauruhoe andesites. Calculated bulk mixing curves for MORB-sediment A305 (continuous line) and MORB-Torlesse basement (dashed line) are shown [*Gamble et al.*, 1996]. T is the average composition of the Torlesse metasediments and the horizontal bar delineates the range of their compositions [*Graham et al.*, 1992]. Tick marks are percent of sediment added to the MORB-source end-member

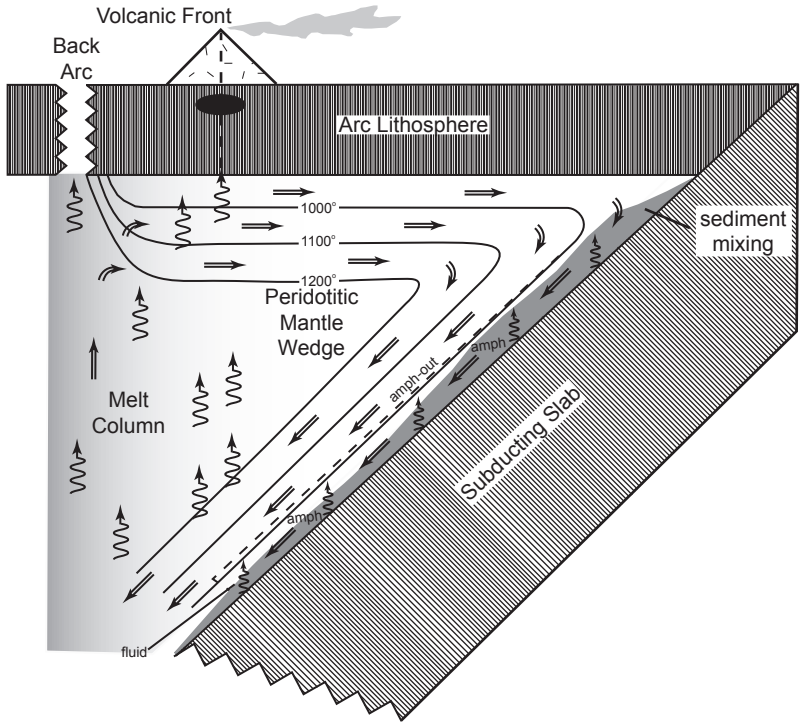

Figure 15. Dynamic petrogenetic model for andesite magma genesis beneath the Kermadec-Taupo Volcanic Arc subduction system [*Tatsumi*, 1986; *Davies and Stevenson*, 1992; *Gamble et al.*, 1996]. Flow lines (arrows with double lines) show mantle flowing from the back-arc region into the mantle wedge, where the isotherms are inverted owing to the cooling effect of the cold subducting "Cretaceous" slab [*Mortimer and Parkinson*, 1996]. Sediment that was deposited on the oceanic crust and thus also subducted is mixed into the wedge assemblage along the interface. Progressive dehydration reactions in the slab lead to fluid transfer from the slab into the mantle wedge. In the juxtaposed wedge, amphibole (amph) is stabilized, but then breaks down over the depth range 112±19 km [*Tatsumi*, 1986], inducing partial melting. In the resulting melt column, the first formed melts accumulating closest to the slab-mantle interface will be most susceptible to fluxing from the slab. Above this zone, melting will continue. The rising melts will eventually pool in the melt column, and the resulting magma finally ascends into the overlying arc lithosphere along fracture conduits, filling magma chambers and triggering eruptions.

Figures 7–10 within, or very close to, the fields of the defined mantle isotopic reservoirs, suggesting that there has been no crustal contamination of the intrusion's magma after having been sourced in the mantle. However, the magma not only inherited the isotopic signature of its mantle source, but also depleted mantle Nd model "ages" ranging from 432.3 Ma to 2923.0 Ma [*Snelling*, 2003b]. The three statistically viable isochron "ages" reported in Table 2 for the Phanerozoic Somerset Dam intrusion are essentially concordant, whereas the isochron "ages" for the Precambrian rock units targeted in this study are discordant, as already noted. Their isotope data plotted in Figures 7–10 are somewhat scattered, largely not coinciding with the fields of the defined mantle isotopic reservoirs. Nevertheless, some trends appear to be apparent in these isotope correlation diagrams. So for ease of visualizing these trends only the isotope ratios for the mafic Precambrian rock units in the Grand Canyon and central Arizona areas are plotted in Figures 16–19, minus the data for the Brahma amphibolites because of the excessive scatter in them, which is probably due to the effects of the metamorphism of the original basalt lavas.

Some obvious trends are evident in the data plotted in Figures 16–19. The effect of the inheritance by the Uinkaret Plateau basalts of the Sr-Nd isotopic signature of their magma's mantle source can be seen in Figure 16 as a linear trend from the field of the mantle array towards increasing $^{87}Sr/^{86}Sr$ ratios. This trend in the $^{87}Sr/^{86}Sr$ ratios obviously coincides with the apparent Rb-Sr isochron defined by the inherited mantle isotopic signature in these Uinkaret Plateau basalts. What is then obvious in Figure 16 is that the data points for the Cardenas Basalt, Grand Canyon diabase sills, Apache Group basalts, and Apache Group diabase sills follow the same poorly defined linear trend as the Uinkaret Plateau basalt data points, except that the Precambrian basalts and diabase sills yield some extremely high $^{87}Sr/^{86}Sr$ isotope ratios. A similar trend towards higher $^{87}Sr/^{86}Sr$ ratios is also evident in Figure 17, while in Figures 18 and 19 the trend is towards higher Pb isotope ratios. Now if the linear trend in the Uinkaret Plateau basalt data in Figure 16 reflects the inherited mantle Rb-Sr isochron whose "age" listed in Table 2 is 1143±220 Ma, then the obvious question is whether the same linear

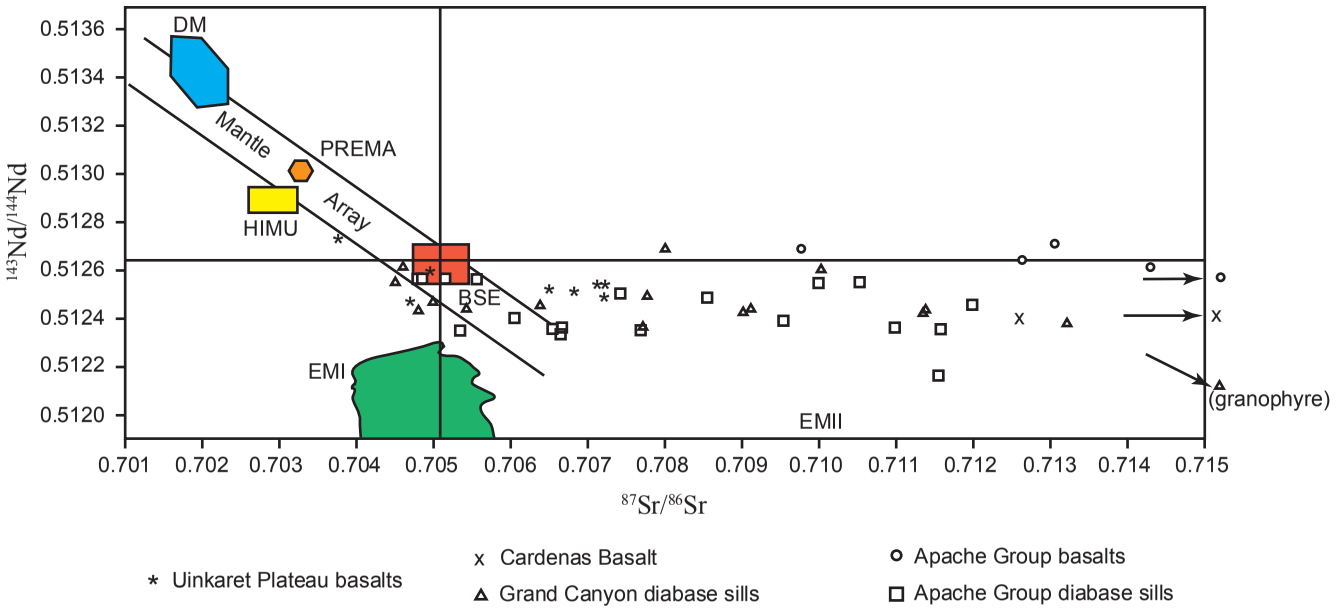

Figure 16. The $^{87}Sr/^{86}Sr$ versus $^{143}Nd/^{144}Nd$ isotope correlation diagram showing the main oceanic mantle reservoirs of *Zindler and Hart* [1986]: DM = depleted mantle; BSE = bulk silicate earth; EMI and EMII = enriched mantle; HIMU = mantle with high U/Pb ratio; PREMA = frequently observed PREvalent MAntle composition. The mantle array is defined by many oceanic basalts, and a bulk silicate earth value for $^{87}Sr/^{86}Sr$ can be obtained from this trend. The whole-rock isotope data for the samples from the selected rock units in this study are variously plotted and labeled on the diagram.

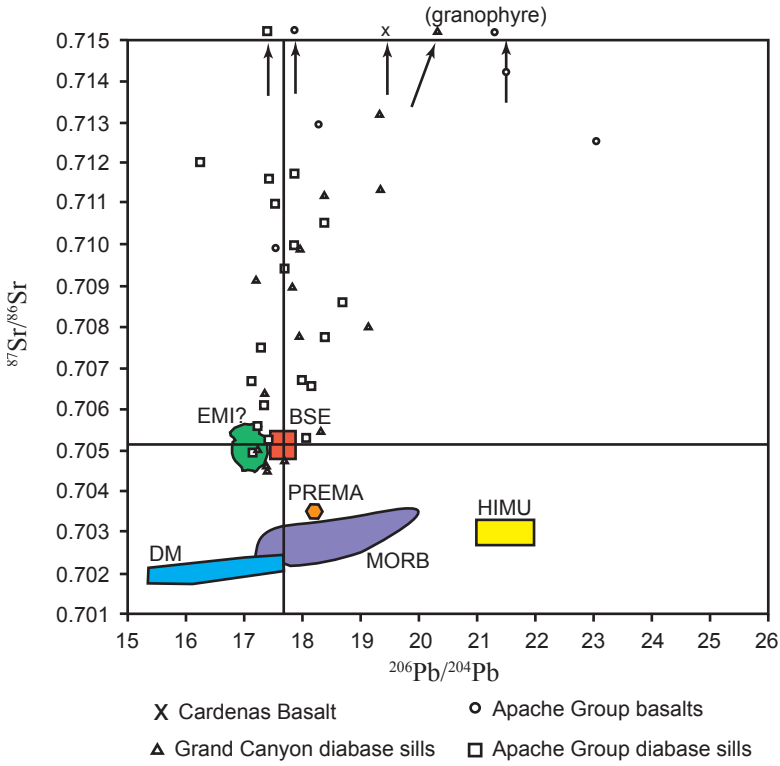

Figure 17. The $^{206}Pb/^{204}Pb$ versus $^{87}Sr/^{86}Sr$ isotope correlation diagram showing the positions of the mantle reservoirs identified by *Zindler and Hart* [1986]: DM = depleted mantle; BSE = bulk silicate earth; EMI and EMII = enriched mantle; HIMU = mantle with high U/Pb ratio; PREMA = frequently observed PREvalent MAntle composition. The $^{206}Pb/^{204}Pb$ value of the bulk silicate earth is taken from *Allègre et al.* [1988]. The whole-rock isotope data for the samples from the selected rock units in this study are variously plotted and labeled on the diagram.

trend in the Precambrian basalts and diabase sills data also reflects their isochron "ages"? Therefore, it is not clear as to whether it is significant that the Rb-Sr isochron "ages" of the Cardenas Basalt (1181±81 Ma [Table 2] or 1103±66 Ma [*Larson et al.*, 1994]) and Bass Rapids diabase sill (1060±24 Ma [Table 2] or 1070±30 Ma [*Elston and McKee*, 1982])

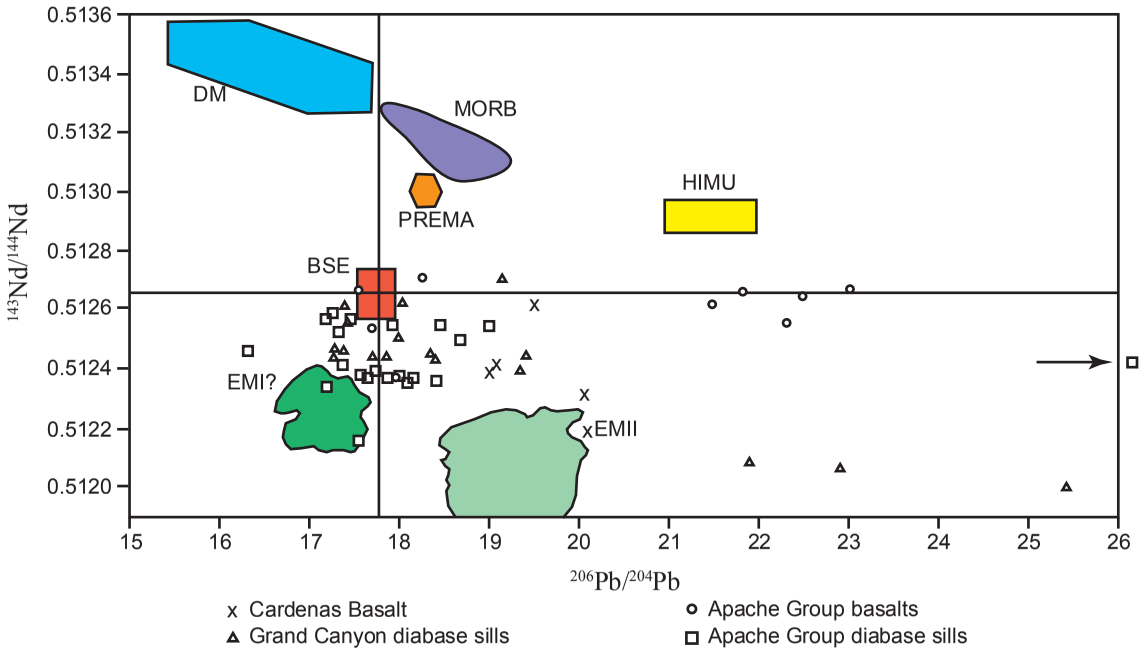

Figure 18. The $^{206}Pb/^{204}Pb$ versus $^{143}Nd/^{144}Nd$ isotope correlation diagram showing the positions of the mantle reservoirs identified by *Zindler and Hart* [1986]: DM = depleted mantle; BSE = bulk silicate earth; EMI and EMII = enriched mantle; HIMU = mantle with high U/Pb ratio; PREMA = frequently observed PREvalent MAntle composition. The $^{206}Pb/^{204}Pb$ value of the bulk silicate earth is taken from *Allègre et al.* [1988]. The whole-rock isotope data for the samples from the selected rock units in this study are variously plotted and labeled on the diagram.

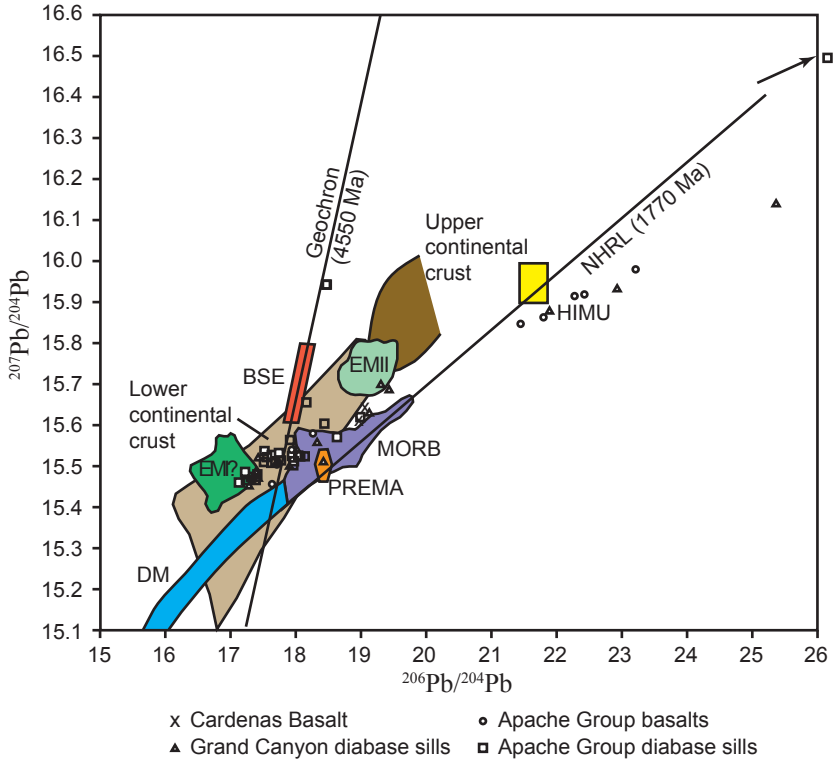

Figure 19. The $^{206}Pb/^{204}Pb$ versus $^{207}Pb/^{204}Pb$ isotope correlation diagram showing the position of the northern hemisphere reference line (NHRL), the slope of which has an age significance of 1770 Ma, and the geochron (4550 Ma). The mantle reservoirs of *Zindler and Hart* [1986] are: DM = depleted mantle; BSE = bulk silicate earth; EMI and EMII = enriched mantle; HIMU = mantle with high U/Pb ratio; PREMA = frequently observed PREvalent MAntle composition. The fields of the upper and lower continental crust, and of MORB (mid-ocean ridge basalts) are shown. The bulk silicate earth value is from *Allègre et al.* [1988]. The whole-rock isotope data for the samples from the selected rock units in this study are variously plotted and labeled on the diagram.

in the eastern and central Grand Canyon are essentially identical with this Rb-Sr mantle isochron "age" for the Uinkaret Plateau basalts in the western Grand Canyon. Given that all these magmas were sourced in the same general area of the mantle beneath the Grand Canyon, it could

be argued that these Rb-Sr isochron "ages" for the Cardenas Basalt and Bass Rapid diabase sill are also the result of their inheritance of the isotopic signature of their magmas' mantle source. On the other hand, the linear trend in the Pb isotope data in Figure 19, which is roughly coincident for these four groups of Precambrian basalts and diabase sills, must reflect their Pb-Pb isochrons, because the isochrons also are all plotted on $^{206}Pb/^{204}Pb$ versus $^{207}Pb/^{204}Pb$ diagrams. This conclusion is confirmed by the agreement between, or concordance of, the Pb-Pb isochron "ages" for these rock units listed in Table 2. But again, given that these magmas were sourced in the same area of the mantle, these Pb-Pb isochron "ages" may also be in some measure the product of the mantle isotopic signature their magmas inherited.

However, the most extreme isotope ratios for the Grand Canyon diabase sills in Figures 16–19 belong to the granophyre layer at the top of the Bass Rapids diabase sill. Because this felsic granophyre is compositionally distinct from the diabase in the body of the sill, it is usually regarded as having separated by in-place differentiation of the parent basaltic magma after intrusion of the sill. But this does not explain how the parent basaltic magma acquired this substantial felsic component, which represents 6–7% of the sill's volume. The granophyre's extremely high isotope ratios, principally $^{87}Sr/^{86}Sr$ and $^{206}Pb/^{204}Pb$, are consistent with the granophyre being derived by crustal contamination of the parent basaltic magma, just as the demonstrated crustal contamination of a basalt magma to produce the Mt. Ngauruhoe andesite lavas is likewise reflected in higher isotope ratios (Figures 7–10). Continental crustal rocks of felsic composition typically have higher isotope ratios, and this includes sedimentary and metamorphosed sedimentary rocks such as those intruded by the Bass Rapids diabase sill. Figure 20 is the diagrammatic section through the Bass Rapids sill showing the granophyre capping on the diabase and the contact hornfels above and beneath the sill. Selected whole-rock geochemical and isotope data are shown beside the respective samples of the diabase and granophyre, plus two samples from the contact hornfels beneath the sill. It is immediately apparent that the high $^{87}Sr/^{86}Sr$ and $^{206}Pb/^{204}Pb$ ratios present in the granophyre are matched by similar

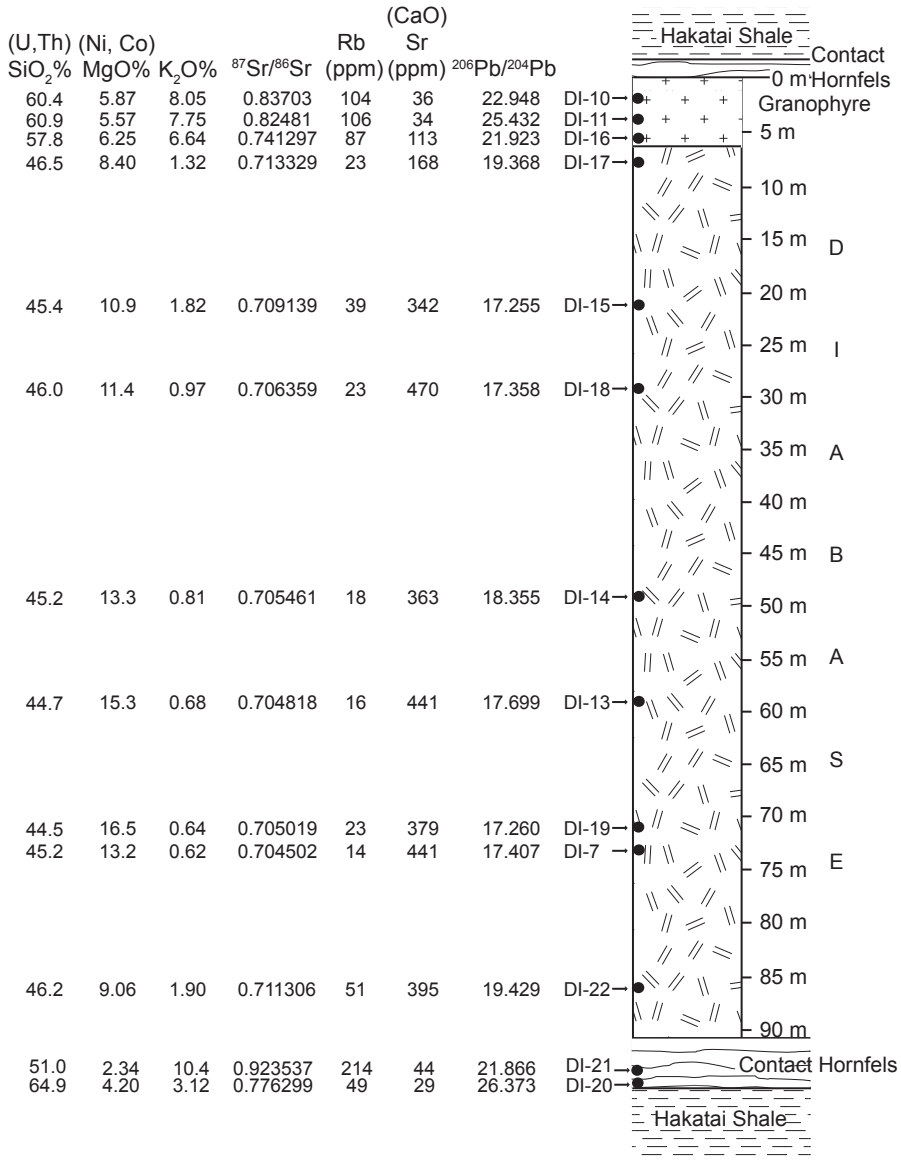

Figure 20. Diagrammatic section through the Bass Rapids sill showing the granophyre "capping" on the diabase, the contact hornfels, the location of samples, and selected whole-rock geochemical and isotope data.

isotope ratios in the contact hornfels. Indeed, the values of these isotope ratios closely correlate with some of the major and trace elements in these rocks, which in turn reflect the minerals that host these elements and therefore the isotopes. For example, the diabase is characterized by the mineral olivine, which is reflected in the diabase's MgO content (and high levels of Ni and Co), compared with the high quartz and K-feldspar content of the granophyre, reflected in its high SiO_2 and K_2O (and high trace U and Th) contents. Because Rb substitutes for K in the K-feldspar crystal lattice, there are higher trace amounts of Rb in the granophyre. In contrast, the diabase is dominated by plagioclase, which is Ca-dominated feldspar, and because Sr substitutes for Ca in the plagioclase crystal lattice, the diabase has a higher trace Sr content. It can thus be seen that the higher isotope ratios follow these mineralogical and geochemical differences between the diabase and the granophyre. But the contact hornfels beneath the sill has similar contents of these major and trace elements, and isotopes, to those in the granophyre. The hornfels, of course, represents the host Hakatai Shale intruded by the basaltic magma which was metamorphosed in contact with the diabase as it crystallized, due primarily to the heat of the magma. That there has been some isotopic contamination of the diabase by both the contact hornfels and the granophyre is evident from the intermediate values of the isotope ratios in the diabase samples adjacent to the granophyre and hornfels respectively. This could perhaps suggest that some of the crustal contamination was provided in-place from the Hakatai Shale wall rock to the sill. The contact hornfels zone is thicker below the sill than above it, but the granophyre is at the top of the sill exclusively, due to its lighter density that would have caused it to float to the top of the basaltic magma as it crystallized and cooled.

The Cardenas Basalt lavas, which are regarded as the extrusive equivalent of the same magma responsible for the Bass Rapids and other diabase sills in Grand Canyon, similarly exhibit very high $^{87}Sr/^{86}Sr$ isotope ratios (Figures 16 and 17), though not as high $^{206}Pb/^{204}Pb$ isotope ratios (Figures 17–19). Figure 21 shows the type section of the Cardenas Basalt with the relative locations of the samples used in this study and selected whole-rock geochemical and isotope data obtained

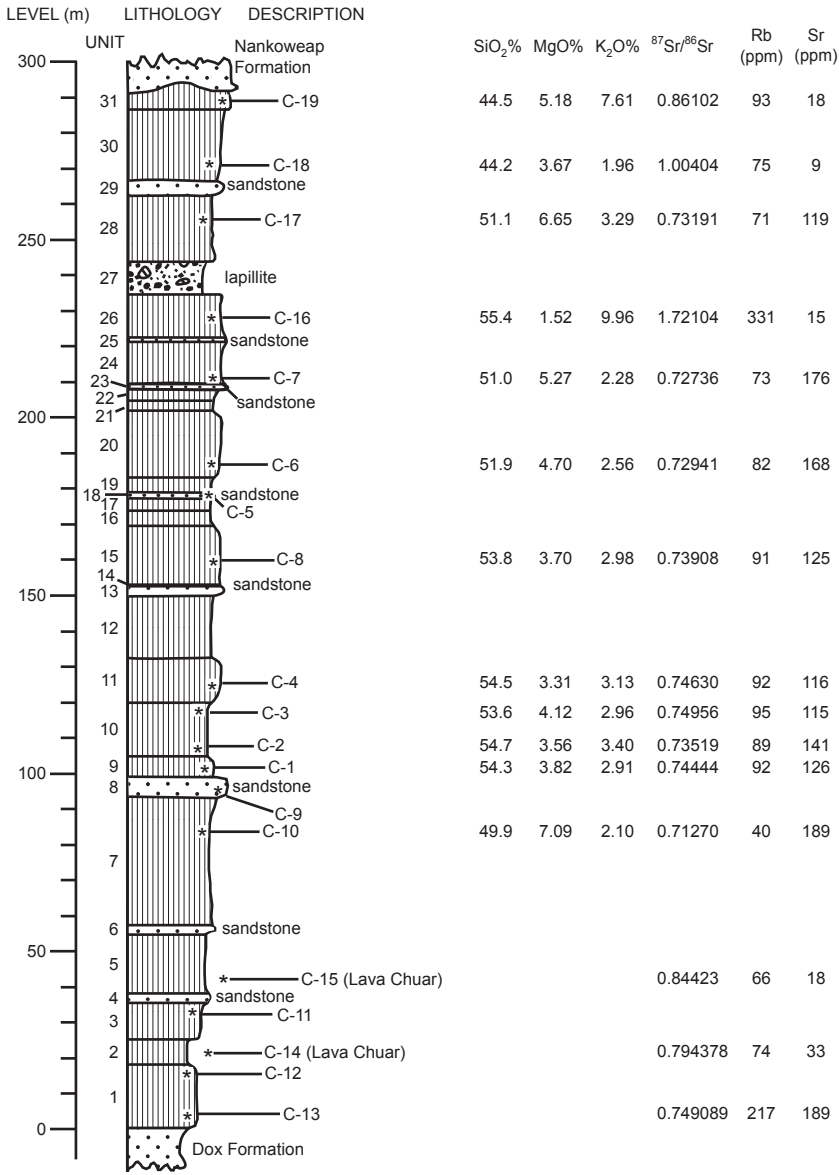

	SiO_2%	MgO%	K_2O%	$^{87}Sr/^{86}Sr$	Rb (ppm)	Sr (ppm)
C-19	44.5	5.18	7.61	0.86102	93	18
C-18	44.2	3.67	1.96	1.00404	75	9
C-17	51.1	6.65	3.29	0.73191	71	119
C-16	55.4	1.52	9.96	1.72104	331	15
C-7	51.0	5.27	2.28	0.72736	73	176
C-6	51.9	4.70	2.56	0.72941	82	168
C-8	53.8	3.70	2.98	0.73908	91	125
C-4	54.5	3.31	3.13	0.74630	92	116
C-3	53.6	4.12	2.96	0.74956	95	115
C-2	54.7	3.56	3.40	0.73519	89	141
C-1	54.3	3.82	2.91	0.74444	92	126
C-10	49.9	7.09	2.10	0.71270	40	189
C-15 (Lava Chuar)				0.84423	66	18
C-14 (Lava Chuar)				0.794378	74	33
C-13				0.749089	217	189

Figure 21. The measured type section of the Cardenas Basalt in Basalt Canyon, eastern Grand Canyon (after *Hendricks and Lucchitta* [1974]). Their unit numbers are shown. The relative locations of the samples collected are also shown, including two samples from nearby Lava Chuar Canyon. Selected whole-rock geochemical and isotope data are also shown.

from them. Of course, there is no felsic equivalent of the granophyre capping in the Bass Rapids diabase sill among the lava flows of the Cardenas Basalt, simply because differentiation and flotation of any felsic crustal contamination requires some time to occur as in the intrusive sill with its coarse-grained diabase, whereas the fine-grained basalt lavas cooled very rapidly. Thus any felsic crustal contamination in the basalt magma when it was extruded would have been retained in-place within the resultant basalt lavas, making them compositionally more felsic than the pure basalt magma that crystallized to form the diabase in the sills. That this is the case can be seen by comparing the selected major and trace elements in the Cardenas Basalt listed in Figure 21 with those in the diabase of the Bass Rapids sill listed in Figure 20. It is immediately apparent that the basalt lavas have higher SiO_2 and K_2O contents and a lower MgO content than the diabase in the sill. Thus the upper member flows of the Cardenas Basalt, for which these elements are listed in Figure 21, are mostly classified as basaltic andesites. Their higher trace Rb content compared with the diabase in the sill parallels their higher K_2O contents and results in higher $^{87}Sr/^{86}Sr$ isotope ratios similar to those in the granophyre and the contact hornfels of the Bass Rapids sill. Even the lower member flows of the Cardenas Basalt, which are alkali basalt lavas that more truly reflect the original mantle-derived basalt magma, contain the same high $^{87}Sr/^{86}Sr$ isotope ratios, indicative of crustal isotopic contamination during ascent of the basalt magma through the crust via conduits. Another possibility is that the crustal isotopic contamination occurred as a result of post-crystallization alteration of the lava flows, given that their high K_2O content and low Sr content could reflect the sericitization (alteration to the fine-grained white mica sericite) of their plagioclase, as observed in thin sections. However, as the bulk geochemistry and mineralogy of these lava flows define them as basaltic andesites, regardless of any post-crystallization alteration, so the crustal contamination they contain is a primary feature, due to such crustal contamination being incorporated in the basalt magma during its passage through the crust from the mantle where it was sourced.

One other means of demonstrating that crustal contamination of the

basaltic magma occurred during intrusion of the Bass Rapids diabase sill is to show that there has been interaction of the basaltic magma as it was intruded and crystallized with the sill's Hakatai Shale wall rock. The two samples of the contact hornfels below the Bass Rapids sill (Figure 20) were also submitted for radioisotope analyses. The resultant data were then included with all the radioisotope data for the diabase sill and granophyre "capping," and further regression analyses were undertaken using the *Isoplot* program [*Ludwig*, 2001] to plot isochrons and obtain isochron "ages." Figures 22–25 are the resultant isochron plots, with a K-Ar isochron "age" of 847±110 Ma (Figure 22), a Rb-Sr isochron "age" of 1082±33 Ma (Figure 23), and a Pb-Pb isochron "age" of 1280±100 Ma (Figure 25). In each of these three cases the isochron regression lines have excellent statistics, with the MSWD at or near unity, meaning the assigned errors match the observed scatter.

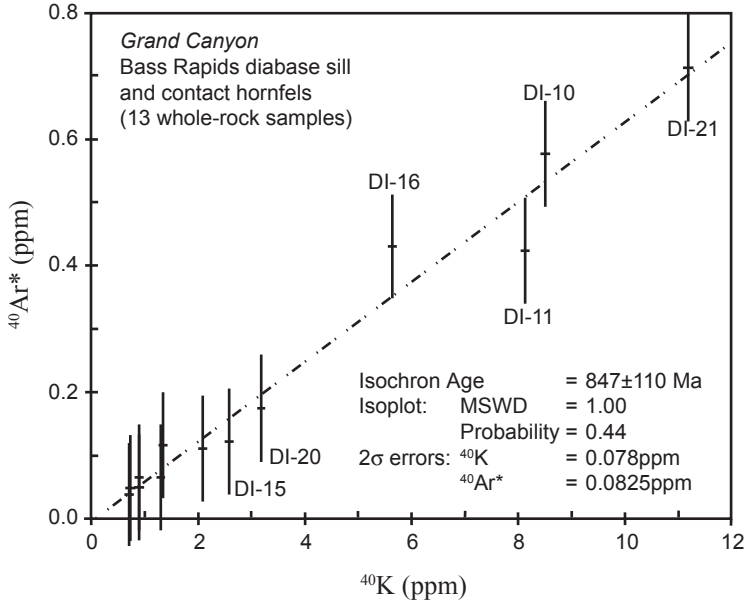

Figure 22. ^{40}K versus $^{40}Ar^*$ isochron diagram for the Bass Rapids sill (diabase and granophyre) and its contact hornfels in Grand Canyon. All thirteen whole-rock samples (some labeled as per Figure 20) were used in the isochron and "age" calculations. The bars represent the 2σ uncertainties.

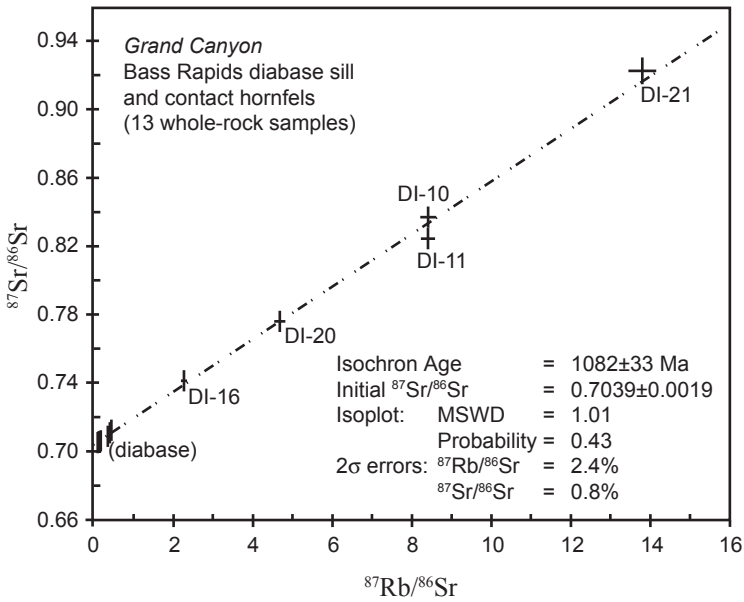

Figure 23. $^{87}Rb/^{86}Sr$ versus $^{87}Sr/^{86}Sr$ isochron diagram for the Bass Rapids sill (diabase and granophyre) and its contact hornfels in Grand Canyon. All thirteen whole-rock samples (some labeled as per Figure 20) were used in the isochron and "age" calculations. The bars represent the 2σ uncertainties.

Furthermore, these isochron "ages" are concordant with the isochron "ages" obtained for the respective radioisotope systems using just the diabase and granophyre samples from the sill itself (Table 2), and the 2σ uncertainties of these isochron "ages" that include the two hornfels samples are overall significantly smaller. In other words, including the hornfels samples with the sill samples in the *Isoplot* analyses yields even better isochron "ages," with the same pattern of discordancy between the radioisotope systems. Furthermore, the hornfels samples plot with the granophyre samples for all of the radioisotope systems, including the Sm-Nd radioisotope system in Figure 24. Indeed, the two hornfels samples combined with the three granophyre samples yield their own five-point Sm-Nd isochron distinct from the DI-13 mineral Sm-Nd isochron that can be fitted to the eight diabase samples [*Snelling et al.*, 2003a; *Austin*, 2005]. The "age" obtained from this granophyre plus

hornfels isochron of 626±280 Ma does not have the best statistics and does not appear to coincide with any known geologic event. However, this obvious relationship between the contact hornfels and the granophyre does confirm that there has been interaction between the granophyre and the contact hornfels as a result of the hydrothermal alteration of the granophyre occurring during the contact metamorphism with the Hakatai Shale to produce the hornfels. Hydrothermal conditions have been shown to cause rare earth element mobility in rhyolite and granite [*Poitrasson et al*., 1995], to which the granophyre is compositionally identical. Thus, as suggested by *Snelling et al*. [2003a] and *Austin* [2005], the Nd isotopes were obviously perturbed during this hydrothermal

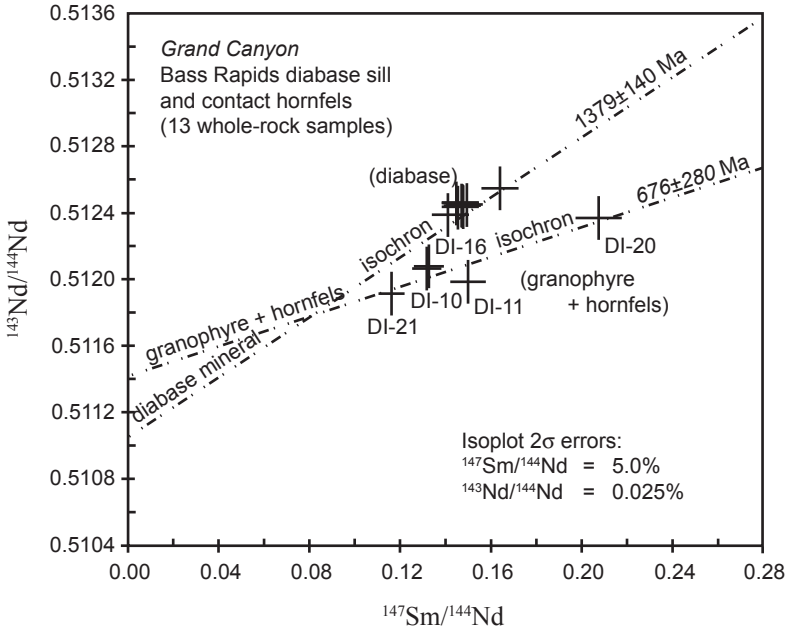

Figure 24. $^{147}Sm/^{144}Nd$ versus $^{143}Nd/^{144}Nd$ isochron diagram for the Bass Rapids sill (diabase and granophyre) and its contact hornfels in Grand Canyon. All thirteen whole-rock samples (some labeled as per Figure 20) are plotted, with the bars representing the 2σ uncertainties. The diabase mineral isochron of sample DI-13 [*Snelling et al*., 2003; *Austin*, 2005] passes through the eight diabase samples. An apparent isochron can be fitted to the five granophyre and hornfels samples.

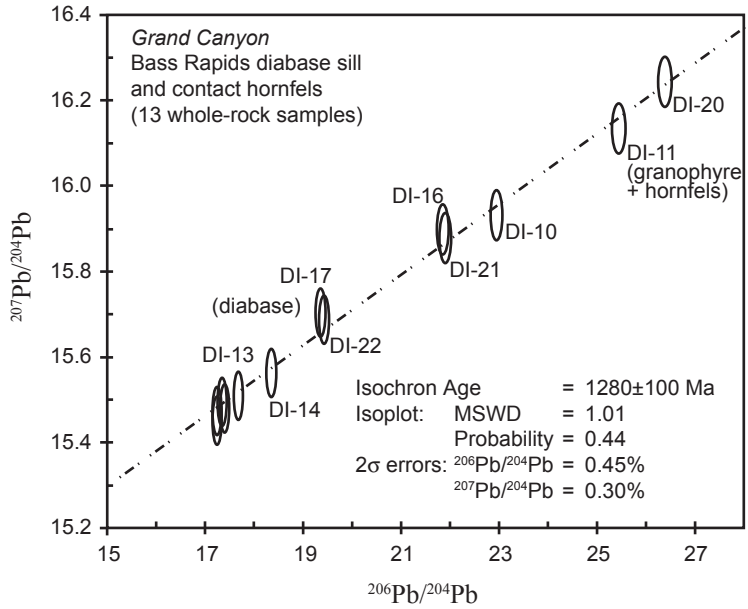

Figure 25. $^{206}Pb/^{204}Pb$ versus $^{207}Pb/^{204}Pb$ isochron diagram for the Bass Rapids sill (diabase and granophyre) and its contact hornfels in Grand Canyon. All thirteen whole-rock samples (many labeled as per Figure 20) were used in the isochron and "age" calculations. The ellipses represent the 2σ uncertainties.

alteration by exchange between the hornfels and the granophyre. It is also clear from Figures 22, 23, and 25 that there has also been exchange in the other radioisotope systems between the granophyre and the hornfels on the one hand, and the granophyre and hornfels with the diabase on the other, because otherwise the radioisotope data for the hornfels, granophyre, and diabase would not have plotted on the same respective isochrons. Indeed, this radioisotope equilibration between the sill and the hornfels is to be expected, because it would have been the heat from the intruding basaltic magma that combined with the connate water in the wall-rock shale that resulted in the contact metamorphism which produced the hornfels between the sill and the shale both above and below the sill. Thus there was crustal contamination of the basaltic magma as it intruded into the shale, that crustal contamination being contributed from the shale itself. The process could have also included

sufficient felsic contamination into the basaltic magma at both the lower and upper contacts of the sill from the shale wall rock itself to produce the granophyre that "floated" to the top of the basaltic magma as it crystallized and cooled to accumulate as the "capping" on the sill. The fact that the contact metamorphism and this crustal contamination coincided with the sill intrusion event would explain why, as would be expected, the hornfels samples plot on the same isochrons as the diabase and granophyre samples from the sill itself.

It is the coincidence of the granophyre and hornfels radioisotope data with the diabase radioisotope data on the same isochrons in the K-Ar (Figure 22), Rb-Sr (Figure 23), and Pb-Pb (Figure 25) radioisotope systems that provides the overall spread in the radioisotope data to yield good isochrons and isochron "ages" with excellent statistics. Indeed, it is because the granophyre and hornfels Sm-Nd radioisotope data are not consistent with the Sm-Nd radioisotope data for the diabase samples that a whole-rock Sm-Nd isochron cannot be plotted for the sill in Sm-Nd radioisotope system (Figure 24). Furthermore, as already noted, in the K-Ar, Rb-Sr, and Pb-Pb radioisotope systems it is the spread in the radioisotope data provided by the granophyre and hornfels samples that actually make the isochrons and isochron "ages" possible, so this implies that the crustal contamination of the basaltic magma to produce the sill with its granophyre "capping" and contact hornfels adjoining it was crucial for the radioisotope methods to succeed in "dating" the sill. However, because it is clear from the isochron diagrams (Figures 22–25) that the isochrons representing the isochron "ages" of the sill do fit with the respective radioisotope data for the diabase samples only, this would imply that radioisotope decay was still necessary to produce these isochrons and isochron "ages." Nevertheless, the 6–7% crustal contamination of the basaltic magma (determined by the volume of the granophyre as a proportion of the total volume of the sill) contributed significantly to the respective radioisotope systematics, and thus to the resultant "statistically robust" isochrons and isochron "ages" for the sill. Of course, if the basaltic magma inherited this radioisotope signature from its mantle source, it may be that a significant quantity of the radioisotope decay indicated by the isochron "ages" occurred in

the mantle source, this mantle radioisotope signature then equilibrating by exchange with the crustal contamination of the basaltic magma in the sill during the contact metamorphism. However, this does not preclude some significant radioisotope decay then occurring in the sill subsequent to its intrusion, crystallization and cooling.

6.4 Resultant Implications for Radioisotope Dating

There are several observations that are clearly evident from the foregoing discussion of radioisotopes in the Precambrian Bass Rapids sill. First, the sill's Rb-Sr isochron "age" is virtually identical to the mantle Rb-Sr isochron "age" of the recent Uinkaret Plateau basalts that outcrop in the western Grand Canyon not all that far from the Bass Rapids sill. Because the basaltic magma that intruded to form the Bass Rapids sill was sourced in the same area of the mantle under the Grand Canyon region as was the basaltic magma for the Uinkaret Plateau basalts, this similarity in Rb-Sr isochron "ages" could be interpreted to mean that the Rb-Sr isochron for the Bass Rapids sill is similarly an inherited mantle isochron. However, it could equally be valid to interpret the similarity in the Rb-Sr isochron "ages" to imply that after the basaltic magma for the Bass Rapids diabase sill separated from the mantle source, the parent Rb isotopes in both the sill and the magma's mantle source experienced the same amount of radioisotope decay, the signature of which was then inherited very recently by the magma which was extruded as the Uinkaret Plateau basalt flows when it was sourced in the same mantle area.

Second, the isochron "ages" for the Bass Rapids sill obtained from the four radioisotope systems are discordant, with the α-decaying isotopes yielding older isochron "ages" than the β-decaying isotopes, and the longer the half-life (and/or the heavier the atomic weight) of the α- or β-decaying isotope the greater the isochron "age" compared to that derived from the other respective α- or β-decaying isotopes. If all four radioisotope systems are "dating" the same geologic event (the formation of the sill), then this pattern is consistent with the four parent radioisotopes decaying at different accelerated rates, the α-decaying parent isotopes having their radio-

decay accelerated more than that of the β-decaying parent isotopes. However, this pattern of discordance is not also evident in the limited data available for the other radioisotope systems in the Uinkaret Plateau basalts. It might be argued that there is some similarity in the Sm-Nd isochron "ages," but the 2600 Ma Pb-Pb isochron "age" for the Uinkaret Plateau basalts [*Austin*, 1994] is more than double the Pb-Pb isochron "age" of the Bass Rapids sill. Furthermore, even though there is no comparative K-Ar isochron "age" available for the Uinkaret Plateau basalts, their K-Ar model "ages" are very recent and contrast markedly with the K-Ar model "ages" for the Bass Rapids sill. However, whereas the Cardenas Basalt is regarded as the extrusive equivalent of the intrusive diabase sills derived from the same basaltic magma, even though the Cardenas Basalt and Bass Rapids sill yield essentially the same Rb-Sr isochron "age," the other radioisotope systems yield different isochron "ages" for the Cardenas Basalt and Bass Rapids sill. Indeed, the K-Ar isochron "age" for the Cardenas Basalt is much less than that for the Bass Rapids sill, even though the former may have been affected by excess $^{40}Ar^*$ when the latter was not.

Third, there is unequivocal evidence of both the Bass Rapids sill and the Cardenas Basalt having been affected by crustal contamination which had to be responsible for some perturbing of the radioisotope systems, especially the Rb-Sr and Sm-Nd radioisotope systems. That this crustal contamination involved radioisotope exchange between the intruding basaltic magma and the shale wall rock to the sill is evident from the fact that the contact hornfels and granophyre "capping" within the sill both plot on the same isochrons as the diabase, dramatically improving the compositional spread in the radioisotopes and thus resulting in excellent statistics for the isochron fits and isochron "ages" in the K-Ar, Rb-Sr, and Pb-Pb radioisotope systems. Nevertheless, this radioisotope exchange during contact metamorphism of the shale wall rock by the intruding basaltic magma must have equilibrated in both the granophyre and the contact hornfels, because in both the Rb-Sr and Pb-Pb radioisotope systems the mineral isochrons yielded by diabase samples are essentially identical to the whole-rock isochrons obtained using both the diabase samples and the granophyre and hornfels

samples. Nevertheless, the crustal contamination did affect the mantle-derived magma, with its inherited radioisotopes, of both the Cardenas Basalt and Bass Rapids diabase sill, and the differences between their isochron "ages" in some of the radioisotope systems may be due to the crustal contamination remaining mixed in the rapidly-cooled Cardenas Basalt compared to its separation into the distinct granophyre phase "capping" the slower-cooled Bass Rapids diabase sill.

All these considerations—isochron discordances, inheritance of mantle source isotopic signatures, and mixing of crustal contamination—must render radioisotope "dating" highly questionable at best, and useless at worst, as the absolute "dating" method it is so unanimously and forthrightly claimed to be. Obviously, if radioisotope decay was accelerated at some time or times in the past, and the decay of the different parent radioisotopes was accelerated at different rates, then the radioisotope decay "clocks" could never be relied upon to provide absolute "dates" for rocks in terms of hundreds of millions of years. Furthermore, if some of the radioisotope decay occurred in the mantle, from where magmas were subsequently sourced and inherited the resultant radioisotope signatures, then measuring the radioisotopes today in the lavas or intrusions could not provide "dates" for when the lavas were erupted and the magmas intruded, because it would be unclear just how much of the radioisotope decay had occurred since eruption or intrusion. And finally, if crustal contamination of magmas occurs during their ascent, intrusion and extrusion, modifying the radioisotope content of the magmas, then unless it was known how much modification of the radioisotopes occurred, it would be impossible to be sure whether measurements performed today were actually providing correct absolute "dates" for the formation of the volcanic and intrusive rocks. Indeed, even as volcanic, intrusive and metamorphic rocks are cooling, hydrothermal alteration by fluids expelled from the cooling rocks and/or the groundwaters from surrounding rocks can modify mineralogy, geochemistry, and radioisotope contents of the rocks being "dated" with radioisotopes.

Given that any or all of these complex factors will have affected each of the radioisotope systems, often differently, then it is misleading to

"date" rocks with just one of the radioisotope pairs. As has been shown here, discordancy between the radioisotope systems is the norm, and therefore without a knowledge of the complex history of the rocks being "dated," it is impossible to decide which of the radioisotope pairs is actually truly "dating" the rocks. These three demonstrated effects on the history of the radioisotope systems in rocks, namely, inheritance from the mantle sources and magmas, crustal contamination, and accelerated radioisotope decay, totally discredit the three assumptions on which the radioisotope "dating" methods are based, namely, known initial conditions, the rock remains a closed system, and a constant rate of radioisotope decay, respectively. Thus radioisotope "dating" methods, which have underpinned uniformitarian geology for nearly a century, are totally discredited and are therefore worthless as absolute geologic chronometers.

6.5 Towards a Model for the Behavior of Radioisotopes in Rocks through Earth History

At best, therefore, the radioisotope methods can only provide relative "dates." Thus, the absolute time framework for earth history into which the sequences of rock units and their relative "dates" can be placed and systematized must be sought from another, more reliable source. In endeavoring to piece together the historic past, evidence in the present can only be circumstantial, subject to interpretation based on the assumptions of the researcher. The best and most reliable sources to validate the details of historic events are reputable eyewitness accounts, a similar procedure to the testimonies of eyewitnesses being used in a courtroom to establish what happened at the crime scene. However, no human observers or researchers were present during the earth's early history, so historical geology is conventionally based only on circumstantial evidence. On the other hand, the Bible provides an eyewitness account of the earth's early history, validated by the character and testimony of the Creator Himself (Jesus Christ), followed by the testimonies of subsequent human observers. The early chapters of Genesis that are the Creator's eyewitness account of the earth's

earliest history are unmistakably historical narrative [*Boyd*, 2005].

The unequivocal testimony of the Biblical record is that the earth, universe and life were created by God in six literal days only 6000–7000 years ago, and that subsequently there was a global catastrophic Flood which destroyed pre-Flood life and buried it in the strata that accumulated as the earth was totally reshaped. Thus the behavior of radioisotopes in rocks through the earth's history needs to be understood and modeled within this Biblical framework with its 6000–7000 year absolute timescale.

In the Bible framework of earth history there were two clearly-stated periods of non-uniformitarian, accelerated geological processes—Creation and the Flood (2 Peter 3:3–7). Early in the Creation week before life was created, and during the Flood when life was preserved on the Ark, the bulk of the earth's present geologic record would have been produced by catastrophic processes not now in operation, and this must have included accelerated radioisotope decay. It is likely that by the end of Day 1 of the Creation week, the early earth that had been created beneath the globe-covering water had already been differentiated internally into its core, mantle, and initial crust divisions [*Austin et al*., 1994]. It is not inconceivable that accelerated radioisotope decay was part of the creative means God used to produce this internal differentiation of the initial earth [*Baumgardner*, 2000]. This accelerated radioisotope decay would have meant that by the end of Day 1, the earth's mantle and crustal rocks would have already acquired a radioisotope signature that if measured then and interpreted by present-day uniformitarian assumptions would have been already as much as 1000 Ma or more "old." This should not be confused with any day-age concept, but should be recognized as only an apparent long-"ages" history during a single literal day if the catastrophic processes involved are ignored. Crustal formation would have continued through Day 2 and reached its climax accompanied by catastrophic global tectonic processes during the first half of Day 3 when the first dry land surface was produced. With the earth now ready for the creation of plant and animal life to populate the earth, the bulk of God's geologic creative work would have been finished during Day 3, so that with the

curtailment of catastrophic geologic processes during Day 3 the burst of accelerated radioisotope decay would also have stopped, leaving some mantle and crustal rocks with apparent radioisotope "ages" already as much as 3000–4000 Ma. Other strata that had progressively developed during this period of catastrophic crustal formation and tectonics would have acquired progressively younger relative radioisotope "ages," due to the radioisotope systems often having been reset as these rock strata formed.

Through the remainder of the Creation week, and through the pre-Flood period, both geological processes and radioisotope decay would probably have occurred at rates similar to today's rates for these processes. This was necessary for the well-being and proliferation of plants and animals on the earth's surface. However, with the onset of the Flood, uniformitarian conditions were replaced by catastrophic geologic processes and plate tectonics, again accompanied by a burst of accelerated radioisotope decay [*Austin et al*., 1994; *Humphreys*, 2000]. The physical evidence for this second episode of accelerated radioisotope and nuclear decay includes the abundant radiohalos and fission tracks respectively in granites and volcanic layers formed during the Flood [*Snelling*, 2000b, 2005a, b; *Snelling and Armitage*, 2003; *Snelling et al*., 2003b]. Again, as the geologic record of the Flood accumulated, those volcanic and intrusive rocks that were progressively erupted and intruded often had their radioisotope systems reset during their formation to provide apparent relative "ages" of less than approximately 600 Ma.

A by-product of radioisotope decay is heat, so these bursts of accelerated radioisotope decay would have produced enormous quantities of heat that would need to be dissipated quickly to avoid vaporizing the rocks, as pointed out by *Snelling* [2005a]. *Humphreys* [2000, 2005] has tentatively suggested a process that might be capable of quickly dissipating this unwanted excessive heat, but an adequate viable mechanism is yet to be fully elucidated.

In the light of the evidence of prolific isochron discordances between the radioisotope systems, inheritance of radioisotope signatures by magmas from their mantle sources, and the changes in the radioisotope

contents of magmas due to some mixing in some of them of crustal contamination, many anomalies in this relative "age" progression during the early Creation week and Flood accumulation of the geologic record would have occurred. Indeed, inheritance and mixing of radioisotopes from mantle and crustal sources continue to be evident in modern and recent volcanic rocks. It would seem that the isochron discordances between the radioisotope systems are most pronounced in Precambrian rock units, though that conclusion may be heavily biased by the majority of the rock units targeted in this study being of Precambrian designation. More pronounced isochron discordances in Precambrian rock units are consistent with many of the rocks so designated having had their origin during the early part of the Creation week, when the burst of accelerated radioisotope decay would seem to have been equivalent to perhaps as much as 3000–4000 Ma worth at today's decay rates. Such a large amount of accelerated radioisotope decay would have increased potential for discordances between the radioisotope systems, the α-decayers being accelerated more than the β-decayers, and in general the longer the half-life, and/or the heavier the atomic weight, of the parent isotope the greater the acceleration. In contrast, if the second burst of accelerated radioisotope decay during the Flood was only equivalent to approximately 600 Ma worth at today's rates, then the potential for isochron discordances between the radioisotope systems would be much diminished, and this is certainly reflected in the Phanerozoic rock unit targeted in this study. Furthermore, just how often the radioisotope signatures inherited by magmas from their mantle sources are not reset during magma ascent, intrusion and extrusion is very difficult to gauge, because of the apparent dominating effect of accelerated radioisotope decay.

Similarly, it is not always apparent that magmas had crustal contamination mixed into them, because where such crustal contamination is recognizable it only amounts to the equivalent of 5–10% by volume of the magma. Thus, even if crustal contamination of a magma was equivalent to up to 20% of the magma volume, and the crustal contamination was not easily recognized because of being mixed and homogenized in the magma, the effect of accelerated

radioisotope decay would dominate overall and still produce isochron discordances between the radioisotope systems. Furthermore, the nature and composition of the crustal contamination can result in one or more of the radioisotope systems being perturbed more than the others, so this might explain where the patterns of isochron discordances are not the same, instead of any trend according to atomic weights of the parent isotopes. For example, in several of the targeted rock units the Pb-Pb isochron "ages" are older than the Sm-Nd isochron "ages," whereas according to the dominant pattern of isochron discordances the longer half-life α-decay of ^{147}Sm should have been accelerated more, and thus should have produced older isochron "ages" than the shorter half-life α-decayers ^{238}U and ^{235}U. And finally, the mobility of $^{40}Ar^{*}$ within rocks can often result in either its loss or accumulation in excess of that produced by *in situ* radioisotope decay of its parent ^{40}K, so that widely divergent K-Ar model "ages" may result even in adjacent samples from the same outcrop, and K-Ar isochron "ages" can also be perturbed. Thus, superimposed on an overall younging trend in the relative "ages" upwards through the geologic record are many anomalies due to these various factors.

In conclusion, while all the observations made and issues discussed by *Snelling* [2000a], and summarized in the introduction to this report, have been vindicated in this overall study, the radioisotope "ages" measured in the earth's crustal rocks cannot be simply explained solely by a model in which inheritance and mixing of radioisotopes in the mantle and crust have occurred due to the two catastrophic episodes of mantle-crust geodynamics (early in the Creation week and during the Flood). The weight of the available evidence favors the conclusion that accelerated radioisotope decay has been the dominant influence on the behavior of radioisotopes in rocks through earth history, "swamping" any effects of inheritance and mixing of radioisotopes in the mantle and crust. And the quantity of the accelerated radioisotope decay appears to equate to that conventionally measured. Not only do the radiohalos and fission tracks in Flood rocks provide physical evidence of 500 million years worth of accelerated radioisotope decay in these rocks equivalent to conventional determinations using radioisotope "dating," but Precambrian (pre-Flood) strata yield radioisotope "ages" of the

right order of magnitude commensurate with the claimed "age" of the earth based on concordant radioisotope isochron "ages" for meteorites [*Dalrymple*, 1991; *Austin*, 2000]. Thus, because of these two bursts of accelerated radioisotope decay being the apparent time contributor to the resultant radioisotope "ages" obtained for the earth's crustal rocks, the systematic trend of radioisotope "dates" in the geologic record can still be used for relative dating. Nevertheless, there will also be anomalous "ages" due to the contributions of inheritance and mixing of radioisotopes in and from mantle and crustal sources. However, the only reliable framework for understanding the earth's geologic history is that provided in the Bible, and that emphasizes a young created earth and a subsequent global Flood, the two events which have catastrophically built the earth's crustal geologic record and shaped its surface.

7. Conclusions

Potassium-Ar, Rb-Sr, Sm-Nd, and Pb-Pb radioisotope analyses of ten targeted rock units that span the geologic record from the recent to the early Precambrian demonstrate that pronounced discordancy between model and isochron "ages," and between isochron "ages," is always present, contrary to the perception that when two or more radioisotope dating methods are applied to the same rocks they yield the same radioisotope "ages." This indicates that there is a fatal problem with the radioisotope "dating" methods, and with the assumptions on which they are based.

For the seven Precambrian rock units studied there is a clear pattern to the significant discordances that exist between the different radioisotope pairs, the K-Ar and Rb-Sr isochron "ages" always being younger than the Sm-Nd and Pb-Pb isochron "ages." In other words, the β-decayers yield younger isochron "ages" than the α-decayers. Furthermore, within each decay mode it is also generally true that the longer the half-life, and/or the heavier the atomic weight, of the parent radioisotope the older the isochron "age" yielded. Therefore, it is obvious that the constant-decay-rates assumption of conventional radioisotope "dating" must be invalid, because for any of these rock units all four radioisotope pairs are supposed to be "dating" the same

geologic event. The only way to reconcile these systematic discordances between the radioisotope pairs is changing decay rates in the past. Thus it is concluded that at some time or times in the past the decay of the α-emitters (^{238}U, ^{238}U, and ^{147}Sm) had to have been accelerated more than the decay of the β-emitters (^{87}Rb and ^{40}K), and in general, the longer the present half-life and/or the heavier the atomic weight of the α- or β-emitter, the more its decay was accelerated relative to the other α- or β-emitters.

However, a further complication to this pattern is that the radioisotope endowment of the mantle sources of basaltic magmas can sometimes be inherited by the magmas without resetting of the radioisotope "clocks" during ascent, intrusion, and extrusion in the earth's crust, thus producing anomalous radioisotope "ages." Furthermore, the radioisotope systems may also be perturbed by crustal contamination during ascent, intrusion, and extrusion, by actual mixing of crustal rock into the magma, or by the transfer of radioisotopes and other trace elements into the magma by hydrothermal and other forms of alteration, again producing anomalous "ages." Thus the known initial conditions and closed system assumptions foundational to the radioisotope "dating" methods are also demonstrably subject to failure, so that together with non-constant accelerated decay rates in the past, radioisotope dating cannot possibly yield absolute "ages" for the earth's crustal rocks.

The dominant process to have affected the radioisotope systems is the accelerated radioisotope decay, which has produced a systematic younging trend of relative ages upwards through the geologic record, with anomalous "ages" occasionally superimposed on the trend by mantle inheritance of radioisotopes by magmas and/or by crustal contamination mixing radioisotopes into magmas. But such effects appear to have only been limited, crustal contamination perhaps only being 5–10% (up to 20% at most) of magma volumes. Additionally, the mobility of ^{40}Ar* within rocks often results in either its loss or accumulation in excess of that produced by *in situ* radioisotope decay of ^{40}K, so that widely divergent K-Ar model "ages" may result, even in adjacent samples from the same outcrop, and K-Ar isochron "ages" can be perturbed.

Within the Biblical framework of a young created earth and a

subsequent global Flood, there would have been two bursts of accelerated radioisotope decay accompanying catastrophic geological processes. These would have been during the early part of the Creation week and during the Flood, with upwards of four billion years worth (at today's rates) of radioisotope decay at the beginning of earth history, and about 600 million years worth subsequently during the Flood. Thus the relative "ages" provided by radioisotope "dating" methods may still be useful, except the demonstrated discordances can make it difficult to decide which is the "correct" relative "age."

8. Future Work

While the ten targeted rock units in this study have been adequate to draw the above conclusions with confidence, radioisotope studies of more rock units would undoubtedly enhance the demonstration that isochron discordances are systematically present and destroy the viability of the radioisotope "dating" methods. Because of so few Phanerozoic rock units being targeted in this present study, further radioisotope studies should include several more Phanerozoic rock units, particularly some from the Paleozoic. This could be useful in determining whether there is a difference in the isochron discordance pattern in rock units formed during the Flood compared with those formed pre-Flood and during the Creation week. Because of the expense of radioisotope analyses it may also be worthwhile to conduct literature searches to obtain radioisotope data on rock units that have already been "dated" by three or four of the main radioisotope dating methods. Furthermore, where possible radioisotope data from relevant rock units should be obtained for the Lu-Hf and Re-Os radioisotope "dating" methods. Because ^{176}Lu and ^{187}Re are β-decayers, it would be possible to thus demonstrate whether they follow the pattern of the longer the half-life, and/or the heavier the atomic weight, the older the isochron "age." In building a comprehensive radioisotope database for each selected rock unit, if literature searches only provide radioisotope data for several of the radioisotope systems, then such data could be supplemented by collecting samples of those rock units and submitting them for analyses of the other radioisotope systems. And

finally, the copious radioisotope data on meteorites needs to be compiled in order to closely examine the claimed concordance of isochron "ages" for them. It remains a puzzle as to why the meteorite isochron "ages" are apparently concordant, when those for the Precambrian rock units tested in this study are discordant. The meteorite radioisotope data are also relevant to the question of just how much accelerated radioisotope decay has occurred during the earth's history.

Acknowledgments

Many people contributed to this research, and their help and support is gratefully acknowledged. Dr. Kurt Wise and Dr. Steve Austin assisted with some of the sampling of many of the rock units targeted in this study, and access and support of many of the sampling programs were provided by various raft crews on a number of trips through the Grand Canyon. The Grand Canyon National Park granted permission to collect rock samples and undertake the analyses of them. Answers in Genesis (Australia) provided logistical support for the Mt. Ngauruhoe and Somerset Dam fieldwork. William (Bill) Hoesch helped with the processing of many rock samples in the ICR rock laboratory. Of course, the analytical work undertaken by the various laboratories used in this research was crucial, and the excellent analytical data they provided are appreciated and acknowledged. Even though they may not agree with some aspects of the interpretation of the data and the conclusions of this study, the help and the work of Dr. Richard Reesman at Geochron Laboratories in Cambridge, Massachusetts, of Dr. Yakov Kapusta at Activation Laboratories in Ancaster, Ontario, of Dr. Richard Armstrong of the PRISE Laboratory in the Research School of Earth Sciences at the Australian National University in Canberra, and of Professor G. Lang Farmer at the University of Colorado at Boulder were all appreciated. Of course, none of the field or analytical work required for this study would have been possible without the donations to the RATE project from many supporters, and they are profusely thanked for those donations. Finally, the advice and encouragement of the other members of the RATE group, especially Dr. Steve Austin, is also acknowledged.

Appendix: The Case Studies—Descriptions and Sampling

A1. Mt. Ngauruhoe, New Zealand

Mt. Ngauruhoe is an andesite stratovolcano within the Tongariro volcanic massif of the Tongariro Volcanic Center of the Taupo Volcanic Zone, North Island, New Zealand (Figure 26) [*Cole et al*., 1986;

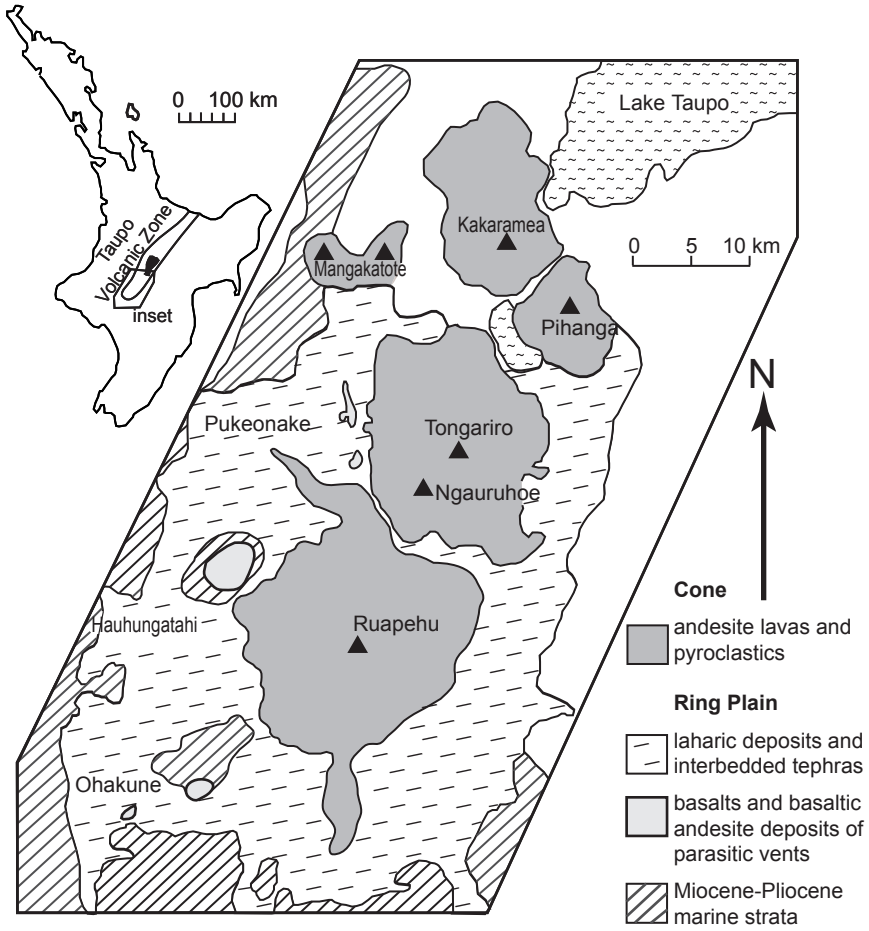

Figure 26. Location and deposits of the Tongariro Volcanic Center, Taupo Volcanic Zone, North Island, New Zealand (after *Cole et al.* [1986]; *Hackett and Houghton* [1987, 1989]). Note the location of Mt. Ngauruhoe.

Graham and Hackett, 1987; *Hackett and Houghton*, 1987]. *Snelling* [1998, 2003a] has summarized the geological setting of the Tongariro Volcanic Center that includes the still active Ruapehu volcano. The Tongariro volcano itself is a large volcanic massif that consists of at least twelve composite cones, Ngauruhoe being the youngest and most active for at least the last 2500 years [*Grindley*, 1965; *Topping*, 1973; *Cole et al*., 1986; *Nairn and Wood*, 1987; *Williams*, 1994]. Ngauruhoe has been one of the most active volcanoes in New Zealand, with more than seventy eruptive episodes since 1839, when the first steam eruption was recorded by European settlers [*Gregg*, 1960; *Nairn and Wood*, 1987; *Williams*, 1994]. The first lava eruptions seen by European settlers occurred in 1870, and then there were pyroclastic (ash) eruptions every few years, with major explosive activity in 1948. The next lava extrusion was in February 1949, when a series of hot block and ash flows down the northwestern slopes of the volcano was followed by lava flows with a subsequently estimated volume of about 575,000 m^3 [*Battey*, 1949; *Gregg*, 1960] (Figure 27).

The eruption from May 13, 1954 to March 10, 1955 began with an explosive ejection of ash and blocks, followed by an estimated volume of almost 8 million m^3 of lava that flowed from the volcano's crater from June through September 1954. It was claimed to be the largest flow of lava observed in New Zealand (by European settlers) [*Gregg*, 1956, 1960; *Nairn and Wood*, 1987; *Williams*, 1994]. The lava was actually dispelled from the crater in a series of 17 distinct flows on the northwestern and western slopes of the volcano (Figure 27). After the 1954–1955 eruption, Ngauruhoe steamed semi-continuously with numerous small eruptions of ash. Then on February 19, 1975 a series of nine, cannon-like, individual eruptions, accompanied by clearly visible atmospheric shock waves and condensation clouds, followed a 1.5 hour period of voluminous gas-streaming emission which formed a convecting eruption plume between 11 km and 13 km high [*Nairn*, 1976; *Nairn and Self*, 1978; *Nairn and Wood*, 1987; *Williams*, 1994]. Numerous pyroclastic avalanches were also generated by fallback from the continuous eruption column, and these turbulent mixtures of ash, bombs, and larger blocks rolled swiftly down Ngauruhoe's sides at

about 60 km per hour. It was estimated that a minimum bulk volume of 3.5 million m^3 of pyroclastic material was erupted in seven hours on that day, accumulating as sheets of debris on the northwestern slopes of the volcano and in the valley below (Figure 27). There have been no further eruptions since February 1975.

Most of the flows from Ngauruhoe are labradorite (plagioclase)-pyroxene andesite with phenocrysts of labradorite, hypersthene, and rare augite in a hyalopilitic (needle-like microlites set in a glassy

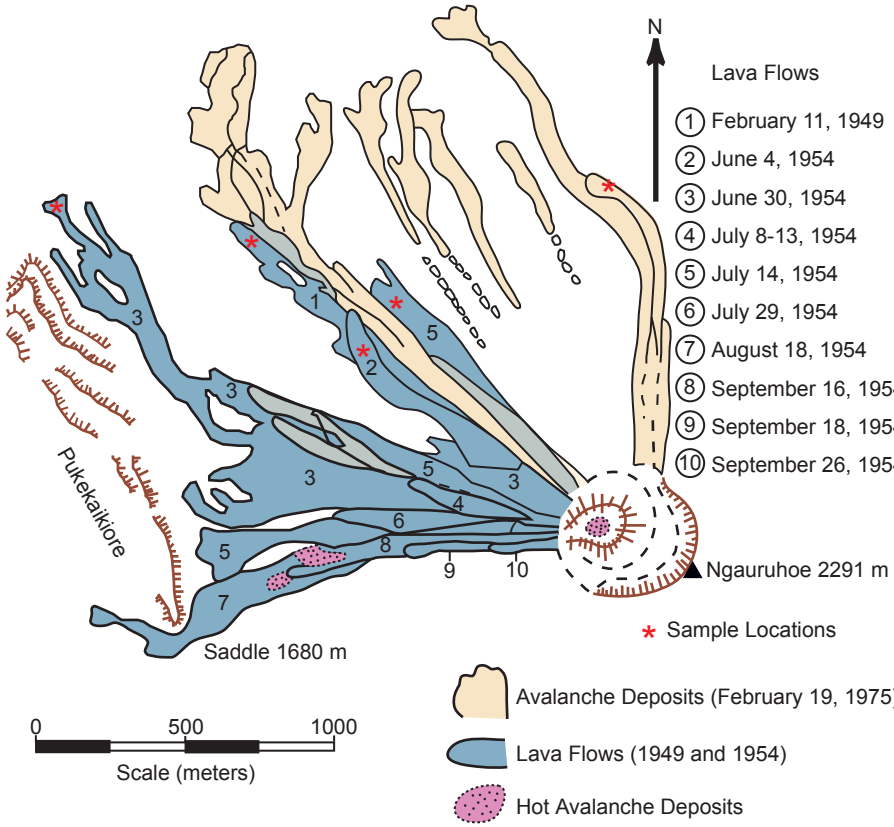

Figure 27. Map of the northwestern slopes of Mt. Ngauruhoe showing the lava flows of 1949 and 1954, and the 1975 avalanche deposits (after *Battey* [1949]; *Gregg* [1956, 1960]; *Nairn and Self* [1978]; *Nairn and Wood* [1987]). The locations of samples collected for this study are marked.

mesostasis) groundmass containing abundant magnetite [*Clarke*, 1960]. However, all lavas, lapilli, and incandescent blocks that have been analyzed from the eruptions in the twentieth century also contain olivine, so that chemically they can be classified as low-silica (or basaltic) andesites, using the classification scheme of *Gill* [1981]. All published analyses show only trivial changes in the compositions of the lavas and pyroclastics between 1928 and 1975 [*Steiner*, 1958; *Clark*, 1960; *Ewart and Stipp*, 1968; *Nairn et al*., 1976; *Cole*, 1978; *Cole et al*., 1983, 1986; *Graham and Hackett*, 1987; *Hackett and Houghton*, 1987*; Nairn and Wood*, 1987]. The porphyritic texture of these andesite lavas consists of phenocrysts consistently amounting to 35–40% by volume, the phenocryst assemblage being dominated by labradorite, but also orthopyroxene (hypersthene) and clinopyroxene (augite) are always major components, with olivine and magnetite present in trace amounts. All the lavas usually contain xenoliths that are usually rounded and invariably consist of fine-grained quartzose material with relict gneissic structure [*Battey*, 1949; *Steiner*, 1958]. Additionally, the andesite lavas contain glomerocrysts and mafic nodules consisting of plagioclase, orthopyroxene, and clinopyroxene with occasional olivine [*Graham et al*., 1995], which probably represent clumps of crystals that formed early in the magma chamber below the volcano.

Eleven samples were collected for the present study—two each from the February 11, 1949, June 4, 1954, and July 14, 1954 lava flows, and from the February 19, 1975 avalanche deposits, as well as three from the June 30, 1954 lava flow [*Snelling*, 1998, 2003a]. The sample locations are marked on Figure 27.

A2. Uinkaret Plateau Basalts, Western Grand Canyon, Arizona

The basaltic rocks of the western Grand Canyon are part of the Uinkaret Volcanic Field on the Uinkaret Plateau (Figure 28). This volcanic field extends northward from the Colorado River approximately 80 km to near the Vermilion Cliffs, and consists of up to 160 volcanic cones ranging in height from 15 to 250 m [*Koons*, 1945]. The lava flows from these volcanic cones are generally less than 8 m thick and cover

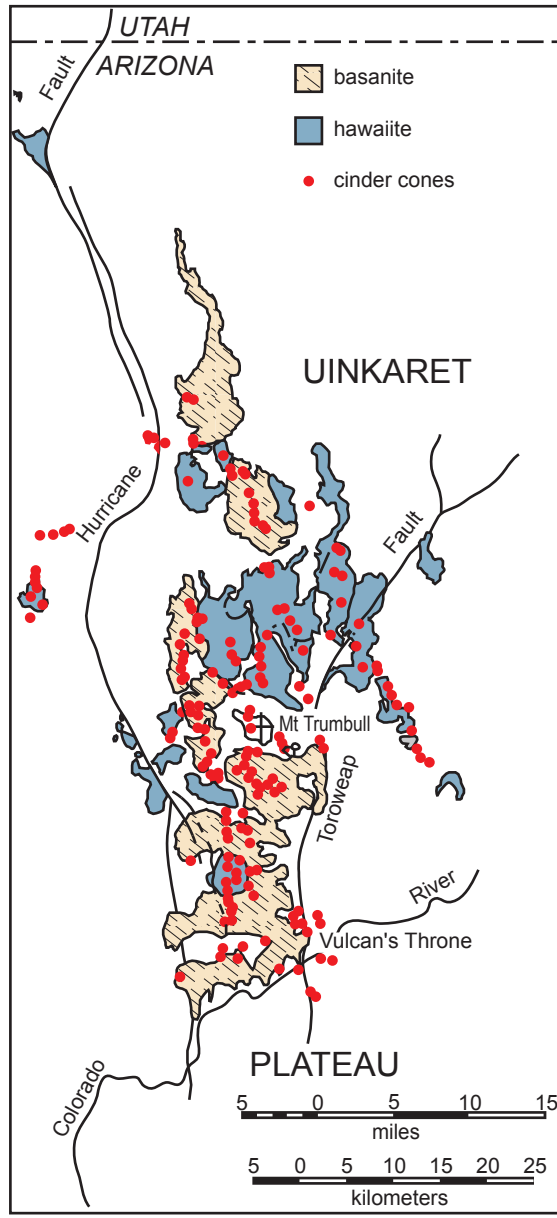

Figure 28. Generalized geologic map of the Uinkaret Plateau in the western Grand Canyon region, showing the distribution of the basaltic rocks (after *Best and Brimhall* [1974]; *Leeman* [1974]).

an area of several hundred km^2. They erupted in association with two north-south trending fissures on the Uinkaret Plateau, which extend north from near the rim of the inner gorge of Grand Canyon [*Maxson*, 1949]. Flows average between approximately 1–2 m thick, and some individual flows cover areas of up to several km^2. The thin and extensive lateral coverage of the flows indicates that they were highly fluid upon eruption. Only a few relatively small eruptive sources occur on the platform south of the inner gorge of Grand Canyon.

More than 150 of these lava flows poured southward into the inner gorge of Grand Canyon as lava cascades [*Hamblin*, 1989, 1990, 1994, 2003]. The most spectacular cascades are found on the north wall of the inner gorge between miles 179 and 182 of the Colorado River (downstream from Lees Ferry), having spilled over the rim of the inner gorge just to the west of Vulcan's Throne, a prominent cinder cone near the north rim of the inner gorge (Figures 28 and 29). One of

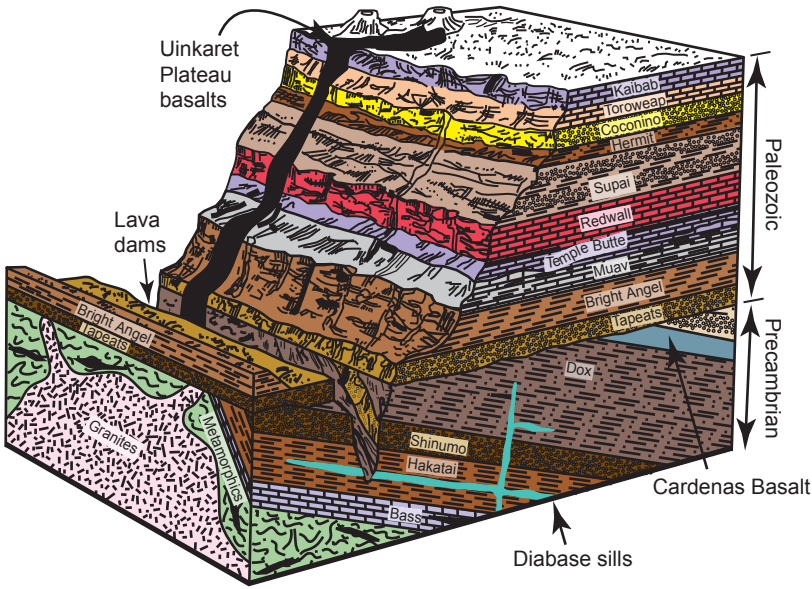

Figure 29. Generalized geologic block diagram showing most of the strata sequence and topographic form below the north rim of Grand Canyon (after *Austin* [1994]). The stratigraphic positions and relationships are shown for the Middle Proterozoic Cardenas Basalt and the likely related diabase sills, and for the Quaternary Uinkaret Plateau basalts and the related lava dams.

these cascades today almost reaches the bank of the Colorado River [*Billingsley and Huntoon*, 1983], while many of the other lava flows once reached the river, where the lavas crystallized and formed dams that temporarily filled the inner gorge of Grand Canyon to different heights, blocking the flow of the Colorado River. Today only erosion remnants of these lava dams remain within the inner gorge of Grand Canyon. When first studied, *McKee and Schenk* [1942] concluded that the lava-dam remnants were part of a large solitary dam structure. However, after more detailed study, *Maxson* [1949] concluded that up to three separate dams, two of which coexisted, once filled the inner gorge. Nevertheless, *Hamblin* [1994], in the most detailed study to date, has concluded that at least thirteen separate lava dams, none of which coexisted, filled the inner gorge during a period between 1.8 Ma to 0.4 Ma of the Pleistocene [*Hamblin*, 1994; *Dalrymple and Hamblin*, 1998]. However, *Rugg and Austin* [1998] argue that the entire span of time from the formation of the first dam to the destruction of the last could have been less than 2000 years.

Maxson [1949] described the volcanic rocks of the Uinkaret Plateau as olivine basalt flows and basaltic cinders. More detailed geochemical and mineralogical analyses by *Best and Brimhall* [1974] showed that the lavas of the western Grand Canyon region comprise a fairly broad and essentially continuous spectrum of compositions within the alkali basalt suite. The recent geologic mapping [*Billingsley and Huntoon*, 1983] has recognized older and younger flows on the Uinkaret Plateau on the basis of strata sequence and filling of valleys. Furthermore, petrographic and geochemical studies [*Best and Brimhall*, 1974] have distinguished two types of alkali basalts—basanites and hawaiites. The most widespread flows on the Uinkaret Plateau (Figure 28) are the hawaiites which are hypersthene (orthopyroxene)-normative [*Best and Brimhall*, 1974; *Fitton*, 1989; *Austin*, 1992]. All the basalt types contain some olivine, including those that form the remnants of the lava dams inside the inner gorge of Grand Canyon. *Austin* [1992] collected a suite of hawaiite samples from scattered locations across the Uinkaret Plateau for radioisotope analyses.

Furthermore, *Rugg and Austin* [1998] collected a sample from the

lava remnants of the Toroweap Dam about 300 m downstream from the site sampled by *McKee et al.* [1968]. The sample was taken from the north side of the Colorado River just above Lava Falls Rapid (mile 179.4) at a somewhat higher elevation than the *McKee et al.* [1968] sample. *Rugg and Austin* [1998] described it as very fine-grained and uniform black, without phenocrysts and without xenoliths, and thus classifiable as a basanite. Subsequently, on another river trip, a sample of the Massive Diabase Dam was collected on March 30, 1999, at mile 202.5 on the north side of the Colorado River, from a basal colonnade about 4 m above the exposed base of the flow, approximately the same site sampled by *Dalrymple and Hamblin* [1998]. The basalt sample was coarse-grained with visible phenocrysts of plagioclase, augite and olivine, devoid of xenoliths, and free of obvious effects of weathering.

A3. Somerset Dam Layered Mafic Intrusion, Queensland, Australia

The Somerset Dam layered mafic intrusion is situated immediately west of the village of Somerset Dam, some 65 km northwest of the city of Brisbane in southeast Queensland on Australia's east coast (Figure 30). The outcrop is somewhat oval shaped, covering an area of about 4 km^2 with a diameter of about 1.5 km (Figure 31) [*Mathison*, 1964, 1967, 1970]. It is a small layered gabbro intrusion with an exposed stratigraphic thickness of 500 m on a steep hillside. It is a well-preserved, well-exposed, steep-sided, discordant intrusion which is undeformed and unmetamorphosed. The roof and floor of the intrusion are not exposed, and an unknown thickness of layered gabbros of the intrusion have been eroded from the top, and are concealed below the exposed sequence. The location and nature of the feeder zone are unknown, yet it probably represents a small, relatively shallow (3–5 km depth), sub-volcanic magma chamber [*Mathison*, 1967, 1987].

Within this gabbro intrusion there is an exposed sequence of twenty-two saucer-shaped macrolayers, 3–50 m thick generally dipping inwards at 10–20° (Figure 31) [*Mathison*, 1967]. The contacts between these prominent layers are sharply defined, generally to within 10 cm, and

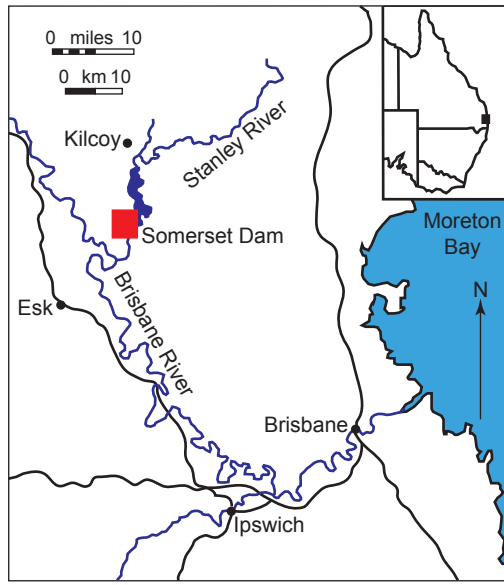

Figure 30. Location map for the Somerset Dam layered mafic intrusion near Brisbane on Australia's east coast (after *Mathison* [1967]).

are phase, modal mineralogy, and textural contacts. These macrolayers appear to be stratigraphically homogeneous. The repetition of these macrolayers has allowed the recognition of at least six well-developed cyclic units, ranging from 30 to 150 m thick (average about 80 m thick). The macrolayers are limited to only four main rock types, which are defined in terms of their essential cumulus mineral phases (distinguished texturally from the intercumulus mineral phases) [*Wager et al*., 1960; *Irvine*, 1982] (Figures 31 and 32). These four rock types constituting the macrolayers are leucogabbro or anorthosite (plagioclase cumulate), troctolite (plagioclase + olivine cumulate), olivine gabbro (plagioclase + augite + olivine cumulate), and oxide (or ferri-) gabbro (plagioclase + augite ± olivine + magnetite + ilmenite cumulate) [*Mathison*, 1967, 1987].

The definition of these cyclic units and which of these macrolayers commences each cycle is strongly influenced by what is expected to be the order of crystallization and the magma fractionation pattern,

because there is commonly no clear field evidence to identify the base or top of a cyclic unit. In the Somerset Dam layered gabbro intrusion, *Mathison* [1964, 1967, 1970, 1975] chose to define each cyclic unit to be the sequence troctolite–olivine gabbro–oxide gabbro–leucogabbro, because troctolite was considered the least fractionated rock type, and cryptic trends generally suggested a reversal at the bases of the

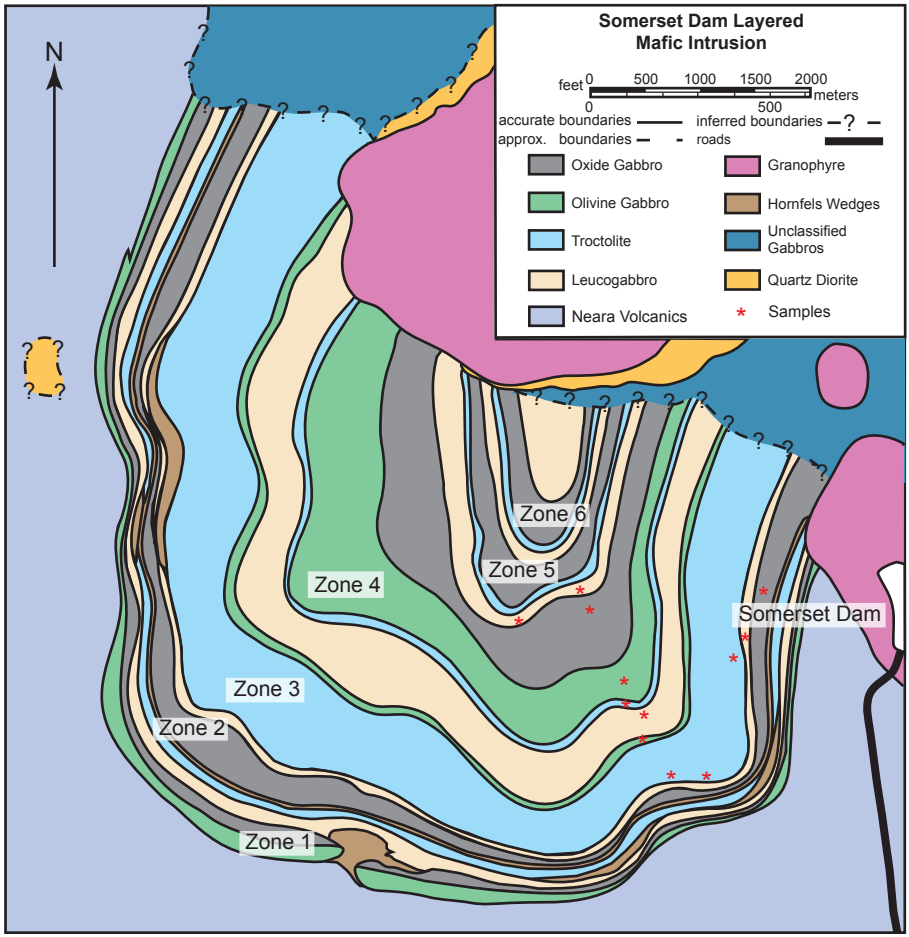

Figure 31. Detailed geologic map of the Somerset Dam layered mafic intrusion, southeast Queensland, Australia (after *Mathison* [1967]).

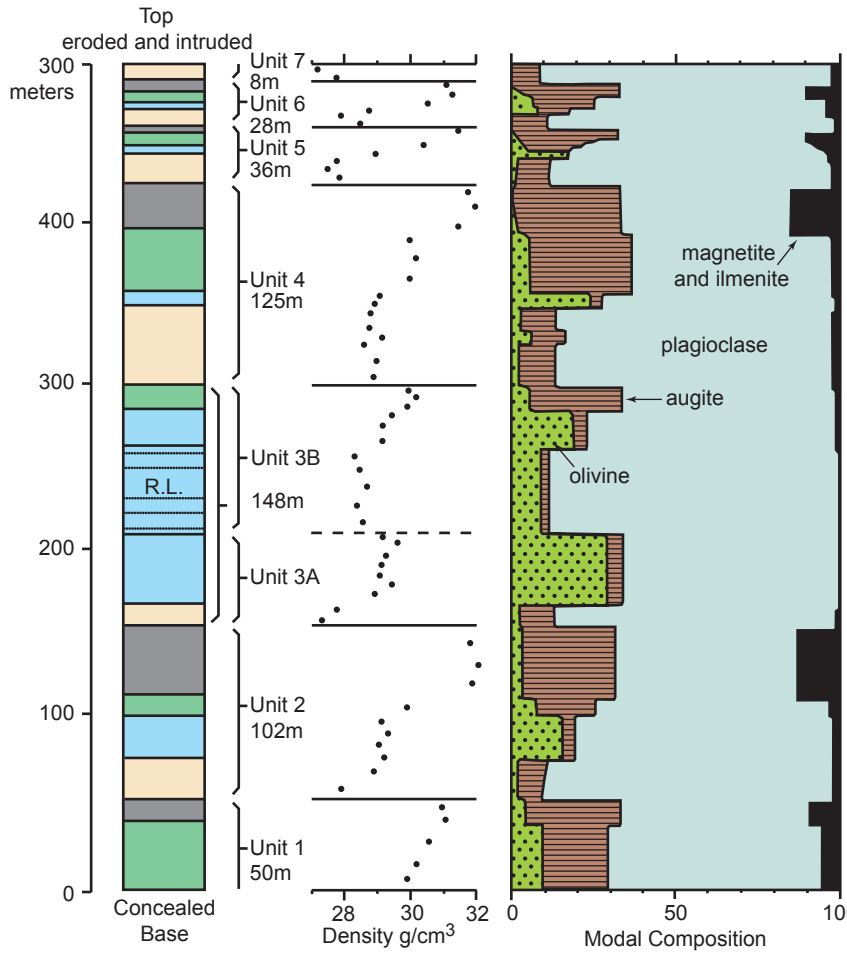

Figure 32. Stratigraphic column for the exposed portion of the Somerset Dam layered mafic intrusion (after *Mathison* [1987]) showing its inferred cyclic units, rock densities, and modal compositions. [= leucogabbro/anorthosite; = troctolite; = olivine gabbro; = oxide (ferri-) gabbro; R.L. = best developed zone of rhythmic layering]

troctolites. However, *Mathison* [1987] revised this choice of sequence in each cyclic unit so that anorthosite was defined as the basal layer and oxide gabbro as the top layer, the choice subsequently followed by

Walker [1998] (Figure 32). This interpretation better fits the inferred order of crystallization, the oxide gabbro being the most fractionated rock type. Of course, the mineralogy, and therefore the whole-rock compositions, of these macrolayers show marked changes between these rock types in this cyclical sequence [*Mathison*, 1967, 1987; *Walker*, 1998; *Snelling*, 2003b]. Despite the remarkable similarity of successive cyclic units, significant differences exist between them in the sequences of macrolayers, thicknesses of individual macrolayers and of the cyclic units, mineral compositions and cryptic patterns, average level of fractionation, and the sizes of reversals (Figure 32).

A total of eighteen whole-rock samples were collected along a farm road that traverses through the intrusion, commencing with samples of the oxide gabbro at the top of cyclic unit 2, and continuing progressively with samples of all the successive macrolayers for units 3 and 4 up to two samples of the anorthosite macrolayer at the base of unit 5 [*Snelling*, 2003b]. The locations of these samples are marked on Figure 31. Details of the petrography of the different macrolayers and the compositions of the minerals in them are provided by *Mathison* [1967, 1987] and are summarized by *Snelling* [2003b]. The samples collected for this study were comparable in major and trace element geochemistry to previous studies [*Mathison*, 1967, 1987; *Walker*, 1998; *Snelling*, 2003b].

A4. Cardenas Basalt, Eastern Grand Canyon

Mafic igneous rocks occur as sills, dikes, and flows in the thick succession of sedimentary strata making up the Middle Proterozoic Unkar Group of the Grand Canyon, Arizona (Figures 29 and 33). The Unkar Group sedimentary sequence is comprised of four formations—in ascending order, the Bass Limestone, Hakatai Shale, Shinumo Quartzite, and the Dox Formation—which are overlain by the 300 m+ thick flow sequence of lavas comprising the Cardenas Basalt [*Hendricks and Stevenson*, 1990, 2003]. The Upper Proterozoic sedimentary strata of the Nankoweap Formation and the Chuar Group overlie this Unkar Group succession, which unconformably rests on the Lower Proterozoic metamorphic and igneous crystalline basement [*Babcock*, 1990; *Ilg et*

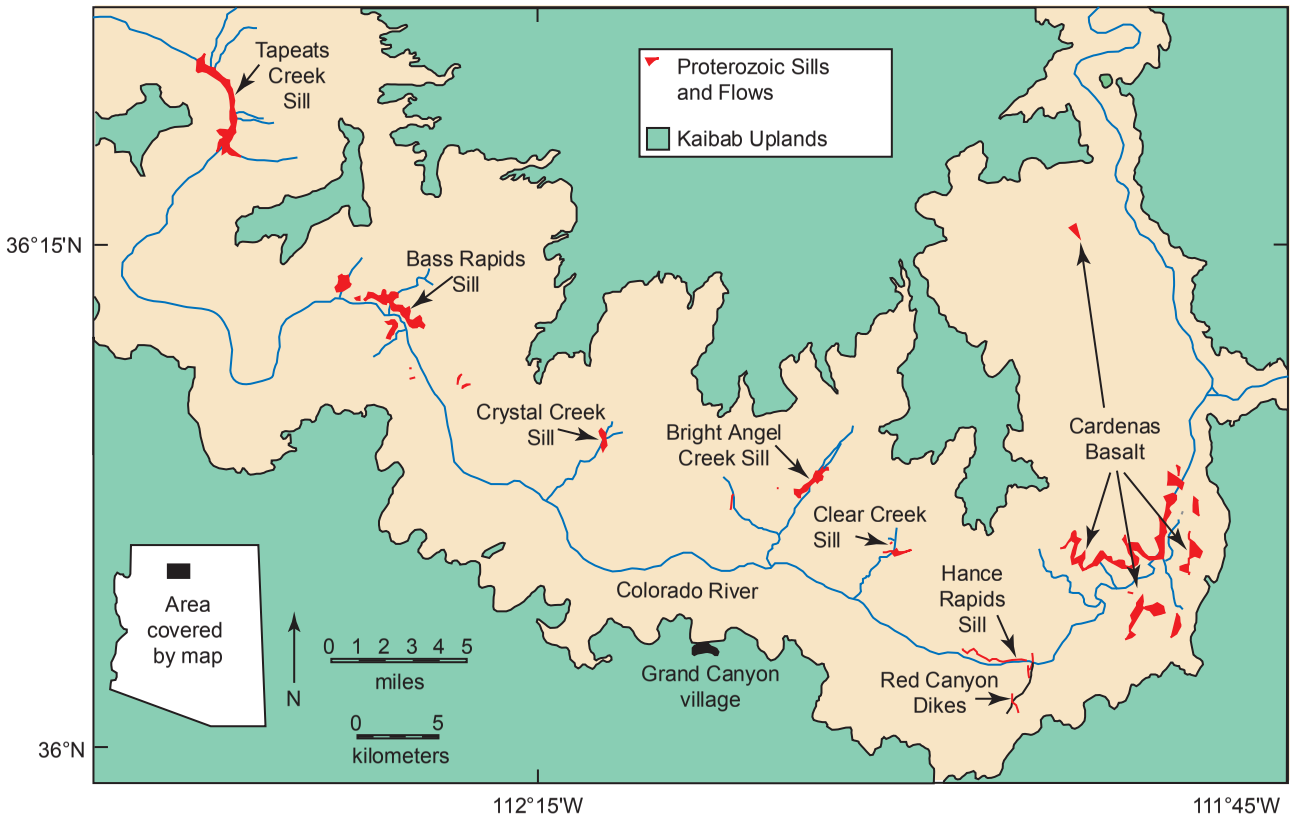

Figure 33. Location of the Cardenas Basalt and the related Middle Proterozoic named diabase sills and dikes in Grand Canyon, northern Arizona (after *Hendricks and Lucchitta* [1974]).

al., 1996; *Karlstrom et al*., 2003] (Figure 29).

The Cardenas Basalt crops out over an area of about 120 km^2 in the eastern Grand Canyon (Figure 33). Most of the Cardenas Basalt lavas are so little altered that primary flow and depositional features are well preserved [*Lucchitta and Hendricks*, 1983]. Several distinctive units within the lavas are good indicators of the depositional environment, and these units are laterally persistent, making it possible to correlate between individual sections. In the type section at Basalt Canyon (Figure 21, p. 447) [*Hendricks and Lucchitta*, 1974; *Hendricks*, 1989; *Larson et al*., 1994], the Cardenas Basalt consists of a 100 m-thick lower member composed of about six, coarsely ophitic flows of olivine basalt which vary in thickness from about 3 to 25 m. Beds of siltstone and sandstone 1.5 to 3 m thick occur between some of the flows. All flows possess vesicular tops and bottoms, and massive to columnar-jointed central portions. Typically this lower member is poorly exposed, weathering to spheroidal masses surrounded by granular debris. Before alteration, this medium-grained olivine basalt was similar in texture and mineralogy to the diabase sills and dikes intruded into the lower Unkar Group sedimentary strata in the central Grand Canyon (Figures 29 and 33). Petrological and geochemical data also appear to suggest that this lower member was originally a spilitic hyaloclastite, which would have been the altered effusive equivalent of those mafic intrusives. However, the spheroidal masses may simply have resulted from onion-skin weathering rather than being suggestive of pillow structures (and underwater extrusion), and therefore, the field evidence could indicate subaerial extrusion of these lower member basalts in a series of low-viscosity pahoehoe flows.

In contrast, the 200 m-thick upper member of the Cardenas Basalt comprises four to six aphyric, intersertal to intergranular flows that change sequentially from basaltic andesite to basalt and then back to basaltic andesite upward through the section (Figure 21). The dramatic change from the easily weathered, greenish ophitic flows of the lower member to the resistant, less-green, finer-grained flows of the upper member is indicative of this abrupt change in magma chemistry. Individual flows vary in thickness from about 20 to 50 m, each flow

being separated from adjacent flows by laterally persistent siltstone and sandstone beds that generally range in thickness from 0.3 to 3 m. The 40 to 50 m-thick lowermost flow displays both large-scale flow banding and rather abrupt thickness variations of about 8–10 m. Amygdaloidal zones, from 2 to 5 m thick, are common near the bases and tops of the flows, and scoriaceous flow breccias are conspicuous at the tops of several of them. Some of the flows exhibit crude columnar jointing in their middle to upper portions, but most also display irregular, hackly fractures. None of the flows exhibits any evidence (pillow structures, hyaloclastites) of interaction with water. Overall, the extent of the lava flow remnants outcropping in the eastern Grand Canyon (Figure 33) suggests an initial volume for the Cardenas Basalt of about 60 km^3. The relationship of the diabase sills and dikes (Figure 33) to the Cardenas Basalt flows remains obscure because direct feeders to the flows and sills have never been recognized.

Hendricks and Lucchitta [1974], *Hendricks* [1989], and *Larson et al.* [1994] describe in detail the petrography and chemistry of the Cardenas Basalt flows. All lower member flows appear to originally have consisted of 10–14 vol.% olivine, 45–50 vol.% plagioclase (labradorite), 18–20 vol.% augite (in subequant ophitic grains that enclose the plagioclase), 5 vol.% titanomagnetite and ilmenite, and 15–20 vol.% glass and crystallites (mesostasis). This mineral association and the ophitic texture mean the rock is appropriately classified as an olivine basalt. All these flows have been affected to some degree by post-extrusion alteration. Whereas it could be expected that this alteration may have changed the original rock chemistry, *Larson et al.* [1994] used an isocon (short for "same concentration") plot to show that these rocks have probably undergone minimal enrichment or depletion of individual major-element oxides during hydration, an important observation relevant to the suitability of these lava flows for radioisotope analyses. Otherwise, the chemistry of these lower member lava flows suggests a tholeiite, but is also compatible with a high-alumina basalt of shoshonitic affinities.

Flows of the upper member vary in texture from intersertal to intergranular, and are much finer grained than those of the lower member. *Larson et al.* [1994] concluded from sporadic occurrence of

pigeonite (clinopyroxene), the aphyric texture, and the modal olivine content ranging from a trace to 10 vol.%, that all of the flows can be classified as tholeiitic olivine basalts or basaltic andesites. The variable chemical alteration of the upper member flows is generally similar to that of the lower member flows, but is often less extensive. *Larson et al.* [1994] also concluded that some of the major element chemical variations between the upper member flows appear to be related to initial differences in the magma composition. SiO_2 and K_2O steadily decrease upwards for the lower four upper-member flows and then increase abruptly in the upper two, whereas CaO and MgO display the opposite behavior. The lowermost upper-member flow, which is the most felsic, corresponds to an andesite, while the three flows above it can be classified as basaltic andesite to basalt, as they become progressively less felsic upward in the sequence. The two uppermost flows also appear to be andesites. Alternately, based on the normative compositions, the more mafic flows are quartz tholeiites, while the more SiO_2-rich flows are tholeiitic andesites (or icelandites).

A total of nineteen samples of the Cardenas Basalt were collected, all but two of them from the Basalt Canyon type section (Figure 21), one of the best and most studied outcrops. Because the Basalt Canyon section has poor exposure of the lower third of the Cardenas Basalt, two samples were collected from the superior exposure of the lower 15 m at Lava Chuar Canyon (Figure 21) [*Austin and Snelling*, 1998].

A5. Diabase Sills, Central Grand Canyon

The diabase sills and dikes of the central Grand Canyon (Figure 33) are believed to be the intrusive equivalents of the Cardenas Basalt lava flows, but they are not found in direct association with them [*Hendricks and Lucchitta*, 1974; *Hendricks*, 1989]. Thus the relationship between them is obscure, because the direct feeders to the flows have never been recognized among the available diabase outcrops. The diabase sills are, in fact, confined to the lower part of the Unkar Group, particularly intruding near the contact between the Bass Limestone and Hakatai Shale, while the related dikes are intruded into all the formations above

the sills along faults that predate, or are contemporaneous with, the sills (Figure 29). These mafic sills crop out in seven locations along a 70–80 km length of the Grand Canyon (Figure 33), whereas the Cardenas Basalt flows are restricted to the area around Basalt Canyon in the eastern Grand Canyon. The sills range in thickness from about 20 m (about 65 ft) near Hance Rapids in the east to more than 200 m (655 ft) near Tapeats Creek in the west. Thicknesses of the other sills include 23 m along Clear Creek, 140 m along Bright Angel Creek, a minimum of 100 m along Crystal Creek, and 100–150 m in the vicinity of Bass Rapids and Shinumo Creek, while nearby in Hakatai Canyon, the latter sill is reported to be 300 m thick [*Noble*, 1914].

All of these diabase sills are composed chiefly of medium-grained ophitic olivine-rich diabase that is uniform in texture and mineralogy, as well as in chemistry, from sill to sill through the Canyon [*Hendricks and Lucchitta*, 1974; *Hendricks*, 1989]. The dikes have a similar composition but are finer grained. All the diabase sills have fine-grained chilled margins about 30 cm to less than 1 m thick, which suggests that the magma was highly fluid at the time of intrusion [*Hendricks and Stevenson*, 1990, 2003]. All the sills show varying amounts of early in-place differentiation and crystal settling that is evidenced by syenite lenses up to 10 m thick and felsite dikes, as well as by layers which are richer in olivine. The sill in the Bass Rapids-Shinumo Creek area is unique in that it displays distinct layers of differentiation and segregation products, with a well-defined 6 m (20 ft) thick granophyre layer on top of the 85 m (280 ft) thick diabase. Contact metamorphism caused by intrusion of the diabase sills resulted in the formation of chrysotile asbestos above the sills where the magma intruded the Bass Limestone. On the other hand, where the sills intrude the Hakatai Shale, it has been altered into a knotted hornfels.

The diabase sills and dikes are mineralogically similar to the lower member flows of the Cardenas Basalt [*Hendricks and Lucchitta*, 1974; *Hendricks*, 1989]. Chemical variation diagrams also indicate a potential common parentage for the diabase in the sills and the lower member flows of the Cardenas Basalt. However, the upper member flows of the Cardenas Basalt are much more silicic than the diabase sills, and

therefore, it has been concluded that they probably were not emplaced during the same phase of igneous activity. Nevertheless, the similarity in mineral composition of the unaltered lower member basalt flows and of the diabase sills suggests that the lavas and the diabase sills were co-magmatic and probably coeval. Indeed, *Larson et al.* [1994] found that the main observable difference between the lower-member basalt flows and the diabase sills is in the color of the augite in thin section, being commonly pink-brown to purplish brown in the diabase due to a content of about 2.5 wt% TiO_2, compared to being colorless to light grey in the basalt due to a content of <1 wt% TiO_2. Thus it has been concluded that the upper member lavas of the Cardenas Basalt (the top two-thirds of the sequence) were extruded after differentiation of the parent magma, which would account for their higher silica content. This conclusion is supported by paleomagnetic observations that suggest the diabase sills may be slightly older than the Cardenas Basalt flows [*Elston and Grommé*, 1974; *Elston*, 1989]. Indeed, *Elston* [1986] indicated that the paleomagnetic evidence suggests the majority of the sills were intruded at the same time that the upper Dox Formation was being deposited. Nevertheless, some of the diabase dikes in the eastern Grand Canyon have paleomagnetic pole positions similar to the Cardenas Basalt and may represent feeders. However, these dikes are not seen connected to either the Cardenas Basalt flows or to the nearby Hance Rapids sill (Figure 33). Nevertheless, the diabase sills and dikes, and the Cardenas Basalt flows are still regarded overall as representing a single volcanic episode, in which the earliest phases were the intrusion of the diabase sills, followed by a period of quiescence during continued deposition of the Dox Formation before the later phases when eruptions of basalt and basaltic andesite flows occurred via a network of thin dikes [*Hendricks and Stevenson*, 1990, 2003].

Larson et al. [1994] also found that, whereas the major-element chemistry of the diabase sills exhibited similarities and dissimilarities with the lower-member flows of the Cardenas Basalt [*Hendricks and Lucchitta*, 1974], the trace and rare earth element data from a sample of the Hance Rapids sill shows very similar variation patterns to those in the lower-member flows of the Cardenas Basalt. Only the Ti

and P contents were markedly higher in the sill, and the negative Eu (europium) anomaly for the sill was smaller than that for the lower-member Cardenas Basalt flows. Thus, *Larson et al*. [1994] suggested a common origin for the diabase of the sills and the basalt of the lower-member flows similar to continental flood basalts, except that the higher Ti and P contents of the diabase may indicate that the magma that fed the intrusions did not also directly feed the flows of the lower member. Alternately, they suggested that the higher silica (SiO_2), Ti, and P contents of the basalt flows were due either to greater crustal contamination of the basalt magma on its passage to the earth's surface, or heterogeneity in the mantle source.

A total of nineteen samples from these diabase sills were collected for this study [*Austin and Snelling*, 1998; *Snelling et al*., 2003a]. These included two samples from the Hance Rapids sill (Figure 33), two samples from the Red Canyon dikes, a single sample from the Bright Angel Creek sill, three samples from the Tapeats Creek sill, and eleven samples from the Bass Rapids sill. The eleven samples collected through the sill at Bass Rapids (north bank of the Colorado River at mile 107.6–108.0) were from a composite section, the same section sampled by *Hendricks and Lucchitta* [1974] some 800 m east of Shinumo Creek. The samples were chosen to represent the overall petrographic variability within the complete thickness of the sill, as depicted in Figure 20 (p. 445), with three samples from the 6 m thick granophyre layer at the top of the sill, and eight samples from the 85 m thick main body of the diabase sill.

The Bass Rapids sill is similar to the other sills within the Unkar Group being composed of olivine diabase, but it is uniquely capped by granophyre (Figure 20), making this sill a classic example of in-place differentiation of a basaltic magma. The 6 m-thick granophyre consists predominantly of K-feldspar (55–60%) and quartz (12–25%), with biotite, plagioclase, some clinopyroxene, and titanomagnetite making up the remaining 20–28%. The rock is holocrystalline, coarse-grained, and has a well-developed granophyric texture in which quartz, plagioclase, biotite, clinopyroxene, and titanomagnetite fill interstices between the orthoclase crystals. The transition between the granophyre

and diabase below occurs over a vertical distance of <1 m and is a zone rich in biotite and accessory minerals [*Hendricks*, 1989]. Apatite makes up as much as 5–10% of the rock, while ilmenite and sphene are prominent, and zircon with reaction halos occurs within the biotite grains.

The olivine diabase interior of the sill is medium- to coarse-grained, containing plagioclase (30–45%), olivine (20–35%), clinopyroxene (15–20%), titanomagnetite and ilmenite (5%), and biotite (1%), with accessory apatite and sphene. The texture is diabasic to subophitic, although a crude alignment of feldspar laths can be seen in many places. The olivine concentration tends to increase towards the center of the sill, whereas the clinopyroxene decreases. Immediately below the granophyre the diabase contains about 5% modal olivine, which increases rapidly to 20–30% through the central part of the sill [*Hendricks and Lucchitta*, 1974]. About 15 m above the base of the sill is an olivine-rich layer that contains about 50% modal olivine, and then the olivine content of the diabase decreases to about 10% near the base. *Hendricks and Lucchitta* [1974] and *Hendricks* [1989] have suggested that this distribution of the olivine in the sill can be explained by the process of flow differentiation, which involves the movement of early-formed olivine grains away from the margins of the sill during flow of the intruding magma [*Bhattacharji and Smith*, 1964; *Bhattacharji*, 1967; *Simkin*, 1967]. It is envisaged that, as the magma intruded up through the conduit and then outward to form the sill, fluid-dynamic forces concentrated toward the center of the moving mass the olivine crystals that had formed early in the cooling history of the magma, even before the emplacement of the sill. As the magma also moved laterally, gravity acting on the olivine crystals would have produced a gradational change in the olivine content from the lower contact upward, while causing an abrupt change in olivine from the upper contact downward. Once emplaced, crystallization of the remaining liquid magma within the sill would then have yielded the remaining minerals in relatively constant proportions [*Simkin*, 1964]. Although there is a general uniformity of the diabase throughout the sill, there are two types of textural variation, first described by *Noble* [1914]. First, there are "lumps" or "balls"

similar in mineralogy to the surrounding diabase, but the plagioclase laths in the lumps are up to 7.5 mm in length and fill embayments in large olivine crystals. Second, pegmatite veins consisting of plagioclase and augite with a very similar texture are found in the upper part of the sill. These textural variations undoubtedly represent segregation features produced during crystallization of the sill.

The lower chilled margin and contact of the Bass Rapids sill with the underlying Hakatai Shale is covered, but is probably similar to the fine-grained chilled margins found in most of the other sills intruding the Unkar Group in Grand Canyon. The upper contact of the sill is marked by the 6 m-thick capping of granophyre, the contact with the overlying Hakatai Shale is sharp (Figure 20), and no xenoliths of Hakatai Shale are found in the granophyre, suggesting that it was not produced by assimilation of the shale. Instead, the transition zone between the granophyre and the diabase beneath it in the sill suggests that the granophyre was a residual magma that "floated" to the top of the sill as the diabase crystallized, so that there was little late-stage mixing of it with the diabase part of the sill [*Hendricks and Lucchitta*, 1974].

Contact metamorphism of the Hakatai Shale has occurred above and below the sill, the shale being altered to a knotted hornfels (Figure 20). This contact metamorphism is greater below the sill than above it. The hornfels below the sill extends for 5 m below the contact and forms a prominent outcrop, from which two samples were collected. No recrystallization of the shale has occurred beyond 5 m below the sill contact, while the mineralogy of the metamorphism (biotite, andalusite, and cordierite[?] porphyroblasts) suggests that it was of low–medium grade.

A6. Apache Group Basalts and Diabase Sills, Central Arizona

In a large area of central and southern Arizona, Middle Proterozoic rocks are represented by the Apache Group, the Troy Quartzite, and co-extensive diabase sills (Figure 34) [*Shride*, 1967; *Wrucke*, 1989]. These sedimentary strata, basalt flows, and diabase sills are regarded, due to their stratigraphic position and lithologic similarities, as correlative

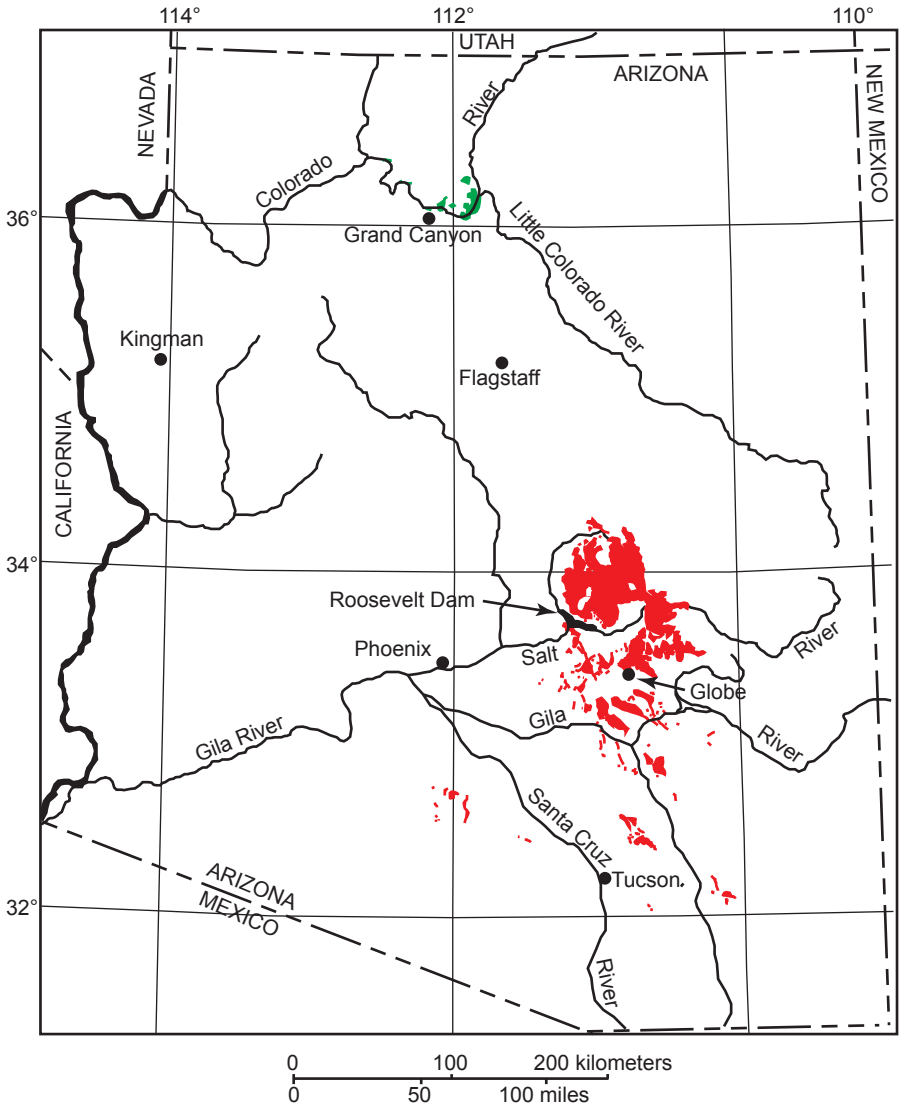

Figure 34. Outcrop areas of the Middle Proterozoic Apache Group, Troy Quartzite, and associated basalts and diabase sills in central and southern Arizona (red), and of the Middle Proterozoic Unkar Group (including the Cardenas Basalt) and associated diabase sills in Grand Canyon, northern Arizona (green) (after *Shride* [1967]; *Wrucke* [1989]).

with the Unkar Group sedimentary strata, Cardenas Basalt, and the related diabase sills in Grand Canyon [*Shride*, 1967; *Elston*, 1989; *Wrucke*, 1989; *Hendricks and Stevenson*, 1990, 2003; *Larson et al*., 1994] (Figure 34). Indeed, *Elston* [1986, 1989] reviewed the correlation of various Middle and Upper Proterozoic sequences on a paleomagnetic basis and found that a paleomagnetic pole from the Mescal Limestone of the Apache Group correlates with poles from the Dox Formation. Furthermore, the diabase sills that intrude both the Apache Group and Troy Quartzite are similar paleomagnetically to the diabase sills in the Unkar Group of Grand Canyon, their respective paleomagnetic poles also correlating with the paleomagnetic poles from mafic intrusions in the Keweenawan Supergroup of the Lake Superior region of the U.S.A. Thus, *Larson et al*. [1994] correlate the diabase sills in the Unkar Group of Grand Canyon and the Apache Group of central Arizona with a number of other Middle Proterozoic mafic and related intrusions around the southwest U.S.A., and in the Belt Supergroup of the northwest U.S.A. and southwestern Canada, as well as those in the Midcontinent Rift System across to the northeastern U.S.A.

The Apache Group and Troy Quartzite crop out in a roughly triangular area of about 20,000 km^2 in central and southern Arizona (Figure 34). The Apache Group sedimentary strata range in thickness from 380 to 490 m and consist, in ascending order, of the Pioneer Shale, the Dripping Spring Quartzite, the Mescal Limestone, and unnamed basalt flows (Figure 35), while the Troy Quartzite has a maximum thickness of 365 m [*Shride*, 1967; *Wrucke*, 1989]. The Pioneer Shale consists of a basal conglomerate overlain by silty mudstone, siltstone, and arkose. The dominant silty mudstone is characteristically greyish-red to dusk red-purple because it largely consists of water-laid rhyolitic tuff [*Gastil*, 1954]. The unconformably overlying Dripping Spring Quartzite also consists of a basal conglomerate overlain by a mostly thick-bedded arkose that grades through a 1–2 m interval into a largely thin-bedded siltstone. The Mescal Limestone unconformably overlies the Dripping Spring Quartzite (Figure 35), and comprises three members: a lower thin- to medium-bedded member of cherty dolomite, or of calcitic limestone that is its metamorphic equivalent, a middle partly massive

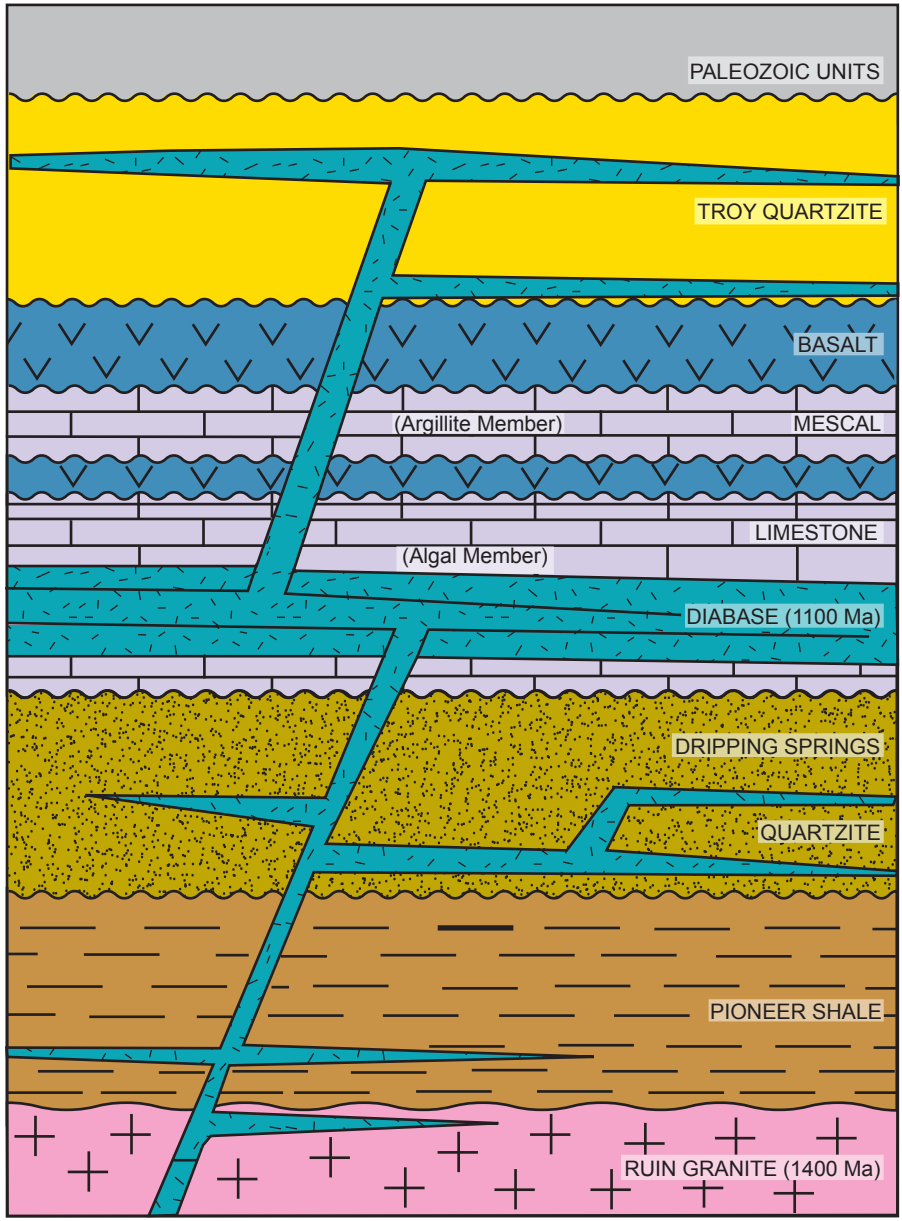

Figure 35. Schematic stratigraphic column of the Apache Group, Troy Quartzite, and associated basalts and diabase sills in central Arizona (modified from *Shride* [1967]; *Wrucke* [1989]).

algal member of similar carbonate, and an upper argillite member. The algal member rests conformably on the lower cherty dolomite member and consists of a thick-bedded dolomite containing columnar branching colonies of stromatolites and biostromes having great lateral continuity, that are overlain by a thin-bedded dolomite with chert that contains filamentous chains and spherules identified as replacements of blue-green algae [*McConnell*, 1974]. The argillite member of the Mescal Limestone (Figure 35) mostly rests directly on the algal member with a disconformable contact, except in a few places where an angular unconformity is evident. It consists of a basal unit of chert, chert breccia, and chert conglomerate overlain by argillite that makes up most of the unit and contains minor amounts of silicified limestone.

Basalt flows occur at two stratigraphic positions high in the Apache Group sequence. Throughout the region the principal occurrences separate the overlying Troy Quartzite from the Mescal Limestone of the Apache Group. At two localities, in the Sierra Ancha mountains north of the Salt River and at Roosevelt Dam (Figure 34), petrographically similar basalt flows with a maximum thickness of 34 m are found between the algal and argillite members of the Mescal Limestone. The two sequences of basalt flows in their juxtaposition below and above the argillite member of the Mescal Limestone are best exposed in cliff faces in the southern part of the Sierra Ancha [*Shride*, 1967]. The sequence of basalt flows stratigraphically above the Mescal Limestone is commonly 10–25 m thick, but locally reaches 75–115 m. Though abundant hematite is disseminated throughout these lava flows they are still recognizable as basalt due to their dark aphyric appearance and evidence of an intersertal to intergranular texture defined by tiny plagioclase laths. The basalt has a highly altered, fine-grained groundmass of albite, chlorite, and other minerals, and sparse to abundant tabular former plagioclase phenocrysts. Vesicles and amygdules are especially abundant in the tops and bottoms of the flows, with ropy flow breccias being conspicuous in places. Thus the basalt formed as subaerial flows which were very fluid. No feeder dikes for these lavas have been found.

The angular relations of the unconformity that separates the Troy Quartzite from the Apache Group are apparent only on a regional scale.

The Apache Group strata were broadly warped, then eroded before deposition of the Troy Quartzite, which thus rests in different places on the different formations of the Apache Group. The Troy Quartzite consists from the base upward of an arkose member, a prominent sandstone member, and a quartzite member, which together obtain a maximum thickness of 365 m.

In nearly every locality where the Apache Group and Troy Quartzite are exposed, diabase sills are associated with them, and dikes, although volumetrically insignificant, are locally numerous. The diabase sills and dikes were emplaced in the Apache Group almost to the exclusion of other formations, but in places extensive bodies also intruded the Troy Quartzite and the older Precambrian basement consisting of metamorphic rocks and the Ruin Granite. Paleozoic formations rest unconformably on the diabase sills, indicating some erosion of the overlying strata after emplacement, and/or a shallow depth of emplacement. Over large areas along the Salt River Canyon and in the Sierra Ancha, the aggregate volume of the diabase sills is as great as the combined volume of the exposed Apache Group and Troy Quartzite strata.

The diabase sills typically are tens of meters thick. The maximum verified thickness of a single diabase sill is about 400 m in the Sierra Ancha [*Shride*, 1967]. Diabase sills as much as 1000 m thick have been reported, but they almost certainly are compound bodies consisting of two or more separate intrusive sheets. Laterally extensive diabase bodies formed by multiple sill intrusions are known throughout the region (exposed in the walls of one of the large open cast mines and of the Salt River Canyon), and can be recognized by the chilled margins of the younger rock against the older, and locally by tabular septa of host strata that commonly remain where a second intrusion was emplaced approximately along the contact with the first. The second intrusion passed around and isolated the remnants of country rock.

All the diabase sills are locally discordant to the host strata. Some cross the layering of the host rocks at low angles as simple tabular bodies having planar contacts, while others have discordant step-like breaks across strata and relatively short vertical and horizontal segments. Sills

commonly end at high-angle contacts that can be distinguished between faults by the chilled diabase along the steep termination, although faults may extend above or below and contain dikes. The diabase sills tend to follow certain stratigraphic horizons with remarkable persistence. For example, sills 0.5 m thick are traceable for 1.5 km, while some thicker sills crop out for at least 30 km. Commonly the diabase sills occur along horizons that separate strata of contrasting competency or along nearby horizons in incompetent rocks. Great volumes of diabase invaded the Ruin Granite at shallow depth below the Apache Group, at horizons a few meters below the top of the Pioneer Shale, within the upper siltstone member of the Dripping Spring Quartzite, within the lower cherty dolomite member of the Mescal Limestone at positions about 12 and 40 m below the upper contact, and between the algal and argillite members of the Mescal Limestone [*Bergquist et al*., 1981]. Diabase sills are widespread along the unconformity between the Mescal Limestone and the Troy Quartzite, and between the Troy Quartzite and the basalt that locally overlies the Mescal Limestone. One thick sill in the Sierra Ancha is in the quartzite member of the Troy Quartzite. Possibly the stratigraphic horizon having the greatest volume of diabase is that near the top of the Pioneer Shale.

The diabase typically is a dark-grey to greenish-black rock that is aphanitic to fine-grained at chilled margins and medium- to coarse-grained and subophitic to ophitic in the interior of the sills. Plagioclase, clinopyroxene, and olivine are the common minerals, so the rock is best classified as an olivine diabase. The distinguishing characteristic of the diabase in these sills compared to similar mafic rocks elsewhere is the unusually coarse grain size of the ophitic and subophitic phases. The plagioclase laths are commonly 1–4 mm long (sometimes 4–8 mm long), and the pyroxene crystals are commonly 5–20 mm across (often 30–50 mm across), in contrast to plagioclase crystals 0.25–2 mm long and pyroxene crystals less than 5 mm across in the well-known Palisade diabase sill in New Jersey [*Walker*, 1940].

Most petrographic studies of the Apache Group diabase have been based on the principal intrusion, the 400 m thick Sierra Ancha sill, emplaced in the upper member of the Dripping Spring Quartzite

[*Nehru and Prinz*, 1970; *Smith*, 1970]. The sills have almost knife-sharp contacts with their host rocks, but the effects of chilling of the diabase can sometimes be seen as far as 10 m from the margins of the sills. The chilled diabase is very fine grained, and progressing to the interior of the sills the diabase becomes a fine-grained felted mat of plagioclase laths and interstitial mafic grains which grade rapidly into subophitic diabase. In the interiors of the sills the ophitic and subophitic diabase consists of plagioclase (labradorite) (45–70%), clinopyroxene (10–40%), orthopyroxene (0–7%), olivine (0–20%), and accessory minerals (3–15%). Augite is the most abundant clinopyroxene and pigeonite is present in small amounts. Hypersthene (orthopyroxene) is sparse, while olivine occurs as small equant grains. Biotite is present in accessory amounts with magnetite, and other accessory minerals include ilmenite, apatite, sphene, zircon, and sparse pyrite and chalcopyrite. Olivine is generally dispersed throughout the sills, although in some of the thicker sills it is concentrated slightly below the middle of the intrusions, similar to the Bass Rapid diabase sill in Grand Canyon.

Felspathic rocks locally are conspicuous in the diabase, and such differentiates include microtroctolite (a plagioclase-olivine rock), aplite (microgranite), pegmatite, and granophyre. Generally these differentiates make up only a small fraction of any sill, except in the 400 m thick Sierra Ancha sill where the microtroctolite that occupies the middle part of the sill is 70 m thick [*Nehru and Prinz*, 1970]. The fair-to-good alignment of the plagioclase crystals parallel to the top and bottom of the microtroctolite zone indicates that the mass was emplaced by flowage differentiation of a crystal mush during the main crystallization phase of the diabase [*Smith*, 1970]. Otherwise, the largest feldspathic masses associated with the Sierra Ancha diabase sill are discontinuous pods of granitic rocks up to 50 m thick at the top of the sill. These consist of various proportions of microgranite and granophyre, and there is some evidence to suggest that, rather than being the result of differentiation of the parent magma during crystallization of the sill, the granophyre represents felspathic country rock material that has become fused at the contact with the diabase [*Smith and Silver*, 1975].

Thermal contact metamorphism resulting from emplacement of the

diabase sills affected the carbonate rocks of the Apache Group on a regional scale, and in many localities caused widespread changes in siliceous rocks [*Wrucke*, 1989]. The dolomite of the Mescal Limestone nearly everywhere was converted to limestone (by removal of Mg, probably by hydrothermal fluids), but the stratification and other sedimentary structures were preserved sufficiently to mask the metamorphosed character of the rocks. Chrysotile asbestos was locally produced in veins by the alteration processes during emplacement of the diabase sills, similar to that produced in the Bass Limestone of Grand Canyon. In the feldspar-rich sedimentary rocks contact metamorphism produced granophyre, and with increased induration, hornfels and spotted hornfels. Where the diabase sills are thin, felspathic rocks were metamorphosed for only a meter or so adjacent to the contact, but where the sills are thick or numerous, entire formations have been affected. Even the basalt flows have been albitized, recrystallized, and veined by epidote adjacent to some diabase sills, confirming that the diabase sills are younger.

Based on chemical analyses of samples from the sills, most of the diabase would be classified as olivine tholeiite with normative hypersthene and olivine, but a few minor sills consist of diabase that is quartz tholeiite, due to having normative quartz. It has been suggested that an original olivine tholeiite magma produced by partial melting in the mantle could have then differentiated at depths of 30–35 km into the high-alumina olivine tholeiite resembling the olivine diabase in most of the sills. However, if the same original olivine tholeiite magma fractionated at shallow crustal depths, a quartz-normative tholeiite magma would have been produced to be emplaced as quartz tholeiite diabase sills. Because the older basalt flows appear to have originally been olivine basalts, it is possible they were derived from the same olivine tholeiite magma that subsequently was intruded as the diabase sills. Emplacement of the diabase sills is thought to have been generally passive, as evidenced by the persistent planar strata above and below both thick and thin sills. Local small-scale folds and minor bedding-plane faults and thrusts found along and near discordant contacts indicate

that some shouldering action took place in response to the intrusive activity. It is envisaged that the diabase magma welled up along feeder dikes and seeped out along bedding planes, inflating the tabular masses of strata by hydraulic action of the magma aided by the buoyancy of the host rocks compared to the denser diabase magma. At some localities, such as now exposed in the Salt River Canyon, continued flooding of the magma caused two or more infiltrations of the diabase to produce adjacent sills, or even sills intruded into other sills. Whether diabase magma inflation was relatively continuous (although episodic at a given locality), or was accomplished in several stages, is not known.

For the purposes of this present study both the Apache Group basalts and the diabase sills were sampled from road cuts along highways. The basalt flows between the algal and argillite members of the Mescal Limestone (Figure 35) were sampled in a road cut south of Globe, and near the wall of the Roosevelt Dam (Figure 34). At the latter location the full sequence of basalt flows was exposed and five samples were collected. Similarly, the basalt flows between the Mescal Limestone and Troy Quartzite (Figure 35) were found exposed in a road cut between the town of Superior and the Ray copper mine, and three samples were collected. Samples of diabase sills intruded into the Apache Group sedimentary strata and the Ruin Granite were sampled from road cuts on State Route 60 north of Globe. Three samples of diabase sills intruded into the Ruin Granite, a sample of a diabase sill intruded near the base of the Pioneer Shale, a sample of a diabase sill intruded into the lower member of the Mescal Limestone, and three samples of a diabase sill intruded into the Dripping Springs Quartzite, as well as samples of diabase dikes cross-cutting the Dripping Springs Quartzite and the Pioneer Shale, were collected. Additionally, twenty-three samples were collected on State Route 60's traverse from the Salt River up the north wall of the Salt River Canyon, where the sills are thick and multiple injections of diabase magma have occurred. These sills intrude between the lower cherty dolomite and algal members of the Mescal Limestone, and between the algal member of the Mescal Limestone and the overlying Devonian Martin Formation, the Troy

Quartzite being missing in this section [*Wrucke*, 1989].

A7. Brahma Schist Amphibolites, Grand Canyon

The east-west trending Grand Canyon transect presents spectacular exposures of the Lower Proterozoic (Paleoproterozoic) rocks that represent the crystalline basement under the Colorado Plateau [*Karlstrom et al*., 2003]. In the Upper Granite Gorge, these rocks are continuously exposed from river mile 78 to 120, while there are discontinuous exposures in the Middle Granite Gorges from mile 127 to mile 137 (Figure 36) ([*Ilg et al*., 1996; *Karlstrom et al*., 2003]. *Powell* [1876] was the first to identify the Precambrian "granite" and "Grand Canyon schist." *Walcott* [1894] identified the Vishnu "terrane" as a complex of schist and gneiss. Subsequently, *Campbell and Maxson* [1938] identified different mappable units called the Vishnu "series" and Brahma "series" [*Maxson*, 1968]. However, Campbell and Maxson under-estimated the structural complexities and probably over-estimated the stratigraphic thickness when they proposed that the combined stratigraphic sequence of these metasedimentary and metavolcanic rocks was 8–16 km thick. This stratigraphic approach was called into question by *Ragan and Sheridan* [1970], and subsequently Brown *et al*. [1979] also emphasized the complex deformational features, so they lumped all of the metasedimentary and metavolcanic rocks together under the name "Vishnu Complex," the approach continued by *Babcock* [1990], who used the term "Vishnu Metamorphic Complex."

More recent detailed field mapping, based on the approach that recognizes the need to simultaneously pursue both tectonic and stratigraphic subdivisions of these Lower Proterozoic rocks, has resulted in a new geologic map (Figure 36) [*Ilg et al*., 1996; *Karlstrom et al*., 2003]. Thus, *Ilg et al*. [1996] and *Karlstrom et al*. [2003] have proposed the new name of Granite Gorge Metamorphic Suite for the entire sequence of metamorphosed volcanic and sedimentary rocks in the Grand Canyon. Furthermore, the new names assigned to the mappable rock units in the Upper and Middle Granite Gorges (Figure 36), as well as the Lower Granite Gorge, are Brahma Schist for the

mafic metavolcanic rocks (after the Brahma "series" of *Campbell and Maxson* [1938]), the Rama Schist for the felsic metavolcanic rocks, and Vishnu Schist for the metamorphosed sedimentary rocks, as probably intended by *Walcott* [1894], recommended by *Noble and Hunter* [1916] (their Vishnu schist), and proposed by *Campbell and Maxson* [1938] (their Vishnu "series"). These metasedimentary and metavolcanic rocks of the Granite Gorge Metamorphic Suite make up about half of the exposed rocks in the Granite Gorges of Grand Canyon, the rest being intrusive rocks (granites, granodiorites, tonalites, and gabbros). Descriptive metamorphic rock names are used for the rocks seen in outcrop and in thin section, and the original sedimentary or volcanic "protoliths" are inferred from rock compositions and a limited number of primary structures that have survived the deposition and metamorphism. Primary structures such as relict pillows and graded bedding show that the original sedimentary rocks were locally deposited on a volcanic sequence, and that the mafic and felsic metavolcanic rocks are commonly interlayered. However, because similar volcanogenic sequences could have been deposited at different times or in separate basins, and such differences would be difficult to unravel due to the subsequent tectonism, this terminology can be considered mainly as lithologic, rather than necessarily stratigraphic.

The Rama Schist consists of quartzofeldspathic schist and gneiss with locally preserved phenocrysts of quartz and feldspar, and possible relict lapilli, that suggest a felsic to intermediate volcanic origin [*Ilg et al*., 1996; *Karlstrom et al*., 2003]. It is dominated by massive fine-grained quartzofeldspathic rocks, but also contains metarhyolites and interlayered micaceous quartzofeldspathic schists and gneisses. The Rama Schist is commonly complexly injected with pegmatite and contains leucocratic layers that may in part reflect preferential partial melting of these rocks due to the peak metamorphic conditions of about 720°C and 6 kbar [*Ilg et al*., 1996; *Hawkins and Bowring*, 1999]. It is also locally interlayered with the mafic Brahma Schist.

The Brahma Schist consists of amphibolite, hornblende-biotite-plagioclase schist, biotite-plagioclase schist, orthoamphibole-bearing schist and gneiss, and metamorphosed sulfide deposits [*Ilg et al*.,

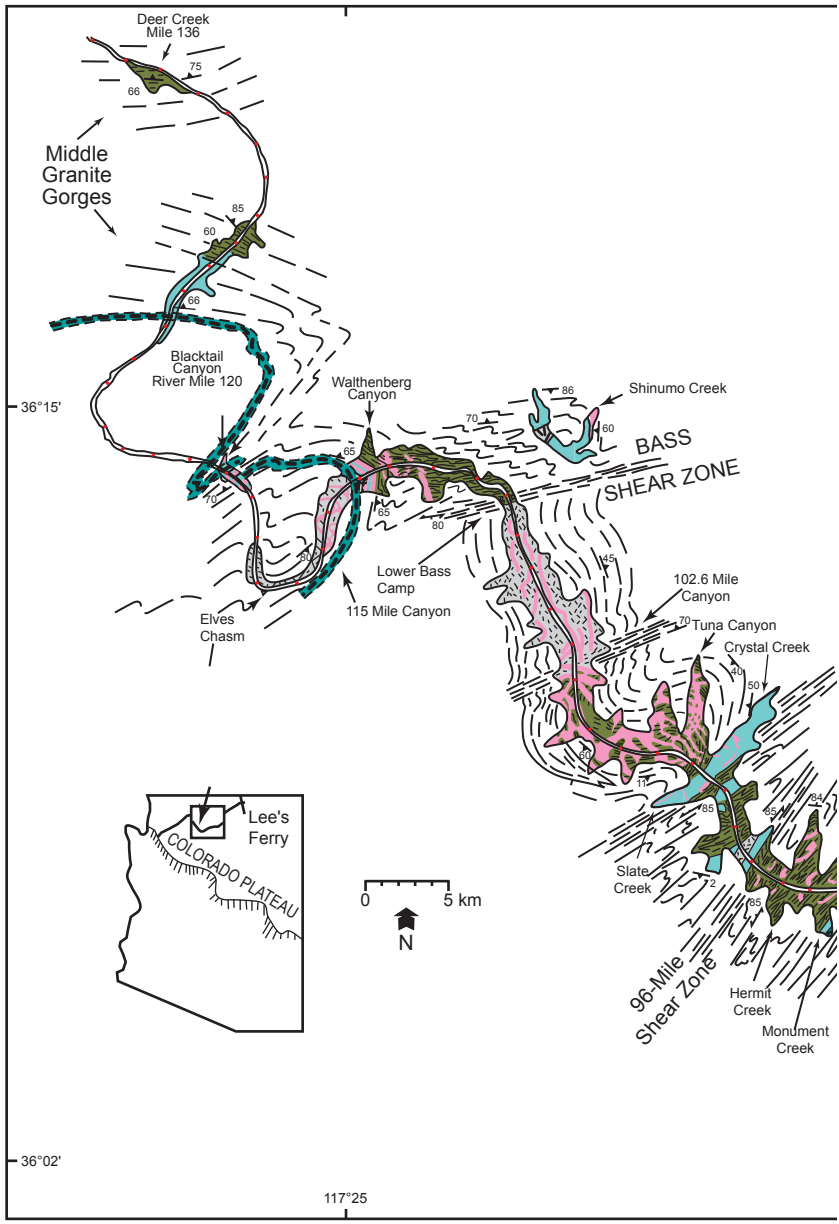

Figure 36. Simplified geologic map of Paleoproterozoic (Lower Proterozoic) rocks in the Upper and Middle Granite Gorges, Grand Canyon, northern Arizona (after *Ilg et al.* [1996]; *Karlstrom et al.*, [2003]). Form lines outside

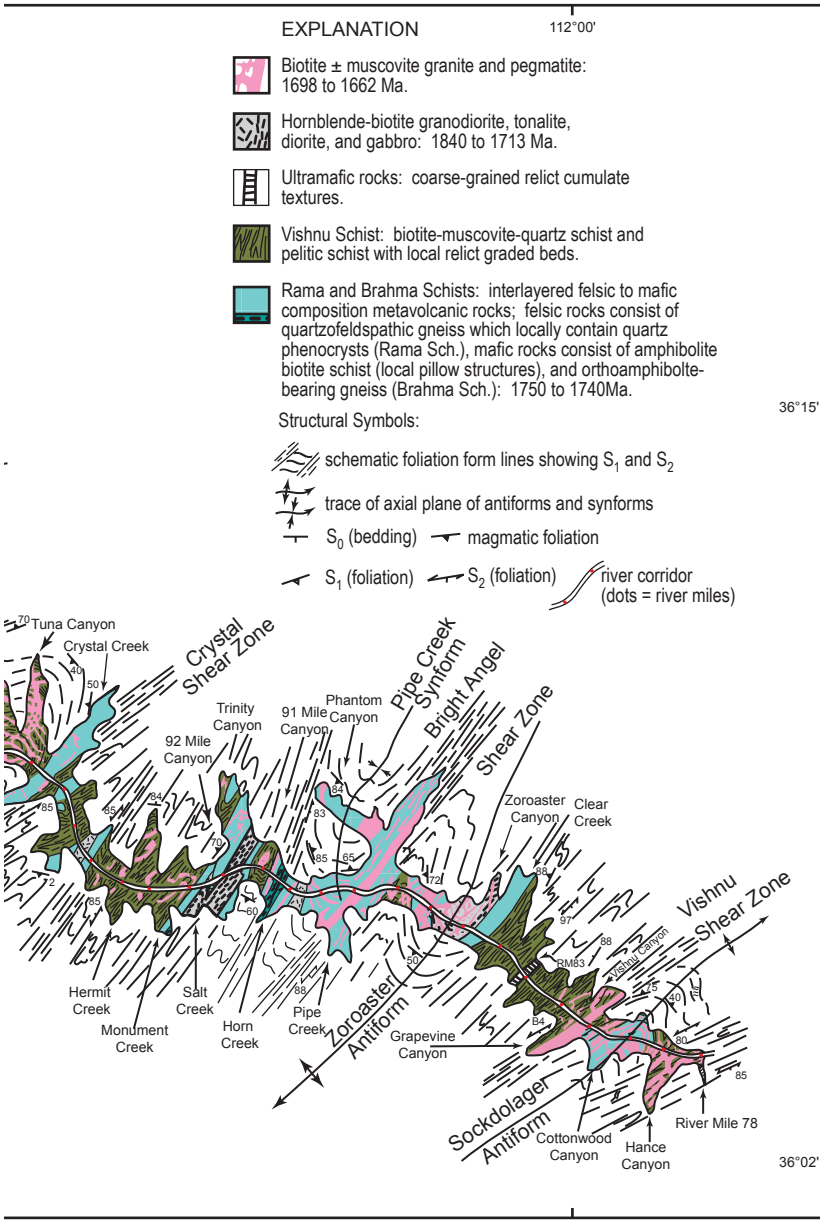

the Paleoproterozoic exposures show their interpretation of the trace of the regional foliation on the map surface. The transect is divided into metamorphic domains that are generally separated by shear zones.

1996]. The petrology and geochemistry of Brahma Schist amphibolites were studied by *Clark* [1978, 1979], who divided the amphibolites and mafic schists into five groups based on field occurrence and mineral assemblage: (1) anthophyllite-bearing and cordierite-anthophyllite-bearing rocks (orthoamphibole schist), (2) "early amphibolites," (3) the Granite Park mafic body (Lower Granite Gorge area), (4) hornblende-bearing dikes, and (5) tremolite-bearing dikes. *Ilg et al.* [1996] agreed with Clark's interpretation that the orthoamphibole-bearing (group 1) rocks are metamorphosed, hydrothermally altered, mafic marine volcanic rocks, and that the "early amphibolites" (group 2) are metamorphosed basalts and basaltic tuffs. Clark's groups 1 and 2 compose the supracrustal Brahma Schist, following *Campbell and Maxson*'s [1938] original usage of the term.

Massive amphibolites (part of Clark's group 2) make up 30–40% of the Brahma Schist. This unit does not typically preserve primary igneous features, but relict pillow structures are present at a number of localities. Massive amphibolites occur in units several meters to tens of meters thick, and are composed of plagioclase and hornblende, plus subordinate quartz, biotite, clinopyroxene, and epidote (plus accessories) [*Clark*, 1978, 1979]. Furthermore, these massive amphibolites have a tholeiitic character and trace element compositions consistent with an island-arc environment. The biotite-plagioclase and hornblende-biotite-plagioclase schists (the remainder of Clark's group 2) make up approximately 50% of the Brahma Schist in the Upper Granite Gorge. Although strong tectonic layering has mostly obscured primary igneous textures, in several locations original textures are preserved, such as subangular quartz + plagioclase + biotite fragments entrained in an amphibolitic matrix, which suggests that some of these rocks may have been volcaniclastic breccias. Interlayered with the biotite schists are discontinuous meter-scale lenses of garnet + diopside + epidote + calcite rocks, the protoliths of these lenses possibly being relatively thin layers of calcareous shale or algal mats interbedded with submarine sediments [*Babcock*, 1990]. The Brahma Schist also contains exposures of orthoamphibole-bearing rocks (Clark's group 1) (Figure 36). They are interpreted to be hydrothermally altered, mafic

marine volcanic rocks [*Vallance*, 1967]. The presence of relict pillow basalt, orthoamphibolite rocks, and associated sulfide mineralization indicates that the Brahma Schist was a product of dominantly mafic submarine volcanism. The Rama and Brahma metavolcanic schists can be complexly interlayered so that contact relationships support variable relative ages between mafic and intermediate metavolcanic rocks. However, in the Upper Granite Gorge, the Rama Schist is underneath and older than the Brahma Schist.

The Vishnu Schist consists of pelitic schist and quartz-biotite-muscovite schists that are interpreted as meta-lithic-arenites and metagreywackes (metamorphosed sandstones and mudstones), with numerous calc-silicate lenses and pods that are interpreted to be concretions [*Ilg et al*., 1996; *Karlstrom et al*., 2003]. Several-kilometer thick sections of meta-lithic-arenite and metagreywacke sequences exhibit rhythmic banded (centimeter- to meter-scale) coarser and finer layers, with locally well-preserved bedding and graded bedding [*Walcott*, 1894; *Brown et al*., 1979] suggesting deposition as submarine turbidites. The original grain sizes in the Vishnu Schist metasedimentary rocks probably range from medium-grained sand to silt and clay, while conglomerates are conspicuously absent, all of which suggests a lack of high-energy proximal facies. The preserved relict graded bedding, association with metavolcanic rocks containing pillow structures, lack of coarse sediments, and geochemical data [*Babcock*, 1990] indicate that these Vishnu metasedimentary units were deposited in submarine conditions on the flanks of eroding oceanic islands (an oceanic island-arc environment). The preserved graded bedding indicates that the Vishnu Schist was deposited stratigraphically above the Brahma Schist, and the accessible exposures indicate that the contact between them is generally concordant, although there is some interlayering of the contact in some places.

For the purposes of this study twenty-seven Brahma Schist amphibolite samples were collected in the Upper and Middle Granite Gorges: (1) three samples from the Cottonwood Canyon area, (2) nine samples from the Clear Creek area, including seven samples from a single 50 m long and 2 m wide amphibolite body just upstream from the

mouth of Clear Creek, (3) one sample from the Cremation Creek area, (4) one sample from near the mouth of Pipe Creek, (5) seven samples from outcrops just upstream of Blacktail Canyon, and (6) six samples from outcrops along the Colorado River between miles 126.5 and 129. All these locations are evident on Figure 36. The small tabular body of amphibolite near the mouth of Clear Creek was intensively sampled because it appeared to show mineralogical variation through its width, perhaps suggesting that it may have been a thin sill rather than a lava flow. Otherwise, all the other samples were of massive amphibolite. In the area just upstream of Blacktail Canyon, there was clear field evidence that the amphibolites represented a series of basaltic lava flows, there being well defined competent layers 3–10 m thick in succession along the outcrop separated by structural breaks accompanied by leaching of the rock (possibly paleoweathering), or in one instance by what appeared to be a thin inter-flow sandstone layer. That sequence of metamorphosed basalt flows was thus systematically sampled.

A8. Elves Chasm Granodiorite, Grand Canyon

All sedimentary and volcanic rocks must be deposited on some older substrate or "basement." However, such "basement" and its "sedimentary cover" often get detached from each other and tectonically interlayered during subsequent deformation, while high-grade metamorphism also obscures the nature of the origin sedimentary and volcanic protoliths, and the original contact relationships. Thus, *Noble and Hunter* [1916] posed this problem and speculated that some of the gneisses of the Grand Canyon might be basement for the schists. However, subsequent investigations recognized that the gneisses are deformed intrusive rocks [*Campbell and Maxson*, 1938; *Brown et al*., 1979; *Babcock*, 1990]. Indeed, the Granite Gorge Metamorphic Suite is intruded by Lower Proterozoic (Paleoproterozoic) granitoid plutons, mafic dikes, and granitic pegmatite dike swarms that together make up about one-half of the crystalline rocks exposed in the Upper Granite Gorge (Figure 36). *Campbell and Maxson* [1938] thought there was a single major period of igneous "invasion," and this led to the convention of lumping all

plutonic rocks of the Grand Canyon under a single name, the Zoroaster Gneiss. This name was subsequently changed to Zoroaster Granite by *Maxson* [1968], and then to the Zoroaster Plutonic Complex by *Babcock et al*. [1979]. However, new mapping by *Ilg et al.* [1996] and geochronology investigations [*Hawkins et al*., 1996] have shown that these plutonic rocks represent a long and complex record of crustal development of the Grand Canyon crystalline basement. As such, these plutonic rocks range widely in conventional ages, in composition from gabbro to granite, in morphology from large plutons to stocks, dikes, and sills, and in tectonic significance.

However, early studies in the Grand Canyon suggested that the quartzofeldspathic Elves Chasm Gneiss and Trinity Gneiss were basement to the supracrustal rocks [*Noble and Hunter*, 1916]. On the other hand, *Babcock et al*. [1974, 1979] suggested that the Elves Chasm and the Trinity Gneisses were formed either by the "granitization" of Vishnu Schist or that they were orthogneisses (metamorphosed intrusives). Later, *Babcock* [1990] interpreted the Trinity Gneiss to be a metamorphosed sequence of interbedded dacitic to andesitic tuffs and flows and sedimentary strata deposited prior to deposition of the Vishnu sediments on top of them. Similarly, *Babcock* [1990] suggested that the orthoamphibole-bearing schist horizon identified by *Clark* [1978, 1979] could be interpreted as a paleosol (former soil horizon), and thus the Elves Chasm Gneiss might be the basement to the supracrustal Vishnu rocks. However, the new mapping by *Ilg et al*. [1996] and the geochronology investigations by *Hawkins et al*. [1996] have shown that the Trinity Gneiss is definitely not basement, but is intrusive into the Granite Gorge Metamorphic Suite. Whereas some layers do have geochemical signatures consistent with a sedimentary parentage [*Babcock*, 1990], they can be interpreted as screens of country rock because the Trinity Gneiss is clearly intrusive into some of them.

However, the Elves Chasm Gneiss is still interpreted as most likely being part of the basement on which the volcanics and sediments were deposited that were then metamorphosed to become the Granite Gorge Metamorphic Suite. Consistent with this interpretation, *Hawkins et al*. [1996] reported a 1840 Ma crystallization age for the Elves Chasm

pluton and interpreted the Elves Chasm Gneiss as therefore an older granodioritic pluton. This conventional age makes the Elves Chasm Granodiorite the oldest rock known in the southwestern United States. The contact around this pluton, which based on radioisotope dating is much older than the Granite Gorge Metamorphic Suite and the plutons that intrude it, is tectonized, but is defined by the high-grade orthoamphibole-bearing gneiss horizon that is exposed adjacent to the Elves Chasm pluton in the Middle Granite Gorge (Figure 36). The contact is gradational over an interval of several meters between the foliated pluton and the distinctive orthoamphibole-bearing gneiss. This orthoamphibole-bearing gneiss suggests a zone of early alteration of the contact zone, possibly a metamorphosed and sheared paleosol as proposed by *Babcock* [1990], or possibly a zone of hydrothermal alteration of mafic marine volcanic rocks [*Vallance*, 1967]. The Elves Chasm pluton itself is dominantly hornblende-biotite tonalite to quartz diorite and is distinguished geochemically from other plutons in the Grand Canyon by its lower concentration of large ion lithophile elements (LILE) and its lower concentration of light rare earth elements relative to heavy rare earth elements [*Karlstrom et al*., 2003].

Eight samples of the Elves Chasm pluton were collected from the outcrops along the river corridor between river miles 112.5 and 117.5 (Figure 36). Samples were carefully selected to be representative of mineralogical and rock type variations within the Elves Chasm pluton.

A9. Beartooth Andesitic Amphibolite, Wyoming

The Beartooth Mountains of southern Montana and northwestern Wyoming are a large uplifted block of Precambrian metasedimentary and metaigneous rocks [*Baadsgaard and Mueller*, 1973; *Mueller and Rogers*, 1973]. The predominant rock types are granitic gneisses and migmatites, but amphibolite, schist, quartzite, and ironstone occur in minor amounts in the southern Beartooth Mountains straddling the Montana-Wyoming border (Figure 37 inset). The amphibolites included in the granitic gneisses were originally interpreted as metamorphosed diabase dikes and small intrusions because of their mapped field

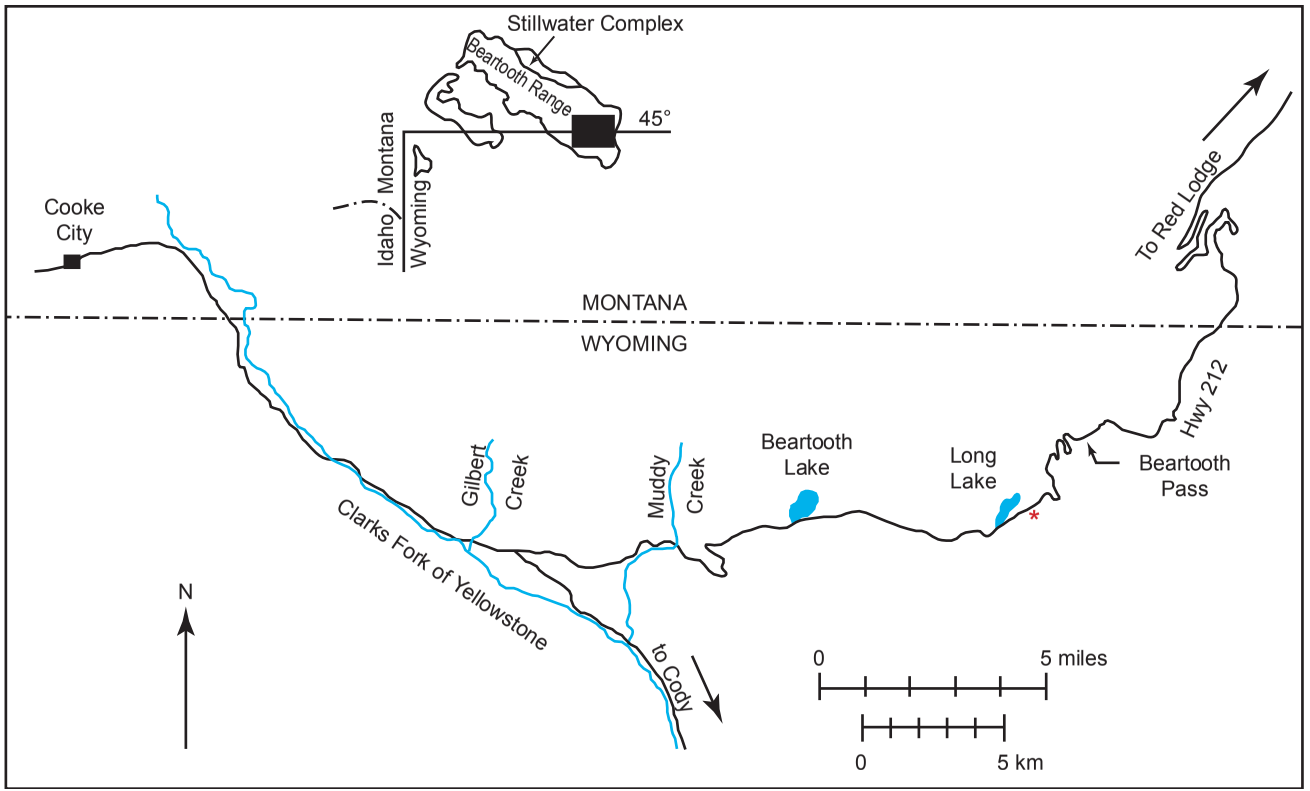

Figure 37. Location maps, showing the Beartooth Mountains of Montana and Wyoming (inset) and the Long Lake-Beartooth Pass area on U.S. Highway 212 (after *Baadsgaard and Mueller* [1973]; *Wooden et al.* [1982]). The location from which the andesitic amphibolite sample was collected is shown *.

relationships as long, narrow, dike-like bodies [*Baadsgaard and Mueller*, 1973]. These amphibolite bodies were easily recognized as older than the unmetamorphosed diabase dikes that clearly cross-cut all the older metamorphosed granitic and mafic rocks. Initial radioisotope dating of all these mafic rocks [*Baadsgaard and Mueller*, 1973] determined that the amphibolites (interpreted as metadiabase dikes) were Archean, whereas the unambiguous dikes of unmetamorphosed diabase were determined to be probably Middle Proterozoic. This distinction was also evidenced from petrographic and geochemical investigations [*Prinz*, 1964; *Mueller and Rogers*, 1973].

More recent detailed mapping and fieldwork, and petrological and geochemical investigations, have clarified the relationship between these amphibolites and the granitic rocks [*Warner et al*., 1982; *Wooden et al*., 1982]. Outcrops were examined and sampled along U.S. Highway 212 west of Beartooth Pass (Figure 37), and a small area beside the highway

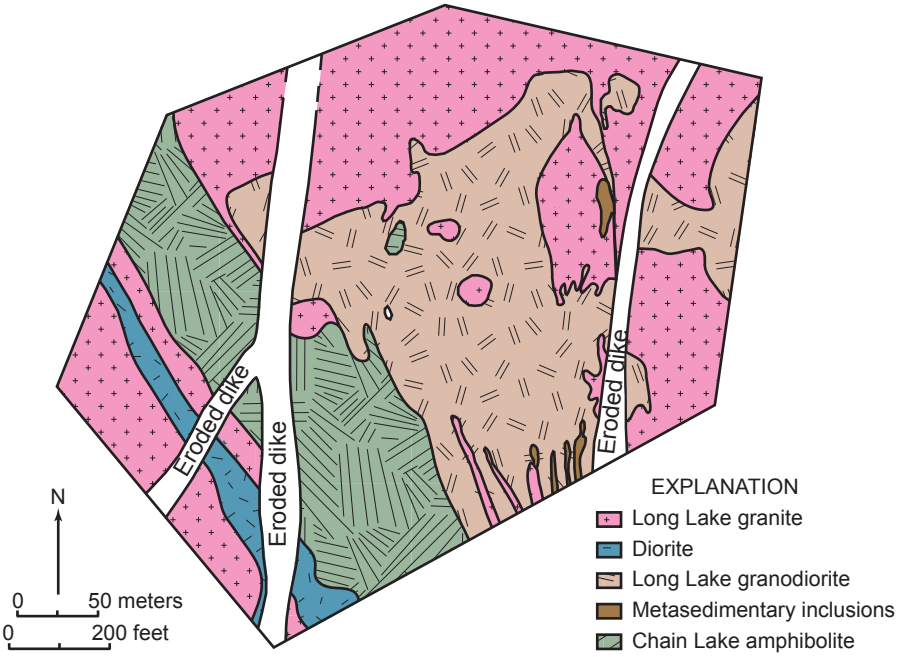

Figure 38. Simplified geologic map of an area adjacent to, and southeast of, Long Lake and U.S. Highway 212, southern Beartooth Mountains, Wyoming (after *Warner et al.* [1982]).

near Long Lake was mapped in detail to elucidate the relationships between the major rock types (Figure 38). The rock units mapped, described and informally named include a basaltic to dioritic unit referred to as the Chain Lake andesitic amphibolite, a series of foliated granitic to tonalitic rocks referred to as the Long Lake granodiorite, and a more massive leucocratic granitic to tonalitic unit referred to as the Long Lake granite. Unnamed diorite and metasedimentary units also occur in the mapped area. The Chain Lake andesitic amphibolite consists of quartz, plagioclase (oligoclase), biotite, and hornblende with accessory sphene (titanite), apatite, epidote, and magnetite with an equigranular texture. It is a metamorphic rock with quartz and plagioclase forming a matrix of equant crystals in which are set pencil-shaped aggregates of biotite and prisms of hornblende. The quartz-plagioclase net consists of approximately 300 μm crystals in fine-grained samples, and approximately 2 mm crystals in coarse-grained samples. Biotite aggregates and hornblende prisms have an aspect ratio between 1:3 and 1:4, with their short dimension approximately 100 μm in fine-grained samples and approximately 500 μm in coarse-grained samples. Hornblende is generally about twice as large as biotite. Grain boundaries are smooth or smoothly scalloped and tend to meet at 120° angles in triple junctions. The crystals do not display zoning. Biotite and hornblende prisms tend to be aligned in a parallel to subparallel array that reflects the hand sample and outcrop lineation. Banding, where present, is defined by variations in the mafic mineral content. This andesitic amphibolite has a relatively restricted composition, with SiO_2 between 55 and 61%, FeO (total) of between 5 and 10%, 2–5% MgO, 3–4% Na_2O, and 0.9–2.6% K_2O. Thus the major element composition is similar to that of many modern andesites, except for slightly lower Al_2O_3 contents. The composition of this andesitic amphibolite is thus very close to that of the original igneous rock and is not the result of alkali metasomatism of basaltic rocks as suggested by *Armbrustmacher and Simons* [1977]. The general homogeneity of the andesitic amphibolite's composition over a large geographic area, the preservation of igneous fractionation trends within the unit, and the survival of many amphibolites of basaltic composition in the same area

support this conclusion [*Wooden et al*., 1982].

This andesitic amphibolite is the dominant type of inclusion in the foliated granitic rocks in the central and southeastern Beartooth Mountains [*Wooden et al*., 1982]. There has been some chemical interaction between the andesitic amphibolites and the foliated granites, with the most common example being the introduction of small (1–5 cm) leucocratic veins into the andesitic amphibolite. There is no obvious evidence of any major metasomatic reaction whereby the andesitic amphibolite could have been produced by interaction between rocks of original basaltic composition and a component of the foliated granites. The andesitic amphibolite is generally well foliated and, as indicated by examination of thin sections, has textures that indicate recrystallization. The interpretation of this andesitic amphibolite unit is that it is definitely older than the foliated granites, and this is confirmed by the field observations which indicate that the andesitic amphibolite has been intruded by the Long Lake granodiorite, which in turn has been intruded by the Long Lake granite [*Warner et al*., 1982]. It has had a more extensive metamorphic-deformational history, its original igneous character being transformed to a metamorphic texture by later deformations. Mineral analyses [*Warner et al*., 1982] suggest final equilibration temperatures of approximately 400°C, a temperature equivalent to metamorphism at the epidote-amphibolite facies, which is confirmed by the presence of epidote in most samples of it. *Wooden et al*. [1982] plotted a composite Rb-Sr isochron for samples of the Long Lake granite, Long Lake granodiorite, and this andesitic amphibolite, which yielded an isochron "age" of 2790±35 Ma. However, they suggested that the Rb-Sr data for the andesitic amphibolite indicated a maximum age of 3100–3000 Ma, and a minimum age of 2800 Ma corresponding to its intrusion by the Long Lake granite. This "age" for the andesitic amphibolite places it among some of the oldest rocks in the continental U. S. A.

A sample of this andesitic amphibolite unit was collected from a prominent outcrop in a road cut on U. S. Highway 212, west of Beartooth Pass, 1.3 km east-northeast of Long Lake (Figure 37). The outcrop sampled is on the east side of the highway, where it has been exposed

by a deep excavation engineered for the highway. Subsequent careful laboratory work to separate the rock into its constituent minerals enabled its mineral composition to be determined as quartz and plagioclase (oligoclase) about 71% of the rock, biotite about 17%, hornblende about 7%, magnetite about 3%, and titanite about 2%.

References

Albarède, F., Time-dependent models of U-Th-He and K-Ar evolution and the layering of mantle convection, *Chemical Geology, 145*, 413–429, 1998.

Alibert, A., and F. Albarède, Isotope and trace element geochemistry of the Colorado Plateau volcanics, *Geochimica et Cosmochimica Acta, 50*, 2735–2750, 1986.

Allègre, C. J., Isotope geodynamics, *Earth and Planetary Science Letters, 86*, 175–203, 1987.

Allègre, C. J., S. R. Hart, and J.-F. Minster, Chemical structure and evolution of the mantle and continents determined by inversion of Nd and Sr isotopic data, I. Theoretical models, *Earth and Planetary Science Letters, 66*, 177–190, 1983a.

Allègre, C. J., S. R. Hart, and J.-F. Minster, Chemical structure and evolution of the mantle and continents determined by inversion of Nd and Sr isotopic data, II. Numerical experiments and discussion, *Earth and Planetary Science Letters, 66*, 191–213, 1983b.

Allègre, C. J., A. Hofmann, and R. K. O'Nions, The argon constraints on mantle structure, *Geophysical Research Letters, 23*, 3555–3557, 1996.

Allègre, C. J., E. Lewin, and B. Dupre, A coherent crust-mantle model for the uranium-thorium-lead isotope system, *Chemical Geology, 70*, 211–234, 1988.

Armbrustmacher, T. J., and F. S. Simons, Geochemistry of amphibolites from the central Beartooth Mountains, Montana-Wyoming, *U. S. Geological Survey Journal of Research, 5*, 53–60, 1977.

Austin, S. A., Isotope and trace element analysis of hypersthene-normative basalts from the Quaternary of Uinkaret Plateau, western Grand Canyon, *Geological Society of America, Abstracts with Programs, 27*(7), A261, 1992.

Austin, S.A. (editor), *Grand Canyon: Monument to Catastrophe*, Institute for Creation Research, Santee, California, 1994.

Austin, S.A., Excess argon within mineral concentrates from the new dacite lava dome at Mount St Helens volcano, *Creation Ex Nihilo Technical Journal, 10*(3), 335–343, 1996.

Austin, S.A., Mineral isochron method applied as a test of the assumptions of radioisotope dating, in *Radioisotopes and the Age of the Earth: A Young-Earth Creationist Research Initiative*, edited by L. Vardiman, A.A. Snelling, and E.F. Chaffin, pp. 95–121, Institute for Creation Research, El Cajon, California, and Creation Research Society, St. Joseph, Missouri, 2000.

Austin, S.A., Do radioisotope clocks need repair? Testing the assumptions of isochron dating using K-Ar, Rb-Sr, Sm-Nd, and Pb-Pb isotopes, in *Radioisotopes and the Age of the Earth: Results of a Young-Earth Creationist Research Initiative*, edited by L. Vardiman, A.A. Snelling, and E.F. Chaffin, pp. 325–392, Institute for Creation Research, El Cajon, California, and Creation Research Society, Chino Valley, Arizona, 2005.

Austin, S.A., and A.A. Snelling, Discordant potassium-argon model and isochron 'ages' for Cardenas Basalt (Middle Proterozoic) and associated diabase of eastern Grand Canyon, Arizona, in *Proceedings of the Fourth International Conference on Creationism*, edited by R.E. Walsh, pp. 35–51, Creation Science Fellowship, Pittsburgh, Pennsylvania, 1998.

Austin, S.A., J.R. Baumgardner, D.R. Humphreys, A.A. Snelling, L. Vardiman, and K.P. Wise, Catastrophic plate tectonics: a global flood model of earth history, in *Proceedings of the Third International Conference on Creationism*, edited by R.E. Walsh, pp. 609–621, Creation Science Fellowship, Pittsburgh, Pennsylvania, 1994.

Baadsgaard, H., and P.A. Mueller, K-Ar and Rb-Sr ages of intrusive Precambrian mafic rocks, southern Beartooth Mountains, Montana and Wyoming, *Geological Society of America Bulletin, 84*(11), 3635–3644, 1973.

Babcock, R.S., Precambrian crystalline core, in *Grand Canyon Geology*, first edition, edited by S.S. Beus and M. Morales, pp. 11–28, Oxford University Press, New York, and Museum of Northern Arizona Press, Flagstaff, Arizona, 1990.

Babcock, R. S., E. H. Brown, and M. D. Clark, Geology of the older Precambrian rocks of the Upper Granite Gorge of the Grand Canyon, *Geology of the Grand Canyon*, edited by W. S. Breed, pp. 2–10, Grand Canyon Natural History Association, Grand Canyon, Arizona, 1974.

Babcock, R. S., E. H. Brown, M. D. Clark, and D. E. Livingston, Geology of the older Precambrian rocks of the Grand Canyon: Part II. The Zoroaster Plutonic Complex and related rocks, *Precambrian Research, 8*, 243–275, 1979.

Battey, M. H., The recent eruption of Ngauruhoe, *Records of the Auckland Institute and Museum, 3*, 389–395, 1949.

Baumgardner, J. R., Computer modeling of the large-scale tectonics associated with the Genesis Flood, in *Proceedings of the Third International Conference on Creationism*, edited by R. E. Walsh, pp. 49–62, Creation Science Fellowship, Pittsburgh, Pennsylvania, 1994a.

Baumgardner, J. R., Runaway subduction as the driving mechanism for the Genesis Flood, in *Proceedings of the Third International Conference on Creationism*, edited by R. E. Walsh, pp. 63–75, Creation Science Fellowship, Pittsburgh, Pennsylvania, 1994b.

Baumgardner, J. R., Distribution of radioactive isotopes in the earth, in *Radioisotopes and the Age of the Earth: A Young-Earth Creationist Research Initiative*, edited by L. Vardiman, A. A. Snelling, and E. F. Chaffin, pp. 49–94, Institute for Creation Research, El Cajon, California, and Creation Research Society, St. Joseph, Missouri, 2000.

Baumgardner, J. R., Catastrophic plate tectonics: the physics behind the Genesis Flood, in *Proceedings of the Fifth International Conference on Creationism*, edited by R. L. Ivey, Jr., pp. 113–126, Creation Science Fellowship, Pittsburgh, Pennsylvania, 2003.

Bergquist, J. R., A. F. Shride, and C. T. Wrucke, *Geologic Map of the Sierra Ancha Wilderness and Salome Study Area, Gila County, Arizona*, U. S. Geological Survey, Miscellaneous Field Studies Map MF-1162A, Scale 1:48,000, 1981.

Best, M. G., and W. H. Brimhall, Late Cenozoic alkali basaltic magmas in the western Colorado Plateau and the Basin and Range Transition Zone, U. S. A., and their bearing on mantle dynamics, *Geological Society of America Bulletin, 85*, 1677–1690, 1974.

Bhattacharji, S., Scale model experiments on flowage differentiation in sills, in *Ultramafic and Related Rocks*, edited by J. Wyllie, pp. 69–70, John Wiley & Sons, New York, 1967.

Bhattacharji, S., and C.H. Smith, Flowage differentiation, *Science, 145*, 150–153, 1964.

Billingsley, G.H., and P.W. Huntoon, *Geologic Map of Vulcan's Throne and Vicinity, Western Grand Canyon, Arizona*, Grand Canyon Natural History Association, Grand Canyon, Arizona, scale 1:48,000, 1983.

Boyd, S.W., Statistical determination of genre in Biblical Hebrew: evidence for a historical reading of Genesis 1:1–2:3, in *Radioisotopes and the Age of the Earth: Results of a Young-Earth Creationist Research Initiative*, edited by L. Vardiman, A.A. Snelling, and E.F. Chaffin, pp. 631–734, Institute for Creation Research, El Cajon, California, and Creation Research Society, Chino Valley, Arizona, 2005.

Brooks, C., S.R. Hart, A. Hofmann, and D.E. James, Rb-Sr mantle isochrons from oceanic regions, *Earth and Planetary Science Letters, 32*, 51–61, 1976a.

Brooks, C., D.E. James, and S.R. Hart, Ancient lithosphere: its role in young continental volcanism, *Science, 193*, 1086–1094, 1976b.

Brown, E.H., R.S. Babcock, M.D. Clark, and D.E. Livingston, Geology of the older Precambrian rocks of the Grand Canyon: Part I. Petrology and structure of the Vishnu Complex, *Precambrian Research, 8*, 219–241, 1979.

Campbell, I., and J.H. Maxson, Geological studies of the Archean rocks at Grand Canyon, *Carnegie Institution of Washington Year Book, 37*, 359–364, 1938.

Clark, M.D., Amphibolitic rocks from the Precambrian of Grand Canyon: mineral chemistry and phase petrology, *Mineralogical Magazine, 42*, 199–207, 1978.

Clark, M.D., Geology of the older Precambrian rocks of the Grand Canyon: Part 3. Petrology of mafic schists and amphibolites, *Precambrian Research, 8*, 277–302, 1979.

Clark, R.H., Petrology of the volcanic rocks of Tongariro subdivision, in *The Geology of the Tongariro Subdivision*, D.R. Gregg, New Zealand Geological Survey Bulletin, n.s. 40, 107–123, 1960.

Cole, J. W., Andesites of the Tongariro Volcanic Centre, North Island, New Zealand, *Journal of Volcanology and Geothermal Research, 3*, 121–153, 1978.

Cole, J. W., K. V. Cashman, and P. C. Rankin, Rare-earth element geochemistry and the origin of andesites and basalts of the Taupo Volcanic Zone, New Zealand, *Chemical Geology, 38*, 255–274, 1983.

Cole, J. W., I. J. Graham, W. R. Hackett, and B. F. Houghton, Volcanology and petrology of the Quaternary composite volcanoes of Tongariro Volcanic Centre, Taupo Volcanic Zone, in *Late Cenozoic Volcanism in New Zealand*, edited by I. E. M. Smith, pp. 224–250, Royal Society of New Zealand, Bulletin 23, 1986.

Dalrymple, G. B., *The Age of the Earth*, Stanford University Press, Stanford, California, 1991.

Dalrymple, G. B., and W. K. Hamblin, K-Ar ages of Pleistocene lava dams in the Grand Canyon, Arizona, *Proceedings of the National Academy of Sciences USA, 95*, 9744–9749, 1998.

Dalrymple, G. B., and M. A. Lanphere, *Potassium-Argon Dating: Principles, Techniques and Applications to Geochronology*, W. H. Freeman, San Francisco, 1969.

Damon, P. E., and J. L. Kulp, Excess helium and argon in beryl and other minerals, *American Mineralogist, 43*, 433–459, 1958.

Davies, G. F., Geophysically constrained mantle mass flows and the ^{40}Ar budget: a degassed lower mantle?, *Earth and Planetary Science Letters, 166*, 149–162, 1999.

Davies, J. H., and G. J. Stevenson, Physical model of source region of subduction volcanics, *Journal of Geophysical Research, 97*, 2037–2070, 1992.

Dickin, A. P., *Radiogenic Isotope Geology*, Cambridge University Press, Cambridge, England, 1995.

Doe, B. R., and R. E. Zartman, Plumbotectonics, in *Geochemistry of Hydrothermal Ore Deposits*, second edition, edited by H. L. Barnes, pp. 22–70, John Wiley & Sons, New York, 1979.

Elston, D. P., Magnetostratigraphy of Late Proterozoic Chuar Group and Sixtymile Formation, Grand Canyon Supergroup, Northern Arizona: correlation with other Proterozoic strata of North America, *Geological*

Society of America, Abstracts with Programs (Rocky Mountain Section), *18*, 353, 1986.

Elston, D.P., Grand Canyon Supergroup, northern Arizona: stratigraphic summary and preliminary paleomagnetic correlation with parts of other North American Proterozoic sessions, in *Geologic Evolution of Arizona*, edited by J.P. Jenney and S.J. Reynolds, pp. 259–272, Arizona Geological Society, Tucson, Digest 17, 1989.

Elston, D.P., and C.S. Grommé, Precambrian polar wandering from Unkar Group and Nankoweap Formation, eastern Grand Canyon, Arizona, in *Geology of Northern Arizona*, edited by T.N.V. Karlstrom, J.A. Swann, and R.L. Eastwood, pp. 97–117, Geological Society of America, Rocky Mountain Sectional Meeting, Flagstaff, Arizona, 1974.

Elston, D.P., and E.H. McKee, Age and correlation of the Late Proterozoic Grand Canyon disturbance, northern Arizona, *Geological Society of America Bulletin, 93*, 681–699, 1982.

Ewart, A., and J.J. Stipp, Petrogenesis of the volcanic rocks of the central North Island, New Zealand, as indicated by a study of $^{87}Sr/^{86}Sr$ ratios, and Sr, Rb, K, U and Th abundances, *Geochimica et Cosmochimica Acta, 32*, 699–736, 1968.

Fitton, J.G., Petrology and geochemistry of Late Cenozoic basalt flows, western Grand Canyon, Arizona, in *Geology of Grand Canyon, Northern Arizona (with Colorado River Guides)*, edited by D.P. Elston, G.H. Billingsley, and R.A. Young, pp. 186–189, American Geophysical Union, Washington, DC, 1989.

Fitton, J.G., D. James, P.D. Kempton, D.S. Ormerod, and W.P. Leeman, The role of lithospheric mantle in the generation of Late Cenozoic basic magmas in the western United States, *Journal of Petrology, Special Lithosphere Issue*, 331–349, 1988.

Galer, S.J.G., and R.K. O'Nions, Residence time of thorium, uranium and lead in the mantle with implications for mantle convection, *Nature, 316*, 778–782, 1985.

Gamble, J.A., J.D. Woodhead, I. Wright, and I. Smith, Basalt and sediment geochemistry and magma petrogenesis in a transect from ocean island arc to rifted continental margin arc: the Kermadec-Hikurangi margin, S.W. Pacific, *Journal of Petrology, 37*(6), 1523–1546, 1996.

Gastil, R. G., Late Precambrian volcanism in southeastern Arizona, *American Journal of Science, 252*, 436–440, 1954.

Gill, J. B., *Orogenic Andesites and Plate Tectonics*, Springer-Verlag, Berlin, 1981.

Graham, I. J., and W. R. Hackett, Petrology of calc-alkaline lavas from Ruapehu volcano and related vents, Taupo Volcanic Zone, New Zealand, *Journal of Petrology, 28*(3), 531–567, 1987.

Graham, I. J., J. W. Cole, R. M. Briggs, J. A. Gamble, and I. E. M. Smith, Petrology and petrogenesis of volcanic rocks from the Taupo Volcanic Zone: a review, *Journal of Volcanology and Geothermal Research, 68*, 59–87, 1995.

Graham, I. J., B. L. Gulson, J. W. Hedenquist, and K. Mizon, Petrogenesis of Late Cenozoic volcanic rocks from the Taupo Volcanic Zone, New Zealand, in the light of new Pb isotope data, *Geochimica et Cosmochimica Acta, 56*, 2797–2819, 1992.

Gregg, D. R., Eruption of Ngauruhoe 1954–55, *New Zealand Journal of Science and Technology, B37*, 675–688, 1956.

Gregg, D. R., *The Geology of Tongariro Subdivision*, New Zealand Geological Survey Bulletin, n.s. 40, 1960.

Grindley, G. W., Tongariro National Park: stratigraphy and structure, *New Zealand Department of Scientific and Industrial Research Information Series, 50*, 79–86, 1965.

Hackett, W. R., and B. F. Houghton, Active composite volcanoes of Taupo Volcanic Zone, in *Central North Island Volcanism*, New Zealand Geological Survey, Record 21, pp. 61–114, 1987.

Hackett, W. R., and B. F. Houghton, A facies model for a Quaternary andesitic composite volcano: Ruapehu, New Zealand, *Bulletin of Volcanology, 51*, 51–68, 1989.

Hamblin, W. K., Pleistocene volcanic rocks of the western Grand Canyon, Arizona, in *Geology of Grand Canyon, Northern Arizona (with Colorado River Guides)*, edited by D. P. Elston, G. H. Billingsley, and R. A. Young, pp. 190–204, American Geophysical Union, Washington, DC, 1989.

Hamblin, W. K., Late Cenozoic lava dams in the western Grand Canyon, in *Grand Canyon Geology*, first edition, edited by S. S. Beus and M. Morales, pp. 385–433, Oxford University Press, New York, and Museum of Northern

Arizona Press, Flagstaff, Arizona, 1990.

Hamblin, W.K., *Late Cenozoic Lava Dams in the Western Grand Canyon*, Geological Society of America, Memoir 183, 1994.

Hamblin, W.K., Late Cenozoic lava dams in the western Grand Canyon, in *Grand Canyon Geology*, second edition, edited by S.S. Beus and M. Morales, pp. 313–345, Oxford University Press, New York, 2003.

Hawkins, D.P., and S.A. Bowring, U-Pb monazite, xenotime and titanite geochronological constraints on the prograde to post-peak metamorphic thermal history of Paleoproterozoic migmatites from the Grand Canyon, Arizona, *Contributions to Mineralogy and Petrology, 134*, 150–169, 1999.

Hawkins, D.P., S.A. Bowring, B.R. Ilg, K.E. Karlstrom, and M.L. Williams, U-Pb geochronological constraints on the Paleoproterozoic crustal evolution of the Upper Granite Gorge, Grand Canyon, Arizona, *Geological Society of America Bulletin, 108*(9), 1167–1181, 1996.

Hendricks, J.D., Petrology and chemistry of igneous rocks of Middle Proterozoic Unkar Group, Grand Canyon Supergroup, Northern Arizona, in *Geology of the Grand Canyon, Northern Arizona (with Colorado River Guides)*, edited by D.P. Elston, G.H. Billingsley, and R.A. Young, pp. 106–116, American Geophysical Union, Washington, DC, 1989.

Hendricks, J.D., and I. Lucchitta, Upper Precambrian igneous rocks of the Grand Canyon, Arizona, in *Geology of Northern Arizona*, edited by T.N.V. Karlstrom, G.A. Swann, and R.L. Eastwood, pp. 65–86, Geological Society of America, Rocky Mountain Sectional Meeting, Flagstaff, 1974.

Hendricks, J.D., and G.M. Stevenson, Grand Canyon Supergroup: Unkar Group, in *Grand Canyon Geology*, first edition, edited by S.S. Beus and M. Morales, pp. 29–47, Oxford University Press, New York, and Museum of Northern Arizona Press, Flagstaff, Arizona, 1990.

Hendricks, J.D., and G.M. Stevenson, Grand Canyon Supergroup: Unkar Group, in *Grand Canyon Geology*, second edition, edited by S.S. Beus and M. Morales, pp. 39–52, Oxford University Press, New York, 2003.

Humphreys, D.R., Accelerated nuclear decay: a viable hypothesis?, in *Radioisotopes and the Age of the Earth: A Young-Earth Creationist Research Initiative*, edited by L. Vardiman, A.A. Snelling, and E.F. Chaffin, pp. 333–379, Institute for Creation Research, El Cajon, California, and Creation Research Society, St. Joseph, Missouri, 2000.

Humphreys, D. R., Young helium diffusion age of zircons supports accelerated decay, in *Radioisotopes and the Age of the Earth: Results of a Young-Earth Creationist Research Initiative*, edited by L. Vardiman, A. A. Snelling, and E. F. Chaffin, pp. 25–100, Institute for Creation Research, El Cajon, California, and Creation Research Society, Chino Valley, Arizona, 2005.

Humphreys, D. R., S. A. Austin, J. R. Baumgardner, and A. A. Snelling, Helium diffusion rates support accelerated nuclear decay, in *Proceedings of the Fifth International Conference on Creationism*, edited by R. L. Ivey, Jr., pp. 175–195, Creation Science Fellowship, Pittsburgh, Pennsylvania, 2003a.

Humphreys, D. R., S. A. Austin, J. R. Baumgardner, and A. A. Snelling, Recently measured helium diffusion rate for zircon suggests inconsistency with U-Pb age for Fenton Hill granodiorite, *EOS, Transactions of the American Geophysical Union, 84*(46), Fall Meeting Supplement, Abstract V32C-1047, 2003b.

Humphreys, D. R., S. A. Austin, J. R. Baumgardner, and A. A. Snelling, Helium diffusion age of 6000 years supports accelerated nuclear decay, *Creation Research Society Quarterly, 41*, 1–16, 2004.

Ilg, B. R., K. E. Karlstrom, D. P. Hawkins, and M. L. Williams, Tectonic evolution of Paleoproterozoic rocks in the Grand Canyon: insights into middle-crustal processes, *Geological Society of America Bulletin, 108*(9), 1149–1166, 1996.

Irvine, P. N., Terminology for layered intrusions, *Journal of Petrology, 23*, 127–162, 1982.

Karlstrom, K. E., B. R. Ilg, M. L. Williams, D. P. Hawkins, S. A. Bowring, and S. J. Seaman, Paleoproterozoic rocks of the Granite Gorges, in *Grand Canyon Geology*, second edition, edited by S. S. Beus and M. Morales, pp. 9–38, Oxford University Press, New York, 2003.

Koons, D. E., Geology of the Uinkaret Plateau, northern Arizona, *Geological Society of America Bulletin, 56*, 151–180, 1945.

Kramers, J. D., and I. N. Tolstikhin, Two terrestrial lead isotope paradoxes, forward transport modeling, core formation and the history of the continental crust, *Chemical Geology, 139*, 75–110, 1997.

Larson, E. E., P. E. Patterson, and F. E. Mutschler, Lithology, chemistry, age and origin of the Proterozoic Cardenas Basalt, Grand Canyon, Arizona,

Precambrian Research, 65, 255–276, 1994.

Leeman, W.P., Late Cenozoic alkali-rich basalt from the western Grand Canyon area, Utah and Arizona: isotopic composition of strontium, *Geological Society of America Bulletin, 85*, 1691–1696, 1974.

Leeman, W.P., Tectonic and magmatic significant of strontium isotopic variations in Cenozoic volcanic rocks from the western United States, *Geological Society of America Bulletin, 93*, 487–503, 1982.

Lucchitta, I., and J.D. Hendricks, Characteristics, depositional environment, and tectonic interpretations of the Proterozoic Cardenas Lavas, eastern Grand Canyon, Arizona, *Geology, 11*(3), 177–181, 1983.

Ludwig, K.R., *Isoplot/Ex (Version 2.49): The Geochronological Toolkit for Microsoft Excel*, University of California Berkeley, Berkeley Geochronology Center, Special Publication No. 1a, 2001.

Mathison, C.I., *Variation in the Somerset Dam Layered Basic Complex*, Unpublished B.Sc. Honours Thesis, University of Queensland, Brisbane, 1964.

Mathison, C.I., The Somerset Dam layered basic intrusion, south-eastern Queensland, *Journal of the Geological Society of Australia, 14*(1), 57–86, 1967.

Mathison, C.I., *The Somerset Dam Layered Basic Intrusion*, Unpublished Ph.D. Thesis, University of Queensland, Brisbane, 1970.

Mathison, C.I., Magnetites and ilmenites in the Somerset Dam layered basic intrusion, south-eastern Queensland, *Lithos, 8*, 93–111, 1975.

Mathison, C.I., Cyclic units in the Somerset Dam layered gabbro intrusion, south-eastern Queensland, Australia, *Lithos, 20*, 187–205, 1987.

Maxson, J.H., Lava flows in the Grand Canyon of the Colorado River, Arizona, *Geological Society of America Bulletin, 61*, 9–16, 1949.

Maxson, J.H., *Geologic Map of the Bright Angel Quadrangle, Grand Canyon National Park, Arizona*, revised, Grand Canyon Natural History Association, Grand Canyon, Arizona, scale 1:48,000, 1968.

McConnell, R.L., Preliminary report of microstructures of probable biologic origin from the Mescal Formation (Proterozoic) of central Arizona, *Precambrian Research, 1*, 227–234, 1974.

McKee, E.D., W.K. Hamblin, and P.E. Damon, K-Ar age of lava dam in Grand Canyon, *Geological Society of America Bulletin, 79*, 133–136, 1968.

McKee, E. D., and E. T. Schenk, The lower canyon lavas and related features at Toroweap in Grand Canyon, *Journal of Geomorphology, 5*, 245–273, 1942.

Mortimer, N., and D. Parkinson, Hikurangi Plateau: a Cretaceous large igneous province in the southwest Pacific Ocean, *Journal of Geophysical Research, 161*, 687–696, 1996.

Mueller, P. A., and J. J. W. Rogers, Secular chemical variation in a series of Precambrian mafic rocks Beartooth Mountains, Montana and Wyoming, *Geological Society of America Bulletin, 84*(11), 3645–3652, 1973.

Mukasa, S. B., A. H. Wilson, and R. W. Carlson, A multielement geochronologic study of the Great Dyke, Zimbabwe: significance of the robust and reset ages, *Earth and Planetary Science Letters, 164*, 353–369, 1998.

Murphy, D. T., B. S. Kamber, and K. D. Collerson, A refined solution to the first terrestrial Pb-isotope paradox, *Journal of Petrology, 44*, 39–53, 2003.

Naeser, C. W., I. R. Duddy, D. P. Elston, T. A. Dumitru, and P. F. Green, Fission-track dating: ages for Cambrian strata and Laramide and post-Middle Eocene cooling events from the Grand Canyon, Arizona, in *Geology of Grand Canyon, Northern Arizona (with Colorado River Guides)*, edited by D. P. Elston, G. H. Billingsley, and R. A. Young, pp. 139–144, American Geophysical Union, Washington, DC, 1989.

Nägler, T. F., and J. D. Kramers, Nd isotope evolution of the upper mantle during the Precambrian: models, data and the uncertainty of both, *Precambrian Research, 91*, 233–252, 1998.

Nairn, I. A., Atmospheric shock waves and condensation clouds from Ngauruhoe explosive eruptions, *Nature, 259*, 190–192, 1976.

Nairn, I. A., C. A. Y. Hewson, J. H. Latter, and C. P. Wood, Pyroclastic eruptions of Ngauruhoe volcano, central North Island, New Zealand, 1974 January and March, in *Volcanism in Australasia*, edited by R. W. Johnson, pp. 385–405, Elsevier, Amsterdam, 1976.

Nairn, I. A., and S. Self, Explosive eruptions and pyroclastic avalanches from Ngauruhoe in February 1975, *Journal of Volcanology and Geothermal Research, 3*, 39–60, 1978.

Nairn, I. A., and C. P. Wood, Active volcanoes of Taupo Volcanic Zone, in *Active Volcanoes and Geothermal Systems, Taupo Volcanic Zone*, New Zealand Geological Survey, Record 22, pp. 5–84, 1987.

Nehru, C.E., and M. Prinz, Petrologic study of the Sierra Ancha sill complex, Arizona, *Geological Society of America Bulletin, 81*(6), 1733–1766, 1970.

Noble, L.F., The Shinumo quadrangle, Grand Canyon district, Arizona, *U.S. Geological Survey, Bulletin 549*, 1914.

Noble, L.F., and J.F. Hunter, Reconnaissance of the Archean Complex of the Granite Gorge, Grand Canyon, Arizona, *U.S. Geological Survey, Professional Paper 98-I*, 95–113, 1916.

Oberthür, T., D.W. Davis, T.G. Blenkinsop, and A. Höhndorf, Precise U-Pb mineral ages, Rb-Sr and Sm-Nd systematics for the Great Dyke, Zimbabwe—constraints on Late Archean events in Zimbabwe craton and Limpopo belt, *Precambrian Research, 113*, 293–305, 2002.

O'Nions, R.K., and I.N. Tolstikhin, Limits on the mass flux between lower and upper mantle and stability of layering, *Earth and Planetary Science Letters, 139*, 213–222, 1996.

Phipps Morgan, J., Thermal and rare gas evolution of the mantle, *Chemical Geology, 145*, 431–445, 1998.

Phipps Morgan, J., and W.J. Morgan, Two-stage melting and the geochemical evolution of the mantle: a recipe for mantle plum-pudding, *Earth and Planetary Science Letters, 170*, 215–239, 1999.

Poitrasson, F., C. Pin, and J.-L. Duthou, Hydrothermal remobilization of rare earth elements and its effects on Nd isotopes in rhyolite and granite, *Earth and Planetary Science Letters, 30*, 1–11, 1995.

Powell, J.W., *Exploration of the Colorado River of the West*, Smithsonian Institution, Washington, DC, 1876.

Prinz, M., Geologic evolution of the Beartooth Mountains, Montana and Wyoming: Part V. Mafic dike swarms of the southern Beartooth Mountains, *Geological Society of America Bulletin, 75*, 1217–1248, 1964.

Ragan, D.N., and M.F. Sheridan, The Archean rocks of the Grand Canyon, Arizona, *Geological Society of America, Abstracts with Programs, 2*(2), 132–133, 1970.

Rugg, S.H., and S.A. Austin, Evidences for rapid formation and failure of Pleistocene "lava dams" of the western Grand Canyon, Arizona, in *Proceedings of the Fourth International Conference on Creationism*, edited by R.E. Walsh, pp.475–486, Creation Science Fellowship, Pittsburgh, Pennsylvania, 1998.

Shride, A. F., Younger Precambrian geology in southern Arizona, *U. S. Geological Survey, Professional Paper 566*, 1967.

Simkin, T., Flow differentiation in the picritic sills of North Skye, in *Ultramafic and Related Rocks*, edited by P. J. Wyllie, pp. 64–69, John Wiley & Sons, New York, 1967.

Smith, D., Mineralogy and petrology of the diabasic rocks in a differentiated olivine diabase sill complex, Sierra Ancha, Arizona, *Contributions to Mineralogy and Petrology, 27*, 95–113, 1970.

Smith, D., and L. T. Silver, Potassic granophyre associated with Precambrian diabase, Sierra Ancha, central Arizona, *Geological Society of America Bulletin, 86*, 503–513, 1975.

Snelling, A. A., The cause of anomalous potassium-argon "ages" for recent andesite flows at Mt Ngauruhoe, New Zealand, and the implications for potassium-argon "dating," in *Proceedings of the Fourth International Conference on Creationism*, edited by R. E. Walsh, pp. 503–525, Creation Science Fellowship, Pittsburgh, Pennsylvania, 1998.

Snelling, A. A., Geochemical processes in the mantle and crust, in *Radioisotopes and the Age of the Earth: A Young-Earth Creationist Initiative*, edited by L. Vardiman, A. A. Snelling, and E. F. Chaffin, pp. 123–304, Institute for Creation Research, El Cajon, California, and Creation Research Society, St. Joseph, Missouri, 2000a.

Snelling, A. A., Radiohalos, in *Radioisotopes and the Age of the Earth: A Young-Earth Creationist Research Initiative*, edited by L. Vardiman, A. A. Snelling, and E. F. Chaffin, pp. 381–468, Institute for Creation Research, El Cajon, California, and Creation Research Society, St. Joseph, Missouri, 2000b.

Snelling, A. A., The relevance of Rb-Sr, Sm-Nd and Pb-Pb isotope systematics to elucidation of the genesis and history of recent andesite flows at Mt Ngauruhoe, New Zealand, and the implications for radioisotopic dating, in *Proceedings of the Fifth International Conference on Creationism*, edited by R.L. Ivey, Jr., pp. 285–303, Creation Science Fellowship, Pittsburgh, Pennsylvania, 2003a.

Snelling, A. A., Whole-rock K-Ar model and isochron, and Rb-Sr, Sm-Nd and Pb-Pb isochron, "dating" of the Somerset Dam layered mafic intrusion, Australia, in *Proceedings of the Fifth International Conference*

on Creationism, edited by R.L. Ivey., Jr, pp. 305–324, Creation Science Fellowship, Pittsburgh, Pennsylvania, 2003b.

Snelling, A.A., Radiohalos in granites: evidence for accelerated nuclear decay, in *Radioisotopes and the Age of the Earth: Results of a Young-Earth Creationist Research Initiative*, edited by L. Vardiman, A.A. Snelling, and E.F. Chaffin, pp. 101–207, Institute for Creation Research, El Cajon, California, and Creation Research Society, Chino Valley, Arizona, 2005a.

Snelling, A.A., Fission tracks in zircons: evidence for abundant nuclear decay, in *Radioisotopes and the Age of the Earth: Results of a Young-Earth Creationist Research Initiative*, edited by L. Vardiman, A.A. Snelling, and E.F. Chaffin, pp. 209–324, Institute for Creation Research, El Cajon, California, and Creation Research Society, Chino Valley, Arizona, 2005b.

Snelling, A.A., and M.H. Armitage, Radiohalos—a tale of three granitic plutons, in *Proceedings of the Fifth International Conference on Creationism*, edited by R.L. Ivey, Jr., pp. 243–267, Creation Science Fellowship, Pittsburgh, Pennsylvania, 2003.

Snelling, A.A., S.A. Austin, and W.A. Hoesch, Radioisotopes in the diabase sill (Upper Precambrian) at Bass Rapids, Grand Canyon, Arizona: an application and test of the isochron dating method, in *Proceedings of the Fifth International Conference on Creationism*, edited by R.L. Ivey, Jr., pp. 269–284, Creation Science Fellowship, Pittsburgh, Pennsylvania, 2003a.

Snelling, A.A., J.R. Baumgardner, and L. Vardiman, Abundant Po radiohalos in Phanerozoic granites and timescale implications for their formation, *EOS, Transactions of the American Geophysical Union, 84*(46), Fall Meeting Supplement, Abstract V32C-1046, 2003b.

Steiner, A., Petrogenetic implications of the 1954 Ngauruhoe lava and its xenoliths, *New Zealand Journal of Geology and Geophysics, 1*, 325–363, 1958.

Sun, S.S., and G.N. Hansen, Evolution of the mantle: geochemical evidence from alkali basalt, *Geology, 3*, 297–302, 1975.

Tatsumi, Y., Formation of the volcanic front in subduction zones, *Geophysical Research Letters, 13*, 717–720, 1986.

Taylor, T.M., N.W. Jones, and S. Moorbath, Isotopic assessment of relative contributions from crust and mantle sources to magma genesis of

Precambrian granitoid rocks, *Philosophical Transactions of the Royal Society of London, A310*, 605–625, 1984.

Tiexeira, W., P.R. Renne, G. Bossi, N. Campal, and M.S. D'Agrella Filho, ^{40}Ar-^{39}Ar and Rb-Sr geochronology of the Uruguayan dike swarm, Rio de la Plata craton and implications for Proterozoic intraplate activity in western Gondwana, *Precambrian Research, 93*, 153–180, 1999.

Topping, W.W., Tephrostratigraphy and chronology of Late Quaternary eruptives from the Tongariro Volcanic Centre, New Zealand, *New Zealand Journal of Geology and Geophysics, 16*, 397–423, 1973.

Vallance, T.G., Mafic rock alteration and isochemical development of some cordierite-anthophyllite rocks, *Journal of Petrology, 8*, 84–96, 1967.

Van Keken, P.E., E.H. Hauri, and C.J. Ballentine, Mantle mixing: the generation, preservation and destruction of chemical heterogeneity, *Annual Review of Earth and Planetary Sciences, 30*, 493–525, 2002.

Wager, L.R., G.M. Brown, and W.J. Wadsworth, Types of igneous cumulates, *Journal of Petrology, 1*, 73–85, 1960.

Walcott, C.D., Precambrian igneous rocks of the Unkar Terrane, Grand Canyon of the Colorado, *U.S. Geological Survey, 14th Annual Report for 1892/93, Part 2,* 497–519, 1894.

Walker, F., The differentiation of the Palisade diabase, New Jersey, *Geological Society of America Bulletin, 51*, 1059–1106, 1940.

Walker, T.B., *The Somerset Dam Igneous Complex, South-East Queensland*, Unpublished B.Sc. Honours Thesis, The University of Queensland, Brisbane, 1998.

Warner, J.L., R. Lee-Berman, and G.H. Simonds, Field and petrologic relations of some Archean rocks near Long Lake, eastern Beartooth Mountains, Montana and Wyoming, in *Precambrian Geology of the Beartooth Mountains, Montana and Wyoming*, compiled by P.A. Mueller and J.L. Wooden, pp. 56–68, Montana Bureau of Mines and Geology, Special Publication 84, 1982.

Williams, K., *Volcanoes of the South Wind: A Field Guide to the Volcanoes and Landscape of the Tongariro National Park*, Tongariro Natural History Society, Turangi, New Zealand, 1994.

Wooden, J.L., P.A. Mueller, D.K. Hunt, and D.R. Bowes, Geochemistry and Rb-Sr geochronology of Archean rocks from the interior of the southeastern

Beartooth Mountains, Montana and Wyoming, in *Precambrian Geology of the Beartooth Mountains, Montana and Wyoming*, compiled by P.A. Mueller and J.L. Wooden, pp. 45–55, Montana Bureau of Mines and Geology, Special Publication 84, 1982.

Wrucke, C.T., The Middle Proterozoic Apache Group, Troy Quartzite and associated diabase in Arizona, in *Geologic Evolution of Arizona*, edited by J.P. Jenney and S.J. Reynolds, pp. 239–258, Arizona Geological Society, Tucson, Digest 17, 1989.

York, D., Least squares fitting of a straight line with correlated errors, *Earth and Planetary Science Letters, 5*, 320–324, 1969.

Zartman, R.E., and S.M. Haines, The plumbotectonic model for Pb isotopic systematics among major terrestrial reservoirs—a case for bidirectional transport, *Geochimica et Cosmochimica Acta, 52*, 1327–1339, 1988.

Zhao, J., and M.T. McCulloch, Sm-Nd mineral isochron ages of late Proterozoic dyke swarms in Australia: evidence for two distinctive events of magma magmatism and crustal extension, *Chemical Geology, 109*, 341–354, 1993.

Zheng, Y.-F., Influences of the nature of the initial Rb-Sr system on isochron validity, *Chemical Geology, 80*, 1–16, 1989.

Zindler, A., and S.R. Hart, Chemical geodynamics, *Annual Review of Earth and Planetary Sciences, 14*, 493–571, 1986.